Theoretical investigations of nonlinear effects in lower hybrid wave heating(Dissertation_全文)

AUTHOR(S):

Fukuyama, Atsushi

THEORETICAL INVESTIGATIONS OF NONLINEAR EFFECTS IN LOWER HYBRID WAVE HEATING

ATSUSHI FUKUYAMA

1980

THEORETICAL INVESTIGATIONS OF NONLINEAR EFFECTS IN LOWER HYBRID WAVE HEATING

ATSUSHI FUKUYAMA

1980

- C O N T E N T S -

Chapter 1 : INTRODUCTION 1

Chapter 2 : SURVEY OF THE LINEAR THEORY OF LOWER HYBRID WAVES 5

2-1 Accessibility condition 6

2-2 Linear mode-conversion 12

2-3 Summary 18

Chapter 3 : NONLINEAR COUPLING OF A PHASED WAVEGUIDE ARRAY WITH LOWER HYBRID WAVES 20

3-1 Linear theory of coupling 23

1. Wave field in the waveguide and in the vacuum 23
2. Wave field in the plasma 26
3. Linear coupling equation 29
4. Numerical results 33

3-2 Density profile modification due to a ponderomotive force 38

1. Formulation 38
2. Basic equations 42

3-3 Effects of the one-dimensional density modification 45

1. One-dimensional model 45
2. Numerical analysis 49

3-4 Discussion 57

Chapter 4 : NONLINEAR PROPAGATION OF LOWER HYBRID WAVES 60

4-1 Basic formulation 62

1. Model and basic equation 62
2. Nonlinear propagation far from the linear mode-conversion point 66

4-2 Nonlinear behaviour near the linear mode conversion point 70

1. Linear analysis 70
2. Model equation 73
3. Numerical analysis 75

4-3 Discussion 80

Chapter 5 : STOCHASTIC HIGH-ENERGY TAIL FORMATION BY A SINGLE WAVE IN A MAGNETIZED PLASMA 82

5-1 Intrinsic stochasticity in RF heating 84

5-2 Hamiltonian formulation for the motion of a charged particle 86

1. Hamiltonian of a test particle 86
2. General formulation 88

5-3 Case of oblique propagation 92

1. Analysis of the primary resonance 92
2. Analysis of the secondary resonance 97
3. Results of numerical analysis 104

5-4 Case of perpendicular propagation 110

1. Analytical treatment 110
2. Results of numerical computations 117

5-5 Discussion 127

Chapter 6 : SUMMARY AND CONCLUSIONS 130

Acknowledgements 134

Appendix A 135

Appendix B 136

References 137

Chapter 1

INTRODUCTION

The problem of plasma heating has been, and is, considered to be one of the central problems in thermonuclear fusion research, in order to ignite magnetically confined plasmas produced in such large-scale devices as tokamaks. For long, the principal heating scheme has relied upon ohmic heating. The ohmic heating alone has been recognized, however, as doubtful, in order to attain an ignition temperature, mainly because plasma heating due to the plasma resistivity, proportional to $T_e^{-3/2}$ with T_e the electron temperature, is overcome by heat loss due to Bremsstrahlung which is proportional to $T_e^{1/2}$, when T_e increases. Actually, an electron temperature, attainable by ohmic heating alone, is predicted to be 3 KeV, since a large current, required to render the ohmic heating efficient, is limited by the MHD stability criterion. In order to produce a high-temperature plasma in which α-particle heating becomes effective, an auxiliary heating scheme has been called for.

At present, the supplementary heating methods currently investigated are a neutral-beam injection, a wave heating (electron cyclotron, lower-hybrid, ion cyclotron and shear Alfven waves), a magnetic compression and a turbulent heating. Because of its simple physical mechanism, the effectiveness of the neutral-beam injection has been experimentally confirmed[1)] as a tool of high-power heating in present-day tokamaks. Future devices containing larger-size and higher-density plasmas require, however, a higher-energy neutral beam which may be capable of heating a central part of the plasma. But it is known that a neuralization effeciency

decreases notably at such a high energy regime. Among various wave heating methods, heating by lower-hybrid (LH) wave is considered to be one of the most promising for supplementary heating which requires an input power of more than several 10 MW. Heating by LH waves with frequencies near 1 ~ 2 GHz is particularly advantageous, mainly because we can use phased-arrays of waveguides as a coupling structure instead of a coil system installed near the plasma surface.

A number of experimental studies of the LH wave heating have been reported both on linear[2,3] and toroidal[4-16] machines. Recent experiments on tokamaks with a RF power input of more than 100 KW have demonstrated efficient heating of bulk plasma ions with no deleterious effect on a plasma confinement.[7,8,10,12] In the latest experiment on JFT-2,[12] a parallel temperature of ions has been observed to increase by about 300 eV during 15 ms RF pulse of 200 KW, accompanied with a slight increase of the electron temperature. These results suggest that an absorbed wave energy has been thermalized and that neither deterioration of the confinement nor enhancement of impurity influx comes about.

In spite of these encouraging experimental results, a heating mechanism is still far from obvious. While a great deal of theoretical effort has been devoted to the study of the linear mechanism of the LH heating, applicability of a linear theory is seriously limited by various nonlinear effects. Because of an intense electric field required for a high-power LH heating, it sounds indeed essential to properly take account of them.

The purpose of this thesis is to analyse several important nonlinear effects encountered in the LH heating, and thereby to estimate their influences on actual heating experiments carried out

on both present and near-future fusion devices.

The mechanism of RF heating is roughly divided into three processes : coupling, propagation and absorption. The coupling of an external wave source with an electromagnetic field in a plasma is a primary factor which determines the heating efficiency. Since an area of access ports mounted on a vessel wall is limited, a power density transmitted into a plasma has to be as large as possible. Problems of how to obtain an optimum coupling and how to maximize a transmitted power density become, therefore, of central interest. On the other hand, propagation characteristics predict a region where wave energy is absorbed. If the wave energy is dissipated near a plasma surface, a rapid energy loss will reduce the heating efficiency. Furthermore, the steepening of a wave packet due to nonlinear effects may generate high-energy particles, while its spreading due to dispersion effects may probably reduce various nonlinear effects. Therefore, analysis of the trajectory of the wave packet and of the deformation of its shape turns out to be the main problem. The absorption mechanism may also determine a position of energy deposition. In a high-temperature fusion plasma, it is natural that the modification of a velocity distribution function of plasma particles has to be taken into account because of very weak collisional effects.

We shall investigate important nonlinear effects originating from each of these three processes, but shall not deal with such parametric phenomena as parametric decay and nonlinear Landau damping. The parametric instabilities of the LH wave have been analysed by a number of authors.[17-20] As for tokamak plasmas, we quote the extensive study by Porkolab[18] who has calculated the

growth rate and the threshold for parametric decay, taking into account the effects of inhomogeneities, such as a density gradient, a finite pump width and a magnetic shear. In fact, decay spectra have often been observed in the LH wave heating experiments on tokamaks,[5-8,10,15] but recent experiments on JFT-2[11] suggest that an amplitude of the decay wave tends to saturate at rather low level with increasing transmitted power. Since a theory which allows to predict a saturation level of the decay-wave amplitude is not yet well established, however, a role played by parametric instabilities in the heating mechanism is still left controversial. The thesis is organized thus.

In Chapter 2, we briefly survey the linear theory of LH waves in toroidal devices. Nonlinear coupling of a waveguide array with LH waves is analysed in Chapter 3, by taking account of a static density depression due to a ponderomotive force. The existence of an upper limit on the transmitted power density is demonstrated. Chapter 4 deals with the nonlinear propagation of LH waves, specifically near the linear mode-conversion point where an electric field is expected to be strengthened. The deformation of wave packet is shown in both linear and nonlinear regimes. Chapter 5 is devoted to the study of the formation of a high-energy tail on the velocity distribution, due to a monochromatic wave propagating through a magnetized plasma. The threshold of a wave amplitude for the onset of an intrinsic stochasticity, which results in the tail formation, is analytically calculated and compared with numerical results. In the last chapter, we present concluding remarks.

Chapter 2

SURVEY OF THE LINEAR THEORY OF LOWER HYBRID WAVES

A feasibility of the auxiliary plasma heating by means of LH waves, first proposed by Stix[21], has been granted as most prospective, thanks to an effective absorption of electromagnetic energies through the conversion of the LH wave into a short wave-length mode which easily couples with plasma particles. Since then, a number of works have been devoted to the theory of the linear LH waves. In this chapter, we shall briefly survey the linear theory of LH waves to revisit their fundamental linear properties required, in the subsequent chapters, to analyse their nonlinear behaviours.

An accessibility condition[22] to the LH resonance is discussed in §2-1, within the framework of the cold-plasma approximation. This condition provides the lower limit of a parallel refractive index in order for externally-excited LH waves to be accessible to the resonance. Section 2-2 deals with the linear mode-conversion[21] near the LH resonance with the aid of the electrostatic approximation. In the last section, we shall summarize the linear theory of the LH heating mechanism.

§2-1. Accessibility condition[23)]

A local property of plasma waves in a weakly inhomogeneous plasma can be explained to a great extent by means of a dispersion relation for a homogeneous plasma. This section deals with the local dispersion relation of plasma waves with frequencies near the LH frequency.

We shall consider a plasma slab immersed in a static magnetic field $B_0\vec{z}$. The plasma is uniform in the y-z plane, while the plasma density n increases in the x-direction. It is assumed that the plasma wave, with amplitude small enough for a linear theory to apply, has a form of a stationary plane wave, $\exp i(k_\perp x + k_\parallel z - \omega t)$; such quantities as ω and $k_\parallel$ which can be controlled externally are assumed to be real and only $k_\perp$ is considered to be complex.

In the cold-plasma approximation, the dielectric tensor $\overleftrightarrow{\varepsilon}$ takes the form,

$$\overleftrightarrow{\varepsilon} = \begin{pmatrix} \varepsilon_\perp & ig & 0 \\ -ig & \varepsilon_\perp & 0 \\ 0 & 0 & \varepsilon_\parallel \end{pmatrix} , \tag{2.1}$$

where

$$\varepsilon_\perp = 1 - \sum_\sigma \frac{\omega_{p\sigma}^2}{\omega^2 - \omega_{c\sigma}^2} ,$$

$$\varepsilon_\parallel = 1 - \sum_\sigma \frac{\omega_{p\sigma}^2}{\omega^2} \tag{2.2}$$

and $$g = \sum_\sigma \frac{\omega_{p\sigma}^2 \omega_{c\sigma}}{\omega(\omega^2 - \omega_{c\sigma}^2)} .$$

$\omega_{p\sigma}$ and $\omega_{c\sigma}$ stand for the plasma and the cyclotron frequencies of the σ-th species, respectively. The wave-number vector $\vec{k}$ and the angular frequency ω of an electromagnetic wave must satisfy the dispersion relation

$$D(\omega,\vec{k}) = \det \overleftrightarrow{D}(\omega,\vec{k}) = 0 \ , \tag{2.3}$$

where the dispersion tensor $\overleftrightarrow{D}$ is defined by

$$\overleftrightarrow{D}(\omega,\vec{k}) = \frac{c^2}{\omega^2}\left(\vec{k}\,\vec{k} - k^2\overleftrightarrow{I}\right) + \overleftrightarrow{\varepsilon} \ . \tag{2.4}$$

When the waves propagate perpendicularly to the static magnetic field ($k_{\parallel}=0$), they can be split into the ordinary and the extraordinary modes. The latter mode

$$N_{\perp}^2 = \frac{k_{\perp}^2 c^2}{\omega^2} = \frac{\varepsilon_{\perp}^2 - g^2}{\varepsilon_{\perp}} \tag{2.5}$$

shows hybrid resonances where $\varepsilon_{\perp}=0$. It has two branches, the resonance frequency of which are called the upper hybrid (UH) frequency ω_{UH} ($\omega_{UH}>|\omega_{ce}|$) and the lower hybrid (LH) frequency ω_{LH} ($\sqrt{\omega_{ci}|\omega_{ce}|}>\omega_{LH}>\omega_{ci}$), respectively. While the UH resonance is mainly related to the motion of electrons, both electrons and ions participate to the LH resonance (LHR). If we assume that $\omega_{ci} \ll \omega \ll |\omega_{ce}|$, the LH frequency, ω_{LH}, can be approximated by

$$\omega_{LH}^2 \simeq \frac{\omega_{pi}^2}{1 + \dfrac{\omega_{pe}^2}{\omega_{ce}^2}} \tag{2.6}$$

and, alternatively, for a given frequency $\omega<\sqrt{\omega_{ci}|\omega_{ce}|}$, the LHR occurs where the plasma density satisfies

$$\frac{\omega_{pe}^2}{\omega_{ce}^2} = \frac{\omega_{per}^2}{\omega_{ce}^2} \equiv q \ , \tag{2.7}$$

where

$$q = \frac{(\omega^2 - \omega_{ci}^2)(1 - \omega^2/\omega_{ce}^2)}{(\omega_{ci}|\omega_{ce}| - \omega^2)(1 + m_e/m_i)} \simeq \frac{\omega^2}{\omega_{ci}|\omega_{ce}| - \omega^2} \ . \tag{2.8}$$

The suffix r indicates the value at the LHR. The extraordinary wave cannot, however, propagate in a region where $\omega_{pe} < \omega_{per}$. Therefore the wave cannot reach the LHR from the outside of a confined plasma.

On the other hand, when there exists nonzero $k_{//}$ determined by a wave source, the LHR is accessible to the wave from the lower density side. The accessibility condition is obtained in the following way. The dispersion relation, eq. (2.3), is a quadratic equation with respect to $k_{\perp}^2$ and the coefficients (2.2) may be approximated by

$$\varepsilon_{\perp} = 1 - h, \ \varepsilon_{//} = 1 - \beta h \quad \text{and} \quad g = \alpha h \ , \tag{2.9}$$

where

$$h = \frac{\omega_{pe}^2}{\omega_{per}^2},$$

$$\alpha \simeq \frac{\omega_{per}^2}{\omega\, \omega_{ce}} \simeq O(\sqrt{m_i/m_e})$$

and $$\beta \simeq \frac{\omega_{per}^2}{\omega^2} \simeq O(m_i/m_e) \ ,$$

in the frequency range $\omega_{ci} << \omega << |\omega_{ce}|$. Except in an extremely low density region $\omega_{pe} \sim \omega$, the solution to eq. (2.3) can be simplified, by virtue of the assumption $\beta h >> 1$, as

$$N_\perp^2 \simeq \frac{\beta h}{2(1-h)} \left\{ N_\parallel^2 - (1-h+qh) \pm \sqrt{\{N_\parallel^2 - (1-h+qh)\}^2 - 4(1-h)qh} \right\} \quad (2.10)$$

with $N_\parallel = k_\parallel c/\omega$. Remark that the slow mode related to the LHR takes the upper sign. In order that the wave can propagate without considerable reflection, the right-hand side (r.h.s) of eq.(2.10) must be real and positive. The sufficient condition for such a solution to exist can be easily obtained from eq.(2.10),

$$N_\parallel > \sqrt{1-h} + \sqrt{qh} \quad , \quad (2.11)$$

and, for $0 < h < 1$, the r.h.s. takes its maximum value $\sqrt{1+q}$ at $h = q/(1+q)$. Therefore the accessibility condition of the LHR from the lower density side is expressed as

$$N_\parallel^2 > N_{\parallel acc}^2 = 1 + q \simeq \frac{\omega_{ci}|\omega_{ce}|}{\omega_{ci}|\omega_{ce}| - \omega^2} \quad . \quad (2.12)$$

If this condition is not satisfied, a slow mode launched by an external wave source may be converted to a fast mode before reaching the LHR and will be reflected back to the lower-density region. Near the plasma boundary $\omega_{pe} \sim \omega$, the solution to eq.(2.3) which describes the slow mode accessible to the LHR is approximated by

$$N_\perp^2 \simeq (\beta h - 1)(N_\parallel^2 - 1) \quad . \quad (2.13)$$

It should be noted here that the wave which satisfies the accessibility condition is evanescent where $\omega_{pe} < \omega$.

When the wave approaches the LHR, the x-component of the electric field E_x as well as $k_\perp$ increases, so that the solution obtained from the electrostatic approximation

$$N_\perp^2 = \frac{\beta h}{1 - h} N_{//}^2 \tag{2.14}$$

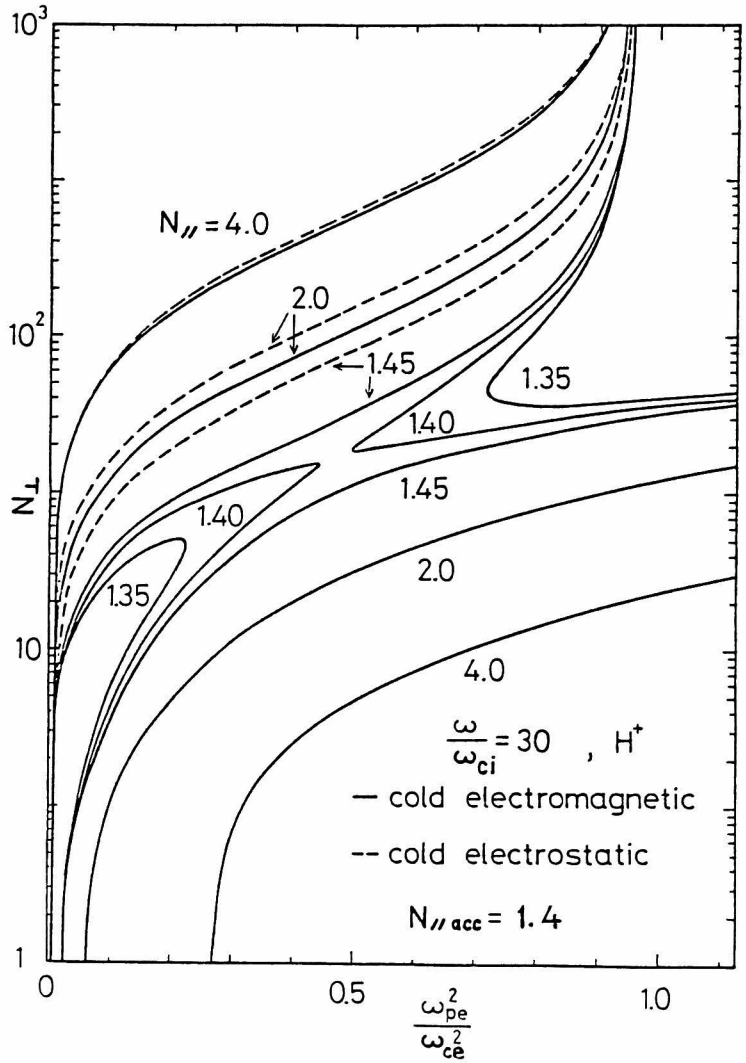

Fig.2.1 Comparison of the solutions to the electromagnetic dispersion relation (2.3) with those obtained from the electrostatic approximation.

can be a good approximation. Comparing eq.(2.14) with eq.(2.10), we obtain a condition for the electrostatic approximation,

$$N_{\parallel} \gg \sqrt{1-h} + \sqrt{q\,h} \quad . \tag{2.15}$$

Therefore if the accessibility condition, eq.(2.12), is well satisfied, the electrostatic approximation can be employed in the study of the LH waves.

Comparison of the exact real solution to eq.(2.3) with that obtained from the electrostatic approximation is illustrated in Fig.2.1, where, as an example, we choose $\omega / \omega_{ci} = 30$ and a mass number $A = 1$. In this case the accessibility condition (2.12) shows $N_{\parallel} = 1.4$. Although there still exists a narrow evanescent gap for $N_{\parallel} = 1.4$, the figure shows that the approximate criterion (2.12) proves to be satisfactory.

§2-2. Linear mode-conversion[23)]

With increasing $k_\perp$, the effect of a finite Larmor radius becomes important in the dispersion relation of plasma waves. Assuming that the electrostatic approximation can be applied, we shall investigate the longitudinal dispersion in a magnetized collisionless plasma composed of electrons and one species of positive ions with Maxwellian velocity distributions. The longitudinal dispersion relation derived from a set of the Vlasov and the Poisson equations is[24)]

$$D_L \equiv \frac{\vec{k}\cdot\overleftrightarrow{D}\cdot\vec{k}}{k^2} = 1 + \chi_e + \chi_i = 0 \ , \tag{2.16}$$

where

$$\chi_\sigma = \frac{\omega_{p\sigma}^2}{k^2}\frac{m_\sigma}{T_\sigma}\left[1 + \sum_{n=-\infty}^{\infty}\frac{\omega}{\omega - n\omega_{c\sigma}}\{W(Z_{\sigma n}) - 1\}\,\Lambda_n(\lambda_\sigma)\right] \ , \tag{2.17}$$

$$Z_{\sigma n} = \frac{\omega - n\omega_{c\sigma}}{k_\parallel v_{T\sigma}} \ , \qquad \lambda_\sigma = \frac{k_\perp^2 v_{T\sigma}^2}{\omega_{c\sigma}^2} \ ,$$

$$\Lambda_n(\lambda_\sigma) = I_n(\lambda_\sigma)\exp(-\lambda_\sigma) \ ,$$

with $I_n(\lambda_\sigma)$ the modified Bessel function of the first kind and $v_{T\sigma}(=\sqrt{T_\sigma/m_\sigma})$ the thermal velocity of the σ-th species. The plasma dispersion function $W(z)$ is defined by

$$W(Z) = \frac{1}{\sqrt{2\pi}}\int_C \frac{x}{x - Z}\exp\left(-\frac{x^2}{2}\right)dx \ , \tag{2.18}$$

where the contour C is chosen, so that the point z lies always above C.

In the frequency range $\omega \ll |\omega_{ce}|$, only the $n=0$ term is retained in the sum for the electronic susceptibility χ_e. As for the ionic susceptibility, we can separate it into a slowly varying part which becomes dominant for a warm plasma and an oscillating part which is apparently singular at the ion cyclotron harmonics, under the condition $k_{\parallel} v_{Ti} \ll \omega_{ci} \ll k_{\perp} v_{Ti} \ll \omega$. This condition is usually satisfied for a plasma with equal temperatures ($T_e \sim T_i$) near the LH reasonance, because otherwise the electron Landau damping prevents the wave from penetrating into a higher-density region. Consequently, we may approximate D_L as[25]

$$
\begin{aligned}
D_L = 1 &+ \frac{\omega_{pe}^2}{k^2} \frac{m_e}{T_e} \left\{ 1 + \{ W(\frac{\omega}{k_{\parallel} v_{Te}}) - 1 \} \Lambda_0(k_{\perp}^2 \rho_e^2) \right\} \\
&+ \frac{\omega_{pi}^2}{k^2} \frac{m_i}{T_i} \left\{ \mathrm{Re}\, W(\frac{\omega}{k_{\perp} v_{Ti}}) - \mathrm{Im}\, W(\frac{\omega}{k_{\perp} v_{Ti}}) \right. \\
&\left. \times \{ \cot \frac{\omega}{\omega_{ci}} \pi - \sum_n \frac{\omega}{\omega - n\omega_{ci}} \frac{1}{n\pi} W(\frac{\omega - n\omega_{ci}}{k_{\parallel} v_{Ti}}) \} \right\} ,
\end{aligned}
\tag{2.19}
$$

where $\rho_\sigma (= v_{T\sigma}/\omega_{c\sigma})$ is the Larmor radius. This dispersion clearly indicates that a wave energy is absorbed by ions through the ion cyclotron harmonic damping, so far as a small-amplitude wave is concerned. We note that in a magnetized plasma the ion Landau damping takes place if $k_{\parallel} \rho_i \gtrsim 1$ or if a small-angle scattering due to the Coulomb collision destroys a phase correlation of the cyclotron motion. In a high-temperature plasma, realizable in a present or a future tokamak, however, the collisional effect may be negligibly small.

In order to discuss the linear mode-conversion near the LHR, we introduce an approximation valid for a warm plasma, $k_\perp \rho_i \lesssim (\omega/\omega_{ci})^{1/2}$. If this condition is fulfilled, the effect of ion cyclotron harmonics in eq.(2.19) can be neglected, since $\mathrm{Im}\, W(\omega/k_\perp v_{Ti})$ is small compared with unity. Furthermore, assuming that $\lambda_e = k_\perp^2 \rho_i^2 (T_e/T_i)(m_e/m_i) \ll 1$, we obtain

$$\mathrm{Re}\, D_L = -\frac{1}{k^2}\left\{\left\{\frac{3\omega_{pi}^2}{\omega^4}\frac{T_i}{m_i} + \frac{3}{4}\frac{\omega_{pe}^2}{\omega_{ce}^2}\frac{T_e}{m_e}\right\}k_\perp^4 - \left\{1 + \frac{\omega_{pe}^2}{\omega_{ce}^2} - \frac{\omega_{pi}^2}{\omega^2}\right\}k_\perp^2 - \left\{1 - \frac{\omega_{pe}^2}{\omega^2}\right\}k_\parallel^2\right\} . \tag{2.20}$$

Then, dispersion relation $\mathrm{Re}\, D_L = 0$ yields

$$\omega^2 = \frac{\omega_{pi}^2}{1 + \frac{\omega_{pe}^2}{\omega_{ce}^2}\left(1 - \frac{3}{4}\frac{k_\perp^2 v_{Te}^2}{\omega_{ce}^2}\right)}\left(1 + \frac{m_i}{m_e}\frac{k_\parallel^2}{k_\perp^2} + 3\frac{k_\perp^2 v_{Ti}^2}{\omega^2}\right) . \tag{2.21}$$

The dispersion curve, together with that obtained from the cold-plasma approximation, is illustrated in Fig. 2.2. It is clear that, for values of $k_\perp \rho_i$ smaller than some critical value, the phase velocity $\omega/k_\perp$ and the group velocity $\partial\omega/\partial k_\perp$, both perpendicular to the magnetic field, have opposite signs (backward wave), and that, for larger $k_\perp \rho_i$, they have the same signs (forward wave). But these same waves are known to be always forward waves along the magnetic field. In order to obtain the density dependence of $k_\perp \rho_i$ for given ω and $k_\parallel \rho_i$, we may transform eq.(2.20) to a dimensionless form

$$(k_\perp \rho_i)^4 - \frac{1-h}{h}\frac{m_i}{m_e}\frac{1}{(1+q)s^2}(k_\perp \rho_i)^2 + \left(\frac{m_i}{m_e}\right)^2 \frac{1}{s^2}(k_\parallel \rho_i)^2 = 0 , \tag{2.22}$$

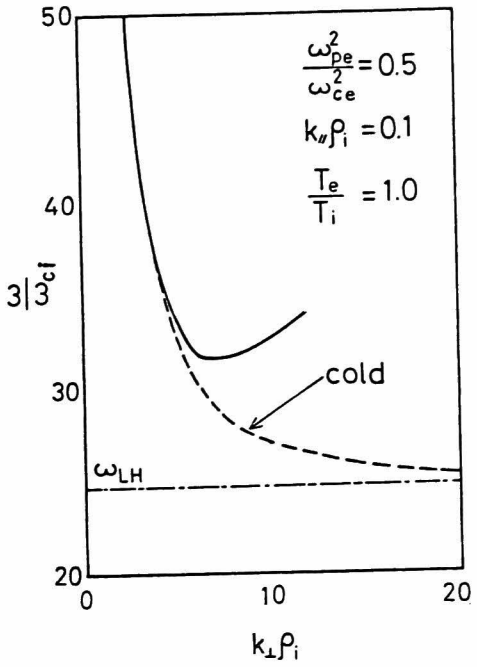

Fig.2.2 Dispersion relation derived from eq.(2.21)

where

$$s^2 = 3\left(\frac{1+q}{q} + \frac{1}{4}\frac{T_e}{T_i}\frac{q}{1+q}\right) = 3\left(\frac{\omega_{ci}|\omega_{ce}|}{\omega^2} + \frac{1}{4}\frac{T_e}{T_i}\frac{\omega^2}{\omega_{ci}|\omega_{ce}|}\right). \quad (2.23)$$

At the critical density ω_{pet}^2 smaller than ω_{per}^2, the cold-plasma mode is converted to a mode with larger $k_\perp\rho_i$ and its group velocity changes sign. When the density is lower than ω_{pet}^2, there exist two real positive $k_\perp^2\rho_i^2$, while, in a higher-density domain, there are complex conjugate solutions corresponding to spatially damped oscillations. The density and the value of $k_\perp\rho_i$ at the critical point (mode-conversion point) can be easily obtained as the double root to eq.(2.22),

$$\frac{\omega_{pet}^2}{\omega_{ce}^2} = \frac{q}{1 + 2(1+q)k_{\parallel}\rho_i s} = \frac{\omega^2}{\omega_{ci}|\omega_{ce}|(1+2k_{\parallel}\rho_i s) - \omega^2} , \tag{2.24}$$

$$k_{\perp}^2\rho_i^2\Big|_{\omega_{pe}^2=\omega_{pet}^2} = \frac{m_i}{m_e}\frac{k_{\parallel}\rho_i}{s} . \tag{2.25}$$

When $k_{\parallel}\rho_i$ increases and/or ω decreases, the mode-conversion point shifts to the lower-density side. Since ω^2 must be smaller than $\omega_{ci}|\omega_{ce}|$, the electron temperature does not considerably alter a location of the mode-conversion point, unless $T_e \gg T_i$. The density dependence of $k_{\perp}\rho_i$ is illustrated in Fig. 2.3 for various values of $k_{\parallel}\rho_i$.

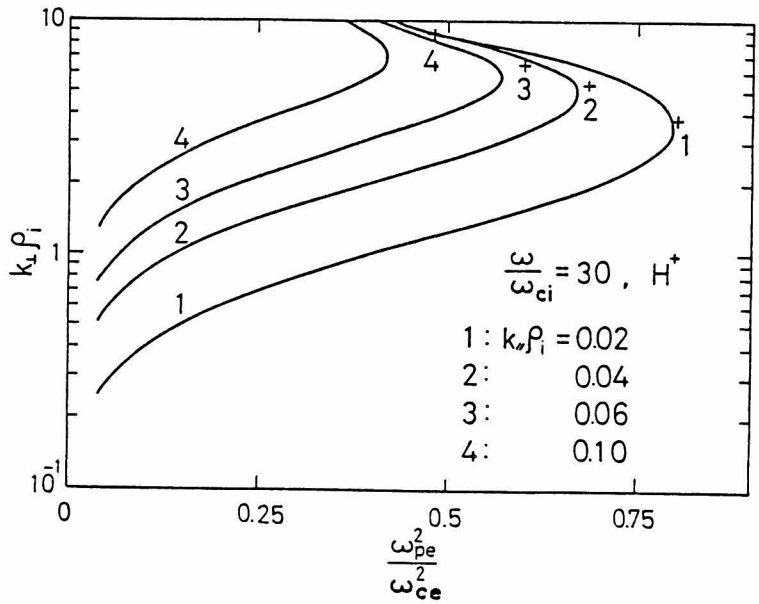

Fig.2.3 Values of $k_{\perp}\rho_i$ as a function of plasma density for various values of $k_{\parallel}\rho_i$. Crosses denote the approximate value calculated from eqs.(2.24) and (2.25).

In view of analysing the behaviour of the LH wave near the linear mode-conversion point, we have to take into account an inhomogeneity of the medium. Since the usual WKB approximation breaks down in the vicinity of the mode-conversion point where $dk_{\perp}/dx$ diverges, analysis of a differential equation describing the linear propagation of LH waves is required.[21,23,26-30] In the case of a plane wave, the wave equation may be reduced to the fourth-order differential equation with respect to x. Four asymptotic solutions of the equation can be connected to each other at the mode-conversion point by means of the saddle point method. If no damping occurs, the incoming LH wave is completely converted to the ion plasma mode. When such damping mechanisms as the collisional, the electron Landau or the ion cyclotron harmonic damping come into play, a considerable part of the wave energy is absorbed in the vicinity of the mode-conversion point where the group velocity in the x-direction approaches zero.[23,28]

After the mode-conversion, the ion plasma mode is greatly affected by the ion cyclotron harmonics because of large values of $k_{\perp}\rho_i$.[23,31,32] Accounting for an inhomogeneity of the static magnetic field, we can show[23] that the ion plasma mode is converted to the ion Bernstein mode and that the latter may be eventually absorbed at a stronger magnetic-field side of the resonance point of the ion cyclotron harmonic.

§2-3 Summary

We now summarize the propagation characteristics of the linear LH wave.

An electromagnetic field, launched by an external wave source, can propagate beyond a thin cutoff layer ($\omega_{pe}<\omega$) close to the vessel wall, if $N_{//}^2 > 1$. When the accessibility condition (2.12) is not satisfied, the incoming slow mode couples with a fast mode and is reflected back to the plasma surface. Waves with $N_{//}^2 > N_{//acc}^2$ penetrate, however, deep into a plasma along the resonance cone which stems from a weak $N_{//}$-dependence of the angle between the group velocity and the static magnetic field. Therefore a well-designed slow wave structure, to be used as an external wave source, is required for an efficient penetration of the wave, as long as the linear theory is concerned.

Since the LH wave is a backward wave, when viewed as a wave propagating in a perpendicular direction, the perpendicular components of the group velocity and the phase velocity have opposite signs. The cold-plasma theory shows that a group velocity of the LH wave is at a right angle to a phase velocity. Therefore, as the perpendicular wave number $k_{\perp}$ increases with a plasma density near the LH resonance, the wave propagates mostly along the magnetic field. In a tokamak plasma, the LH wave usually has to go round the torus several times along the magnetic axis before reaching the LH resonance.

As $k_{\perp}\rho_i$ becomes large, thermal effects have to be taken into account near the LH resonance. The warm plasma analysis predicts the mode-conversion from the cold LH mode to an ion plasma mode on

the lower density side of the LH resonance. Near the mode-conversion point, the perpendicular group velocity becomes small, while the electric field of the wave has a maximum value. The reflected ion plasma mode is converted again to the ion Bernstein mode and an energy associated with any of the two is eventually dissipated by the ions at the ion cyclotron harmonic resonance, if an inhomogeneity of the static magnetic field is taken into account. On the other hand, when $k_{//}$ is large enough to satisfy $\omega \lesssim 3k_{//}v_{Te}$, electrons absorb the wave energy through the electron Landau damping, even if the mode conversion does not occur.

Ray trajectories in a toroidal plasma have been analysed in several literatures.[23,33,34] The cylindrical configuration does not seem to essentially modify the analysis for a slab plasma except that the wave field is concentrated at the center of a plasma column. Toroidal effects, i.e., a shift of the resonance surface and a decrease of $k_{//}$, become important near the resonance surface, but the thermal effect has the tendency of shifting a trajectory apart from the resonance surface and reduces the toroidal effect on the incident LH mode. A recent work[35] suggests, however, that the accessibility condition may be considerably modified due to a change of $k_{//}$ during the rotation around the magnetic axis.

So far we have surveyed the LH heating mechanism within the framework of the linear theory. These linear pictures may be modified to include nonlinear effects which will be treated in the subsequent chapters. The individual concepts, such as the accessibility condition and the linear mode-conversion, remain, as we shall see, indispensable to the nonlinear analyses.

Chapter 3

NONLINEAR COUPLING OF A PHASED WAVEGUIDE ARRAY WITH LOWER HYBRID WAVES

The coupling of an external wave source with an electromagnetic field in a plasma is one of the most important problems in the studies of RF heating, because it is a primary factor which determines the heating efficiency and a maximum power-density transmitted into a plasma.

A phased waveguide array, which is a wave source composed of many waveguides with appropriate phase differences between them, was first proposed by Lallia[36] in order to preferentially excite slow waves with parallel refractive index $N_{\parallel}$ satisfying the accessibility condition (2.12), $N_{\parallel}^2 > N_{\parallel acc}^2$. It also has advantages that an efficient coupling can be obtained without complicated adjustments and that no structure within a vacuum chamber is required. The latter reduces the impurity influx due to the bombardment of high energy particles. Linear coupling of a phased waveguide array with LH waves was recently analysed by Brambilla[37] and developed by several authors.[38-41] Their results have shown that the reflection coefficient R seen from the wave source depends on both the relative phase difference $\Delta\Phi$ of adjacent waveguides and the density profile near the plasma surface, and have been recognized to be in satisfactory agreement with low-power experiments on linear[42] and toroidal machines.[5,9,10]

When the RF power-density increases, however, the experimental results deviate from the linear theory: the reflection coefficient has usually decreased with the power density and in several

experiments it becomes almost independent of $\Delta\Phi$. The recent experiment with high power-density in Petula[9] has shown that the reflection increases when the power density exceeds about 4 KW/cm^2 and that it still depends on $\Delta\Phi$.

In order to explain these nonlinear behaviours of the coupling, we consider the effect of a static density perturbation due to a ponderomotive force of the electromagnetic field on the propagation of the LH wave. It was first treated by Morales and Lee[43] and a number of works on it have been done as they will be refered to in Chapter 4. In a low-density and low-temperature plasma in a scrape-off layer, such nonlinear effects are more essential because the electromagnetic pressure can be comparable to the kinetic pressure in high power-density heating experiments. The effect on the coupling was first analysed by Morales[44] as a time-dependent problem. The density modification, however, is a very slow process compared to the wave propagation, since the former is specified by a characteristic length along the static magnetic field and the sound velocity. Therefore it seems appropriate to treat the density modification as a static process. The one-dimensional problem of the nonlinear coupling due to the static density perturbation has been analysed by Chan and Chiu[45] with a simplified model. The effect of two-dimensional density ripples due to the finite size and/or the higher modes of the waveguide array has been suggested in some literatures,[46] but no concrete work has yet been done.

In this chapter, we wish to clarify a power-density dependence of the coupling and an existence of the upper limit of the transmitted power, by taking account self-consistently of the nonlinear modification of the density profile near the plasma surface. In the

first section, the linear theory of the LH wave launching is summarized and some numerical results are presented. By the use of an appropriate ordering, we derive the nonlinear wave equation in §3-2. The case of a one-dimensional density modification is treated in §3-3, by considering only the fundamental mode of the waveguide array. The numerical computation starting from an asymptotic solution shows the nonlinear behaviour of the reflection to be consistent with the analytical result of an approximation model. The last section is devoted to the discussion of the results obtained.

§3-1. Linear theory of coupling[37)]

§§3-1-1. Wave field in the waveguide and in the vacuum

We consider a waveguide array which is composed of N_p waveguides and mounted on a plane metal wall at $x = 0$. Each waveguide has a width b parallel to the static magnetic field pointed to the z-direction and the separating metal wall has a width d, as are illustrated in Fig.3.1. For simplicity, we neglect the y-dependence of the array by assuming an infinite height of the waveguide. It has been shown in Ref.47 that the finiteness of the height a can be approximated by reducing the wave frequency ω to $\omega\{1 - (\pi c/\omega a)^2\}^{1/2}$ so long as the $N_{//}$-spectrum is not localized around $N_{//} = 1$. We have also assumed a slab geometry in spite of the complex geometry of actual devices, expecting the characteristic length of the device to be larger than the wave length in vacuum.

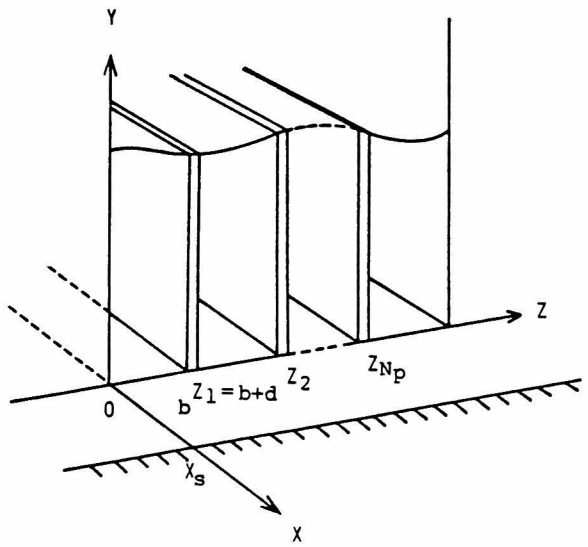

Fig.3.1 Geometry of a model of the phased waveguide array.

The field in the waveguide $(x < 0)$ may be expressed as a sum of transverse magnetic modes which easily couple with slow modes in a plasma: †

$$\begin{cases} E_{wz} = \sum_{p=1}^{N_p} \theta_p(z) \sum_{n=0}^{\infty} (\alpha_{np} e^{i\gamma_n x} + \beta_{np} e^{-i\gamma_n x}) \cos \dfrac{n\pi(z-z_p)}{b} , \\ B_{wy} = \sum_{p=1}^{N_p} \theta_p(z) \sum_{n=0}^{\infty} \left(-\dfrac{k_0}{c\gamma_n}\right) (\alpha_{np} e^{i\gamma_n x} - \beta_{np} e^{-i\gamma_n x}) \cos \dfrac{n\pi(z-z_p)}{b} , \\ E_{wx} = \sum_{p=1}^{N_p} \theta_p(z) \sum_{n=0}^{\infty} \left(-\dfrac{in\pi}{b\gamma_n}\right) (\alpha_{np} e^{i\gamma_n x} - \beta_{np} e^{-i\gamma_n x}) \sin \dfrac{n\pi(z-z_p)}{b} , \end{cases} \quad (3.1)$$

where

$$k_0 = \omega / c, \qquad z_p = (p-1)(b+d)$$

and

$$\gamma_n = \begin{cases} (k_0^2 - n^2\pi^2/b^2)^{1/2} & \text{for} \quad n < k_0 b/\pi , \\ i\,(n^2\pi^2/b^2 - k_0^2)^{1/2} & \text{for} \quad n > k_0 b/\pi . \end{cases}$$

The step function $\theta_p(z)$ has a value of unity only in the p-th waveguide,

$$\theta_p(z) = \begin{cases} 1 & \text{for} \quad z_p < z < z_p + b , \\ 0 & \text{for} \quad \text{elsewhere.} \end{cases}$$

The complex amplitudes α_{np} of the incident components are assumed to vanish for evanescent modes $n > k_0 b/\pi$. Our aim is to calculate the complex amplitudes β_{np} of the reflected components which result from the modes excited by a discontinuity at the waveguide

† We have assumed a time dependence of the form $e^{-i\omega t}$.

mouth ($x = 0$) and by an inhomogeneity of the plasma ($x > 0$).

In the vacumm region between $x = 0$ and the plasma surface $x = x_s$, it is convenient to write the wave field as a superposition of plane waves with different $k_{//}$,

$$\begin{cases} E_{vz} = \int_{-\infty}^{\infty} dk_{//}\, e^{ik_{//}z}\,(\sigma(k_{//})\, e^{ik_{\perp}x} + \rho(k_{//})e^{-ik_{\perp}x}) , \\ B_{vy} = \int_{-\infty}^{\infty} dk_{//}\, e^{ik_{//}z}\,(\frac{-k_0}{ck_{\perp}})(\sigma(k_{//})\, e^{ik_{\perp}x} - \rho(k_{//})e^{-ik_{\perp}x}) , \\ E_{vx} = \int_{-\infty}^{\infty} dk_{//}\, e^{ik_{//}z}\,(\frac{-k_{//}}{k_{\perp}})(\sigma(k_{//})\, e^{ik_{\perp}x} - \rho(k_{//})e^{-ik_{\perp}x}) , \end{cases} \tag{3.2}$$

where

$$k_{\perp} = \begin{cases} (k_0^2 - k_{//}^2)^{1/2} & \text{for} \quad k_{//}^2 < k_0^2 , \\ i\,(k_{//}^2 - k_0^2)^{1/2} & \text{for} \quad k_{//}^2 > k_0^2 . \end{cases}$$

If the plasma is homogeneous along the z-axis, no coupling among components with different $k_{//}$ values takes place and the simple relation $\rho(k_{//}) = Y(k_{//})\sigma(k_{//})$ holds by the use of the reflection coefficient $Y(k_{//})$ seen from the vacuum region. The density ripple along the magnetic field, however, gives rise to the coupling and complicates matters.

The boundary conditions imposed on the $x = 0$ plane are that the tangential electric field E_z is continuous everywhere and that the magnetic field B_y is continuous only in front of the waveguides. The discontinuity on the metal wall is due to the surface current on it. The orthogonality property of the waveguide eigenmodes to the

plane waves being applied to the boundary conditions, we obtain the relations:

$$\begin{cases} \sigma(k_{\parallel}) + \rho(k_{\parallel}) = \sum_{p=1}^{N_p} \sum_{n=0}^{\infty} (\alpha_{np} + \beta_{np})\, F_{np}(k_{\parallel}) \ , \\ \\ \alpha_{mq} - \beta_{mq} = \dfrac{4\pi\gamma_m}{b\varepsilon_m} \displaystyle\int_{-\infty}^{\infty} dk_{\parallel} \frac{1}{k_{\perp}} (\sigma(k_{\parallel}) - \rho(k_{\parallel}))\, F^{*}_{mq}(k_{\parallel}) \ , \end{cases} \tag{3.3}$$

where

$$F_{np}(k_{\parallel}) = \frac{k_{\parallel}}{2\pi i} \frac{1 - (-1)^n e^{-ik_{\parallel}b}}{k_{\parallel}^2 - (n\pi/b)^2} e^{-ik_{\parallel}z_p}$$

and

$$\varepsilon_m = \begin{cases} 2 & \text{for} \quad m = 0 \ , \\ \\ 1 & \text{for} \quad m \geq 1 \ . \end{cases}$$

§§3-1-2. Wave field in the plasma

We consider a cold plasma immersed in a uniform magnetic field $B_0\vec{z}$ with an inhomogeneous density profile $n_0(x)$. Since the wave frequency lies in the LH frequency regime, $\omega_{ci} \ll \omega \sim (\omega_{ci}|\omega_{ce}|)^{1/2} \ll |\omega_{ce}|$ and the plasma density near the surface is low enough to satisfy the condition, $(\omega_{pe}/\omega)^2 \ll |\omega_{ce}|/\omega$, the slow and the fast modes are decoupled. Then the wave equation for the electric field E_{pz} of the slow mode is approximated by

$$\frac{\partial^2}{\partial x^2} E_{pz}(x,z) + \left(k_0^2 + \frac{\partial^2}{\partial z^2}\right)\left[\left(1 - \frac{\omega_{pe}^2(x)}{\omega^2}\right) E_{pz}(x,z)\right] = 0 \ , \qquad (3.4)$$

as it shall be discussed at length in §3-2. The coupling with the fast mode[40,41] as well as the TE mode in the waveguides have been included in analysis in recent literatures.[38] It has been shown that the reflection coefficient and the $N_{//}$-spectrum above $N_{//acc}$ are not drastically modified by these effects. By the use of the Fourier transform of E_{pz}, the wave field may be expressed as

$$\begin{cases} E_{pz} = \int_{-\infty}^{\infty} dk_{//}\, e^{ik_{//}z}\, E(k_{//},x) \ , \\ B_{py} = \int_{-\infty}^{\infty} dk_{//}\, e^{ik_{//}z}\, \dfrac{ik_0}{ck_\perp^2}\, \dfrac{\partial E(k_{//},x)}{\partial x} \ , \\ E_{px} = \int_{-\infty}^{\infty} dk_{//}\, e^{ik_{//}z}\, \dfrac{ik_{//}}{k_\perp^2}\, \dfrac{\partial E(k_{//},x)}{\partial x} \ . \end{cases} \qquad (3.5)$$

In order to simplify the discussion, we assume a linear density profile, such that the surface density is μ_s times the cutoff density $n_{co} = m_e \varepsilon_0 \omega^2 / e^2$ and the density gradient is characterized by the length L_n,

$$\frac{n_0(x)}{n_{co}} = \frac{x - x_s}{L_n} + \mu_s \ . \qquad (3.6)$$

By substituting eqs.(3.5) and (3.6) into eq.(3.4), we obtain the ordinary differential equation for the Fourier component,

$$\frac{d^2}{dx^2} E(k_{//}, x) - \frac{k_0^2 - k_{//}^2}{L_n} \left(x - x_s + L_n(\mu_s - 1) \right) E(k_{//}, x) = 0 \ . \qquad (3.7)$$

A general solution to eq.(3.7) is expressed by a linear combination of the two Airy functions, Ai and Bi.[48] Since the solution has to satisfy the radiation condition which means that there exists no wave source deep in the plasma, we obtain the solution in the form,

$$E(k_{//}, x) = C(k_{//})\, P(k_{//}, x) \ , \qquad (3.8)$$

where

$$P(k_{//}, x) = \begin{cases} \mathrm{Ai}[\kappa(x - x_s + L_n(\mu_s - 1))] & \text{for} \quad k_{//}^2 < k_0^2 \ , \\ \mathrm{B}_-[\kappa(x - x_s + L_n(\mu_s - 1))] & \text{for} \quad k_{//}^2 > k_0^2 \ , \end{cases} \qquad (3.9)$$

$$\mathrm{B}_-(\xi) = \mathrm{Bi}(\xi) - i\, \mathrm{Ai}(\xi) \ ,$$

$$\kappa^3 = \frac{k_0^2 - k_{//}^2}{L_n}$$

and $C(k_{//})$ is a complex function of $k_{//}$ to be determined by the boundary condition at $x = x_s$. In the deep interior of the plasma, the asymptotic forms of Ai and Bi are applicable and we can write

$$\mathrm{Ai}(\xi) \sim \frac{1}{2\sqrt{\pi}}\,\xi^{-1/4}\exp\left[-\frac{2}{3}\,\xi^{3/2}\right] \qquad \text{for } \xi \to \infty\ ,$$

$$\mathrm{B}_{-}(\xi) \sim \frac{1}{\sqrt{\pi}}\,(-\xi)^{-1/4}\exp\left[-i\left(\frac{2}{3}\,(-\xi)^{3/2}+\frac{\pi}{4}\right)\right] \qquad \text{for } \xi \to -\infty\ . \tag{3.10}$$

The former evanescent mode decays exponentially and the latter travelling mode approaches to a backward wave which transports wave energy in the x-direction.

§§3-1-3. Linear coupling equation

The continuity of the tangential components of the electromagnetic field at the plasma surface $x = x_s$ yields the relations,

$$\begin{cases} \sigma(k_{//}) + \rho(k_{//}) = C(k_{//})\left[P(k_{//}, x_s)\cos k_{\perp}x_s - \dfrac{P'(k_{//}, x_s)}{k_{\perp}}\sin k_{\perp}x_s\right]\ , \\ \sigma(k_{//}) - \rho(k_{//}) = -i\,C(k_{//})\left[\dfrac{P'(k_{//}, x_s)}{k_{\perp}}\cos k_{\perp}x_s + P(k_{//}, x_s)\sin k_{\perp}x_s\right]\ , \end{cases} \tag{3.11}$$

where $P'(k_{//}, x_s) = \mathrm{d}P(k_{//}, x)/\mathrm{d}x\big|_{x=x_s}$. Finally, substituting eqs.(3.11) into eq.(3.3), we obtain the linear coupling equation for α_{np} and β_{np} as

$$\sum_p \sum_n (\delta_{nm}\delta_{pq} + K_{nmpq})\beta_{np} = \sum_p \sum_n (\delta_{nm}\delta_{pq} - K_{nmpq})\alpha_{np}\ , \tag{3.12}$$

where

$$K_{nmpq} = \frac{4\pi\gamma_m}{b\varepsilon_m} \int_{-\infty}^{\infty} dk_{//} \frac{1}{ik_{\perp}} F_{np}(k_{//}) F^{*}_{mq}(k_{//})$$

$$\times \frac{[P'(k_{//}, x_s)/k_{\perp}] \cos k_{\perp} x_s + P(k_{//}, x_s) \sin k_{\perp} x_s}{P(k_{//}, x_s) \cos k_{\perp} x_s - [P'(k_{//}, x_s)/k_{\perp}] \sin k_{\perp} x_s}$$

and $\delta_{ab} = 1$ for $a = b$ and 0 for $a \neq b$. We can calculate from eq. (3.12) the reflection coefficient R defined by

$$R = \left(\sum_p \sum_{n=0}^{n_{pr}} |\beta_{np}|^2 \right) / \left(\sum_p \sum_{n=0}^{n_{pr}} |\alpha_{np}|^2 \right) \tag{3.13}$$

with n_{pr} the largest integer not exceeding $k_0 b/\pi$.

In order to elucidate a qualitative behaviour of the reflection coefficient, we restrict ourselves for the moment only to the fundamental mode of the waveguide array. If a number of waveguides is sufficiently large, the power spectrum emitted by the array has a peak around $k_{//} = \Delta\Phi/b$. In this case the reflection coefficient is approximately expressed in terms of the surface impedance $\overline{Z}_s$ normalized by the impedance in vacuum $Z_0 = (\mu_0/\varepsilon_0)^{1/2}$ as

$$R = \left| \frac{\overline{Z}_s - 1}{\overline{Z}_s + 1} \right|^2 \tag{3.14}$$

and

$$\overline{Z}_s = - \frac{\mu_0}{Z_0} \frac{E_z}{B_y} \bigg|_{x=0} = i \frac{k_0^2 - k_{//}^2}{k_0} \frac{E_z}{\partial E_z/\partial x} \bigg|_{x=0} \tag{3.15}$$

$$= i \frac{k_0^2 - k_{//}^2}{k_0} \frac{P(k_{//}, 0)}{P'(k_{//}, 0)}$$

If there is no vacuum region, i.e. $x_s = 0$, $\bar{Z}_s$ may reduce to the limit of a mild density gradient ($|k_0^2 - k_{//}^2|^{1/3} L_n^{2/3} |\mu_s - 1| \ll 1$) :

$$\bar{Z}_s \rightarrow \begin{cases} -i\, Q_B (1 - N_{//}^2)^{2/3} (k_0 L_n)^{1/3} & \text{for } N_{//}^2 < 1, \\ e^{i\pi/6}\, Q_B (N_{//}^2 - 1)^{2/3} (k_0 L_n)^{1/3} & \text{for } N_{//}^2 > 1, \end{cases} \tag{3.16}$$

and to the high density limit ($|k_0^2 - k_{//}^2|^{1/3} L_n^{2/3} (\mu_s - 1) \gg 1$) :

$$\bar{Z}_s \rightarrow \begin{cases} -i\, (1 - N_{//}^2)^{1/2} (\mu_s - 1)^{-1/2} & \text{for } N_{//}^2 < 1, \\ (N_{//}^2 - 1)^{1/2} (\mu_s - 1)^{-1/2} & \text{for } N_{//}^2 > 1, \end{cases} \tag{3.17}$$

with $Q_B = 3^{-1/3} \Gamma(1/3)/\Gamma(2/3) = 1.3717$.

When $N_{//}^2 < 1$, $\bar{Z}_s$ becomes pure imaginary and therefore R is unity, as is expected from the fact that such a mode cannot propagate into the plasma beyond the cutoff point ($\omega^2 = \omega_{pe}^2$). Even if $N_{//}^2 > 1$, R approaches to unity for $\mu_s = 0$ when L_n is either extremely small or large, because $\bar{Z}_s$ becomes zero or pure imaginary, respectively. Consequently, R is expected to have a minimum when the gradient assumes an optimum value. This may be explained thus: When the gradient gets smaller, the cutoff point is shifted into the interior of the plasma, resulting in an increase of the width of an evanescent region and therefore in an enhancement of the reflection coefficient

On the contrary, when the gradient gets steeper, a matching is hardly obtained due to an abrupt mode-conversion and thus an increase of the reflection coefficient may be expected.

The electric field in front of the waveguide array and in the plasma can be expressed in terms of α_{np} and β_{np} as

$$E(k_{//},0) = \sum_p \sum_n (\alpha_{np} + \beta_{np})\, F_{np}(k_{//}) \tag{3.18}$$

and

$$E(k_{//},x) = P(k_{//},x) \times \sum_p \sum_n \frac{(\alpha_{np} + \beta_{np})\, F_{np}(k_{//})}{P(k_{//},x_s)\cos k_\perp x_s - [P'(k_{//},x_s)/k_\perp]\sin k_\perp x_s} , \tag{3.19}$$

for $x > x_s$. The power density of the LH wave is calculated from the x-component Γ_x of the Poynting vector. If we assume that a quantity X varies in time as $X = X(x,z)e^{-i\omega t} + \text{c.c.}$, Γ_x is given by

$$\mu_0 \Gamma_x = 2\,\mathrm{Re}(\vec{E} \times \vec{B}^*) = -2\,\mathrm{Re}(E_z B_y^*) . \tag{3.20}$$

Remark that, if the time dependence of the form $X = \mathrm{Re}[X(x,z)e^{-i\omega t}]$ is assumed, the factor 2 in eq.(3.20) should be replaced by 1/2. Our definition of $E_z(x,z)$ gives a half of the peak value of the actual E_z. The $k_{//}$-spectrum of the power density $\Gamma_x(k_{//})$, defined such as $\Gamma_x = \int_{-\infty}^{\infty} dk_{//} \Gamma_x(k_{//})$, may be expressed as

$$\Gamma_x(k_{//}) = \frac{4\pi k_0}{\mu_0 c}\,\mathrm{Im}\left\{\frac{E(k_{//},x)E'^*(k_{//},x)}{k_0^2 - k_{//}^2}\right\} . \tag{3.21}$$

It is easy to show that $\Gamma_x(k_{//})$ vanishes whenever $k_{//}^2 < k_0^2$ and that the phase velocity of E_z in the x-direction must be negative for Γ_x to be positive. The latter is consistent with the backward character of the LH wave. Also can we readily demonstrate, by differentiating eq.(3.21) with respect to x and using eq.(3.7), that $\Gamma_x(k_{//})$ does not depend on x. By the use of this conservation property and the asymptotic form of eq.(3.10), we may rewrite eq.(3.21) as

$$\Gamma_x(k_{//}) = \frac{4\pi k_0}{\mu_0 c} \frac{|C(k_{//})|^2}{\pi(k_{//}^2 - k_0^2)^{2/3} L_n^{1/3}} \qquad \text{for} \quad k_{//}^2 > k_0^2 \ . \quad (3.22)$$

§§3-1-4. Numerical results

In this subsection, we summarize numerical results on the linear coupling. Various parameters used here have been chosen to simulate the experiment in JFT-2.[10] They are: the wave frequency $f = 750\,\mathrm{MH_z}$, the cutoff density $n_{co} \sim 7 \times 10^{15}\mathrm{m}^{-3}$, the number of waveguides $N_p = 4$, the width of a waveguide $b = 0.014\,\mathrm{m}$ and the width of a metal wall $d = 0.001\,\mathrm{m}$. In numerical calculations, we have taken 16 modes in a waveguide and have assumed spatial periodicity along the magnetic field with a period 64 times longer than the array so that numerical errors are estimated to be less than about 1%.

Figures 3.2 to 6 show the reflection coefficient R as a function of the phase difference $\Delta\Phi$. The position x_s of the plasma surface is set to zero except in Fig.3.6. The dependence on the

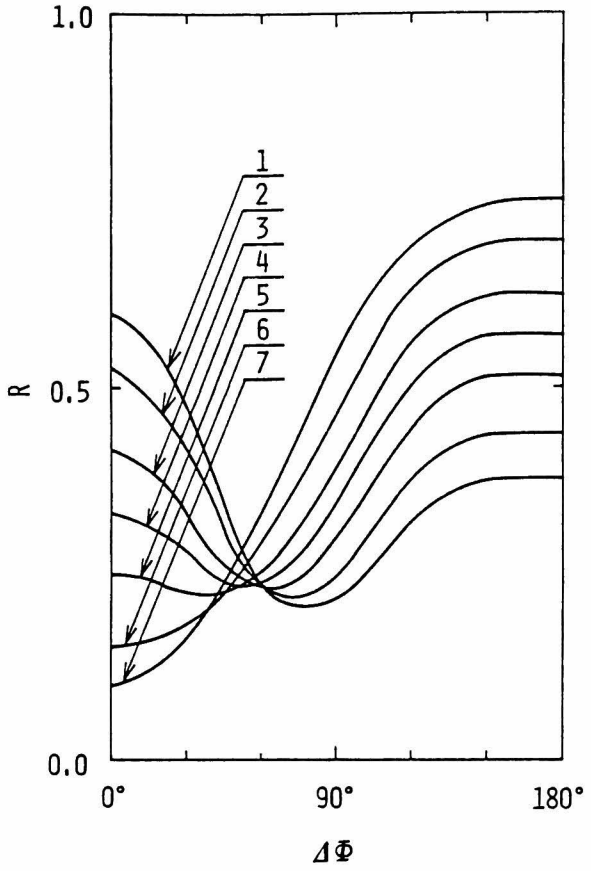

Fig.3.2 Reflection coefficient R versus $\Delta\Phi$ with $\mu_s = 0$: for
(1) $L_n = 1\times10^{-5}$m,
(2) $L_n = 2\times10^{-5}$m,
(3) $L_n = 5\times10^{-5}$m,
(4) $L_n = 1\times10^{-4}$m,
(5) $L_n = 2\times10^{-4}$m,
(6) $L_n = 5\times10^{-4}$m and
(7) $L_n = 1\times10^{-3}$m.

density gradient L_n for $\mu_s = 0$ is illustrated in Fig.3.2. In case where $\Delta\Phi = 0$, R increases with decreasing L_n, since, for a steeper gradient (small L_n), components with small $N_{//}$ are reflected at the cutoff point and come back to the array. On the other hand, they remain between the cutoff point and the metallic wall of the vessel on both sides of the array for a small gradient (large L_n). On the other hand, in case where $\Delta\Phi = \pi$, the evanescent region ($\omega_{pe} < \omega$) becomes larger for a smaller gradient, and thus the reflection coefficient increases.

When $\mu_s \neq 0$, as are seen in Fig.3.3 ($\mu_s = 20$) and Fig.3.4 ($\mu_s = 100$), we can observe that R becomes less sensitive to L_n as μ_s increases. This is a reasonable result, because the inhomogeneity is less important if the total density is large enough. The results

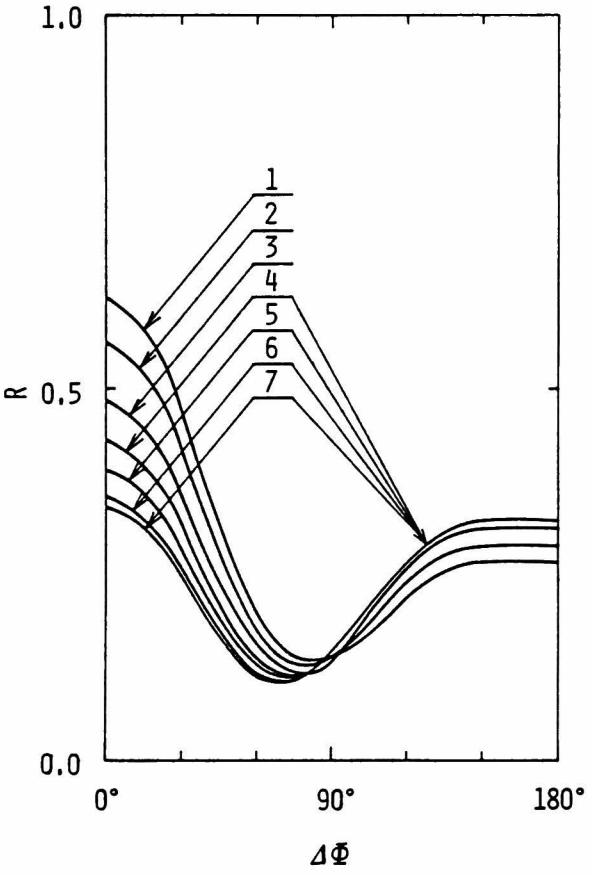

Fig.3.3 Reflection coefficient R versus $\Delta\Phi$ with $\mu_s = 20$, for the same values of L_n as in Fig.3.2.

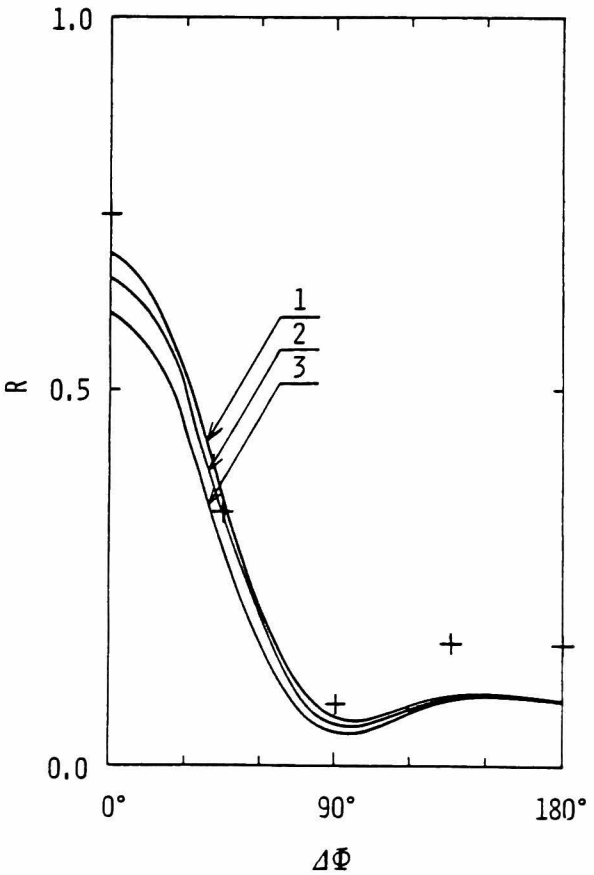

Fig.3.4 Reflection coefficient R versus $\Delta\Phi$ with $\mu_s = 100$: for
(1) $L_n = 1 \times 10^{-5}$ m,
(2) $L_n = 2 \times 10^{-5}$ m and
(3) $L_n = 1 \times 10^{-3}$ m

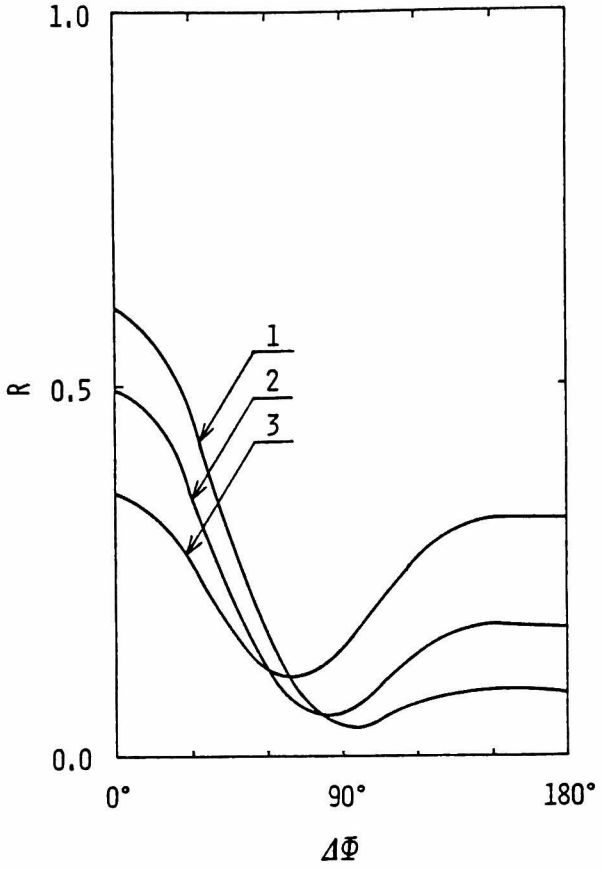

Fig.3.5 Reflection coefficent R versus $\Delta\Phi$ with $L_n = 5\times10^{-4}$ m and $x_s = 0$: for
(1) $\mu_s = 100$,
(2) $\mu_s = 50$ and
(3) $\mu_s = 20$.

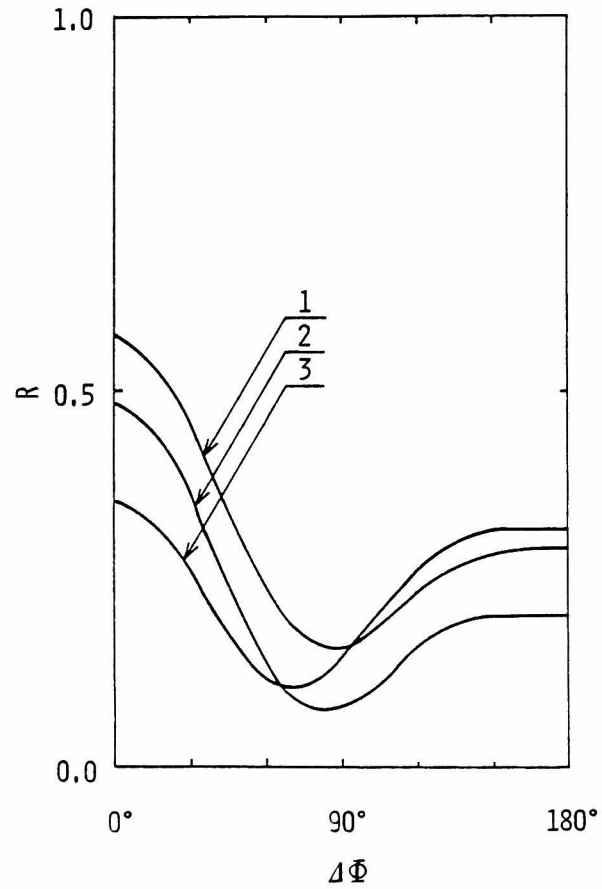

Fig.3.6 Reflection coefficient R versus $\Delta\Phi$ with $L_n = 5\times10^{-4}$ m and $x_s = \mu_s/L_s$ where $L_s = 2\times10^{-6}$m, for the same values of μ_s as in Fig.3.5.

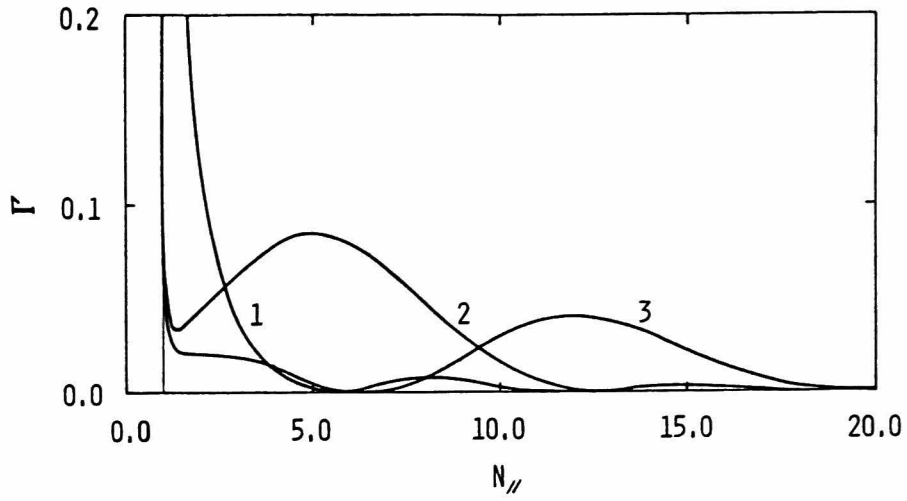

Fig.3.7 Power spectra versus $N_{//}$ with $\mu_s = 20$ and $L_n = 5 \times 10^{-4}$m : for (1) $\Delta\Phi = 0°$, (2) $\Delta\Phi = 90°$ and (3) $\Delta\Phi = 180°$.

of the low-power experiment (3 KW) in JFT-2 are indicated by crosses in Fig.3.4. The surface density $n_s \sim 100 n_{co}$ is consistent with the scrape-off layer density measured by means of an electrostatic probe.[49] It should be noted that this density is rather high compared with the assumption $(\omega_{pe}/\omega)^2 << |\omega_{ce}|/\omega$. Even if this inequality does not holds, we may neglect the coupling to the fast mode, whenever $N_{//}^2 \gg 1$. Therefore the effect of the fast mode on the reflection is expected to be small for large $\Delta\Phi$.

In Fig.3.5 and 6, the influence of a thin vacuum layer in front of the waveguide array is considered. The coupling is found to vary appreciably only for large values of both μ_s and $\Delta\Phi$.

The power spectra for $\mu_s = 20$ and $L_n = 5 \times 10^{-4}$m are shown in Fig.3.7. The peak of the spectrum shift toward large $N_{//}$ with increasing $\Delta\Phi$. Since only the fraction of the power satisfying $N_{//}^2 < N_{//acc}^2$ can penetrate deep into the plasma, larger $\Delta\Phi$ is preferable for the heating of a central part of the plasma column.

§3-2. Density profile modification due to a ponderomotive force[50]

§§3-2-1. Formulation

We start from a set of Maxwell and two-fluid MHD equations. The former is required to deal with the coupling between an electromagnetic field and a low-density plasma, while the latter is relevant to the neglect of the wave-particle interaction. They read as

$$\vec{\nabla} \times \vec{E} = - \frac{\partial \vec{B}}{\partial t} , \tag{3.23.a}$$

$$\vec{\nabla} \times \vec{B} = \frac{1}{c^2} \frac{\partial \vec{E}}{\partial t} + \mu_\sigma \sum_\sigma q_\sigma n_\sigma \vec{v}_\sigma , \tag{3.23.b}$$

$$\frac{\partial n_\sigma}{\partial t} + \vec{\nabla} \cdot (n_\sigma \vec{v}_\sigma) = 0 , \tag{3.23.c}$$

$$\frac{\partial \vec{v}_\sigma}{\partial t} + (\vec{v}_\sigma \cdot \vec{\nabla}) \vec{v}_\sigma = \frac{q_\sigma}{m_\sigma} (\vec{E} + \vec{v}_\sigma \times \vec{B}) - \frac{T_\sigma}{m_\sigma} \vec{\nabla} (\ln n_\sigma) , \tag{3.23.d}$$

where m_σ, q_σ, n_σ, $\vec{v}_\sigma$ and T_σ denote, respectively, the mass, the charge, the number density, the fluid velocity and the temperature of the σ-th species. The unperturbed density profile $n_0(x)$ at $z \to \pm\infty$, where there exists no electromagnetic wave, is assumed to increase in the x-direction. A uniform magnetic field B_0 is applied along the z-axis and the temperature gradient is neglected for the sake of simplicity. The electromagnetic field excited by the external wave source has no y-dependence and is assumed to propagate in the x - z plane.

In order to obtain a nonlinear equation which accounts for

a nonlinear coupling of the LH wave with the low-density, low-temperature plasma near the wave source, the wave amplitude is assumed to be of the order of ε and the temperature to be of the order of ε^2, with ε a small expansion parameter. Thus we assume the ratio of the electromagnetic pressure to the kinetic pressure at the cutoff to be of the order of unity, i.e. $\varepsilon_0 |E|^2 / n_{co} T \sim O(1)$ with n_{co} the cutoff density. Now we look for a solution of the form

$$X(x,z,t) = X^{(0)}(x,z) + \sum_{n=1}^{2} \varepsilon^n \sum_{\ell=-2}^{2} X_\ell^{(n)}(x,z)\, e^{-i\ell\omega t} + \text{c.c.} , \qquad (3.24)$$

for a wave frequency ω.

In order to properly take into account the effect of the ponderomotive force, we have to persue a calculation up to the order of ε^2. Substituting eq.(3.24) into eqs.(3.23), we obtain to the first order in ε the dispersion relation for a cold plasma

$$\overleftrightarrow{D} \cdot \vec{E}_1^{(1)} = \begin{pmatrix} \varepsilon_\perp + \dfrac{c^2}{\omega^2}\dfrac{\partial^2}{\partial z^2} & -ig & -\dfrac{c^2}{\omega^2}\dfrac{\partial^2}{\partial x \partial z} \\ ig & \varepsilon_\perp + \dfrac{c^2}{\omega^2}\left(\dfrac{\partial^2}{\partial x^2} + \dfrac{\partial^2}{\partial z^2}\right) & 0 \\ -\dfrac{c^2}{\omega^2}\dfrac{\partial^2}{\partial x \partial z} & 0 & \varepsilon_\parallel + \dfrac{c^2}{\omega^2}\dfrac{\partial^2}{\partial x^2} \end{pmatrix} \cdot \begin{pmatrix} E_{1x}^{(1)} \\ E_{1y}^{(1)} \\ E_{1z}^{(1)} \end{pmatrix} = \vec{0} , \qquad (3.25)$$

where

$$\varepsilon_\perp = 1 - \sum_\sigma \frac{\omega_{p\sigma}^{(0)2}}{\omega^2 - \omega_{c\sigma}^2} , \qquad \varepsilon_\parallel = 1 - \sum_\sigma \frac{\omega_{p\sigma}^{(0)2}}{\omega^2}$$

and $$g = \sum_{\sigma} \frac{\omega_{p\sigma}^{(0)2}\,\omega_{c\sigma}}{\omega(\omega^2 - \omega_{c\sigma}^2)} \quad .$$

$\omega_{p\sigma}$ and $\omega_{c\sigma}$ are the plasma and the cyclotron frequencies of the σ-th species, respectively. Next, eq.(3.23.d) with $n = 2$ and $\ell = 0$ yields

$$[\vec{v}_{\sigma 1}^{(1)} \cdot \vec{\nabla}]\vec{v}_{\sigma 1}^{(1)*} + [\vec{v}_{\sigma 1}^{(1)*} \cdot \vec{\nabla}]\vec{v}_{\sigma 1}^{(1)} = \frac{q_\sigma}{m_\sigma} [\vec{E}_0^{(2)} + \vec{v}_{\sigma 0}^{(2)} \times \vec{B}_0^{(0)} + \vec{v}_{\sigma 1}^{(1)} \times \vec{B}_1^{(1)*} + \vec{v}_{\sigma 1}^{(1)*} \times \vec{B}_1^{(1)}] - \frac{T_\sigma}{m_\sigma} \vec{\nabla} [\ln n_\sigma^{(0)}] \quad . \tag{3.26}$$

In order to express $n_\sigma^{(0)}$ in terms of $\vec{E}_1^{(1)}$, we first calculate $\vec{B}_1^{(1)}$ and $\vec{v}_{\sigma 1}^{(1)}$ from the $n = |\ell| = 1$ version of eqs.(3.23.a) and (3.23.d) and then bring them into the z-component of eq.(3.26). The result is

$$\frac{q_\sigma}{m_\sigma \omega^2} \frac{\partial |E_{1z}^{(1)}|^2}{\partial z} = E_{0z}^{(2)} + \frac{q_\sigma}{m_\sigma} \left(- \frac{1}{\omega^2 - \omega_{c\sigma}^2} \frac{\partial}{\partial z} [|E_{1x}^{(1)}|^2 + |E_{1y}^{(1)}|^2] \right.$$

$$- \frac{\omega_{c\sigma}}{\omega(\omega^2 - \omega_{c\sigma}^2)} \frac{\partial}{\partial z} [E_{1y}^{(1)} E_{1x}^{(1)*} - E_{1y}^{(1)*} E_{1x}^{(1)}]$$

$$\left. - \frac{1}{\omega^2} \frac{\partial}{\partial z} |E_{1z}^{(1)}|^2 \right) - \frac{T_\sigma}{q_\sigma} \frac{\partial}{\partial z} \ln n_\sigma^{(0)} \quad .$$

Now, eliminating $E_{0z}^{(2)}$ from the electron ($\sigma = e$) and the ion ($\sigma = i$) equations, using the charge neutrality condition $n_e^{(0)} = n_i^{(0)} = n^{(0)}$ and integrating over z with $n^{(0)}(x, z \to \pm\infty) = n_0(x)$, we obtain

$$\ln \frac{n^{(0)}(x,z)}{n_0(x)} = -\frac{e^2}{T} \sum_{\sigma=e,i} \left\{ \frac{1}{m_\sigma(\omega^2 - \omega_{c\sigma}^2)} [|E_{1x}^{(1)}|^2 + |E_{1y}^{(1)}|^2] \right. \tag{3.27}$$
$$\left. - \frac{i\omega_{c\sigma}}{m_\sigma \omega(\omega^2 - \omega_{c\sigma}^2)} [E_{1x}^{(1)} E_{1y}^{(1)*} - E_{1x}^{(1)*} E_{1y}^{(1)}] + \frac{1}{m_\sigma \omega^2} |E_{1z}^{(1)}|^2 \right\},$$

where $T = T_e + T_i$. Eqs.(3.25) and (3.27) give a closed set of non-linear equations to the order of ε. The density profile $n^{(0)}$, given by eq.(3.27), describes well the circumstance that the plasma is pushed away by the z-component of the ponderomotive force. The thermal dispersion, the drift due to the perpendicular components of the ponderomotive force and the effect of higher harmonics are neglected, because they are the second-order effects in ε. In the small amplitude limit, it is easy to show that this expression coincides with the generalized formula for the quasi-static density perturbation, $\delta n = -\varepsilon_0[|E|^2 - c^2|B|^2]/T$, recently derived by Kaufman, Cary and Pereira[51]. Remark, however, that the usual electrostatic approximation, $\delta n = -\varepsilon_0|E|^2/T$, which would be valid in a high-density plasma with $\varepsilon_{//} \gg 1$ and $\varepsilon_{\perp} \ll 1$, may not be justified in our case, unless $N_{//}^2 \gg 1$.

§§3-2-2. Basic equations

The frequency range of our concern lies near the lower hybrid frequency ω_{LH}, i.e., $\omega_{ci} \ll \omega \lesssim (\omega_{ci}|\omega_{ce}|)^{1/2} \ll |\omega_{ce}|$. Though a condition for the heating of a plasma center requires $\omega \sim \omega_{LH,max} \sim \omega_{pi,max}$, we restrict ourselves to consider a low-density region in the scrape-off layer where $(\omega_{pe}/\omega)^2 \ll |\omega_{ce}|/\omega$ holds. The latter condition, rather stringent, enables us to decouple the slow mode and the fast mode. The rigorous condition which allows to neglect the coupling with the fast mode is given by $|(\varepsilon_\perp - N_{//}^2)(\varepsilon_\perp - N_{//}^2 - N_x^2)| \gg g^2 \sim \omega_{pe}^4/\omega^2\omega_{ce}^2$, which thus enables us to neglect the effect of the fast mode for waves with large $N_{//}$. These assumptions kept in mind, the coefficients of various terms in eqs.(3.25) and (3.27) can be simplified and we obtain the dispersion relation

$$\overleftrightarrow{D}\cdot\vec{E}_1^{(1)} = \begin{pmatrix} 1 + \frac{c^2}{\omega^2}\frac{\partial^2}{\partial z^2} & 0 & -\frac{c^2}{\omega^2}\frac{\partial^2}{\partial x \partial z} \\ 0 & 1 + \frac{c^2}{\omega^2}\left(\frac{\partial^2}{\partial x^2} + \frac{\partial^2}{\partial z^2}\right) & 0 \\ -\frac{c^2}{\omega^2}\frac{\partial^2}{\partial x \partial z} & 0 & 1 - \frac{\omega_{pe}^{(0)2}}{\omega^2} + \frac{c^2}{\omega^2}\frac{\partial^2}{\partial x^2} \end{pmatrix} \cdot \begin{pmatrix} E_{1x}^{(1)} \\ E_{1y}^{(1)} \\ E_{1z}^{(1)} \end{pmatrix} = \vec{0}\,, \tag{3.28}$$

together with the expression for $n^{(0)}$ as

$$\ln \frac{n^{(0)}}{n_0} = -\frac{e^2}{T}\left\{\left[\frac{1}{m_i\omega^2} - \frac{1}{m_e\omega_{ce}^2}\right]\left[|E_{1x}^{(1)}|^2 + |E_{1y}^{(1)}|^2\right]\right.$$

$$\left. - \frac{i}{m_e\omega\omega_{ce}}\left[E_{1x}^{(1)}E_{1y}^{(1)*} - E_{1x}^{(1)*}E_{1y}^{(1)}\right] + \frac{1}{m_e\omega^2}|E_{1z}^{(1)}|^2\right\} . \tag{3.29}$$

In order for a launched wave to be coupled efficiently with the slow mode in a plasma, we have to excite an electromagnetic field with no E_y-component. Moreover, it is easily shown that the two terms in eq.(3.29) which do not contain the component E_y are related to each other by

$$\left\{\left[\frac{1}{m_i\omega^2} - \frac{1}{m_e\omega_{ce}^2}\right]|E_{1x}^{(1)}|^2\right\} \Big/ \left\{\frac{1}{m_e\omega^2}|E_{1z}^{(1)}|^2\right\}$$

$$= \frac{m_e}{m_i}\frac{N_{//}^2}{N_{//}^2 - 1}\left[1 - \frac{\omega^2}{\omega_{ci}|\omega_{ce}|}\right]\left[\frac{\omega_{pe}^2}{\omega^2} - 1\right] ,$$

when the dispersion relation for a uniform plasma is used. Thus, unless $N_{//}^2 - 1 \lesssim (m_e/m_i)^{1/2}$, the first term can be neglected compared with the term involving $|E_{1z}^{(1)}|^2$. Therefore, eqs.(3.28) and (3.29) are further simplified to give

$$\frac{\partial^2}{\partial x^2}E_z(x,z) + \left[k_0^2 + \frac{\partial^2}{\partial z^2}\right]\left\{\left[1 - \frac{n^{(0)}(x,z)}{n_{co}}\right]E_z(x,z)\right\} = 0 \tag{3.30}$$

and

$$n^{(0)}(x,z) = n_0(x) \exp\left[-\beta \left|E_z(x,z)\right|^2\right] , \qquad (3.31)$$

where $k_0 = \omega/c$ and $\beta = e^2/m_e\omega^2 T = \varepsilon_0/n_{co}T$, and the scripts of E_z have been suppressed for brevity. These are the basic nonlinear equations for the subsequent analysis. We note that similar equations have previously been derived in slightly different ways without rigorous ordering.[45,52)]

§3-3. Effects of the one-dimensional density modification[50)]

§§3-3-1. One-dimensional model

The simplest approach first treated by Chan and Chiu[45)] is to consider only the fundamental mode of the waveguide array. We assume that the electric field has a sharp spectrum with respect to the parallel wave number $k_{//} \sim \Delta\Phi/b$ where $\Delta\Phi$ is a phase difference between adjacent waveguides and b the parallel width of a waveguide. We also assume that the accessibility condition, $N_{//}^2 > N_{//acc}^2$, be satisfied. The former is well satisfied if the array is much longer than the parallel wave length $2\pi/k_{//}$. These assumptions enable us to write $E_z(x,z) = E_z(x)e^{ik_{//}z}$ and to reduce the basic equations (3.30) and (3.31) to the ordinary differential equation

$$\frac{d^2}{dx^2} E_z(x) + (k_0^2 - k_{//}^2)\left(1 - \frac{n_0(x)}{n_{co}} \exp\left[-\beta|E_z(x)|^2\right]\right)E_z(x) = 0 \quad . \qquad (3.32)$$

We should remark that, although the z-dependence does not appear explicitly in eq.(3.32), $E_z(x)$ is assumed to vanish at $z \to \pm\infty$, in order that the plasma be pushed away in the z-direction, resulting in a density depression. Using the linear density profile given by eq.(3.6) and normalizing various quantities to simplify the notations, we obtain

$$\frac{d^2}{d\xi^2} E + \left[\frac{\xi - \xi_s + \mu_s L}{L} e^{-|E|^2} - 1\right] E = 0 \qquad \text{for } \xi > \xi_s \qquad (3.33)$$

and

$$\frac{d^2}{d\xi^2} E - E = 0 \qquad \text{for} \quad 0 < \xi < \xi_s \ ,$$

where $E = \beta^{1/2} E_z(x), \xi = (k_{\prime\prime}^2 - k_0^2)^{1/2} x$ and $L = (k_{\prime\prime}^2 - k_0^2)^{1/2} L_n$.

Since the basic equation (3.33), including the nonlinear term, is not analytically tractable, we try to solve it by using an approximation model with $\mu_s = 0$. When an electromagnetic field is applied, the plasma is pushed away along the magnetic field, resulting in a change of the density profile. Our first task is then to evaluate an effective shift length in the x- direction defined as a shift length of the cutoff point, which is given by $\Delta\xi = (k_{\prime\prime}^2 - k_0^2)^{1/2} \Delta x$. We assume that this global shift of the plasma does not alter the density gradient. According to this model, the region $\xi_s < \xi < \xi_s + \Delta\xi$ becomes empty and, in place of properly accounting for an exact density profile, we approximate it by a shifted one. Thus neglecting the nonlinear term in eq.(3.33), we can rewrite eq.(3.33) as

$$\frac{d^2}{d\xi^2} E + \frac{\xi - (\xi_s + \Delta\xi) - L}{L} E = 0 \qquad \text{for} \quad \xi > \xi_s + \Delta\xi \ . \qquad (3.34)$$

First of all, we wish to evaluate the shift length. Assuming the electric field in a plasma to be approximated by its asymptotic form (3.10) even at the vicinity of the plasma surface, we may determine a cutoff point on a shifted density profile. By means of eqs.(3.10) and (3.20), the electric field intensity at $\xi = \xi_s + L + \Delta\xi$ is evaluated as

$$|E_p|^2 = L^{1/2} (\Delta\xi)^{-1/2} \Gamma \quad ,$$

where Γ is the normalized power-density, (see eq.(3.20))

$$\Gamma = \frac{1}{2} \mu_0 c (N_{//}^2 - 1)^{1/2} \beta \Gamma_x = \mathrm{Im}\left[E \left(dE^* / d\xi \right) \right] . \tag{3.35}$$

Therefore the density modified by the nonlinear effect may be approximated as

$$\frac{n}{n_{co}} \sim \frac{n_0}{n_{co}} \left[1 - |E_p|^2\right] = \left[\frac{\Delta\xi}{L} + 1\right]\left[1 - \frac{L^{1/2}}{(\Delta\xi)^{1/2}} \Gamma\right] .$$

Using the cutoff condition $n = n_{co}$, we can determine $\Delta\xi$ as a function of the power density Γ, i.e., as a solution to the equation

$$\left[\frac{\Delta\xi}{L} \right]^{3/2} - \Gamma \left[\frac{\Delta\xi}{L} + 1 \right] = 0 . \tag{3.36}$$

The electromagnetic fields in the plasma are now given from eq.(3.34) as

$$\begin{cases} E_p(\xi) = C B_-\left[-(\xi - L - \xi_s - \Delta\xi) L^{-1/3} \right] , \\ B_p(\xi) = - \dfrac{ik_0 C}{c(k_{//}^2 - k_0^2)^{1/2} L^{1/3}} B_-'\left[-(\xi - L - \xi_s - \Delta\xi) L^{-1/3} \right] , \end{cases} \tag{3.37}$$

where $B_- = Bi - i\, Ai$ and the prime denotes the derivative with respect to the argument. On the other hand, since the fields in vacuum are represented by

$$\begin{cases} E_v(\xi) = [\sigma e^{-\xi} + \rho e^{\xi}] , \\ \\ B_v(\xi) = \dfrac{ik_0}{c(k_{//}^2 - k_0^2)^{1/2}} [\sigma e^{-\xi} - \rho e^{\xi}] , \end{cases} \tag{3.38}$$

the continuity conditions of the tangential electromagnetic fields on the plasma surface $(\xi = \xi_s + \Delta\xi)$ yield

$$\begin{cases} \sigma e^{-(\xi_s+\Delta\xi)} + \rho e^{(\xi_s+\Delta\xi)} = C B_-[L^{2/3}] , \\ \\ \sigma e^{-(\xi_s+\Delta\xi)} - \rho e^{(\xi_s+\Delta\xi)} = -C B_-'[L^{2/3}] L^{-1/3} . \end{cases}$$

We can then determine the squared amplitude of the electric field $|E_v(0)|^2$ at the waveguide mouth $(\xi = 0)$ as well as the surface impedance $\overline{Z}_s$ defined by (3.15) as

$$\begin{aligned} |E_v(0)|^2 = |\sigma + \rho|^2 &= \pi \Gamma L^{1/3} \\ &\times |B_-[L^{2/3}] \cosh(\xi_s+\Delta\xi) - B_-'[L^{2/3}] L^{-1/3} \sinh(\xi_s+\Delta\xi)|^2 , \end{aligned} \tag{3.39}$$

and

$$\begin{aligned} \overline{Z}_s &= -i \frac{(k_{//}^2 - k_0^2)^{1/2}}{k_0} \frac{\sigma + \rho}{\sigma - \rho} \\ &= i(N_{//}^2 - 1)^{1/2} \frac{B_- L^{1/3} - B_-' \tanh(\xi_s+\Delta\xi)}{B_-' - B_- L^{1/3} \tanh(\xi_s+\Delta\xi)} . \end{aligned} \tag{3.40}$$

It is readily verified that the expression (3.16) for $N_{//}^2 > 1$ is recovered when $L^{2/3} << 1$, since $B_-(0)/B_-'(0) = Q_B e^{-i\pi/3}$. In case where $\xi_s + \Delta\xi \gg 1$, $\overline{Z}_s$ becomes pure imaginary and therefore the reflection coefficient approaches unity.

The above calculations show that, given a power density Γ, we can determine, as a function of Γ, the shift length $\Delta\xi$, the electric field intensity at the waveguide mouth and the reflection coefficient.

§§3-3-2. Numerical analysis

We now wish to solve numerically the basic equation (3.33) in its normalized form. Since a solution must represent a travelling wave with $\Gamma_x > 0$, as was discussed in §§3-1-3, the asymptotic solution to eq.(3.33) for $\xi \to \infty$, correct up to the order of $\eta^{-1/4}$, reads

$$E \sim \frac{a}{\pi^{1/2}} \eta^{-1/4} \left[1 + \frac{a^2}{4\pi} \eta^{-1/2} + \frac{5a^4}{32\pi^2} \eta^{-1} \right] \times \exp\left[-i\left(\frac{2}{3} \eta^{3/2} - \frac{a^2}{2\pi} \eta - \frac{a^4}{4\pi^2} \eta^{1/2} + \phi \right) \right], \tag{3.41}$$

where α and ϕ are real constants and $\eta = \xi/L^{1/3}$. Numerical analysis has been proceeded as follows: The electric field E and its derivative $dE/d\xi$ at an initial point, chosen to be located far from the plasma surface, is calculated by means of eq.(3.41). After preparative calculations, eq.(3.33) is solved toward the waveguide

mouth $\xi = 0$ with the aid of the Adams-Moulton method. The electric field at the waveguide mouth enables us to compute the reflection coefficient R. In the course of numerical calculations, we have confirmed that the power density Γ is conserved and that absolute values of the electric field decreases monotonically in the positive direction. The latter ensures that there is no reflected wave component which would otherwise originate from a wave source at $\xi \to \infty$.

Figs.3.8 to 11 illustrate numerical results obtained with

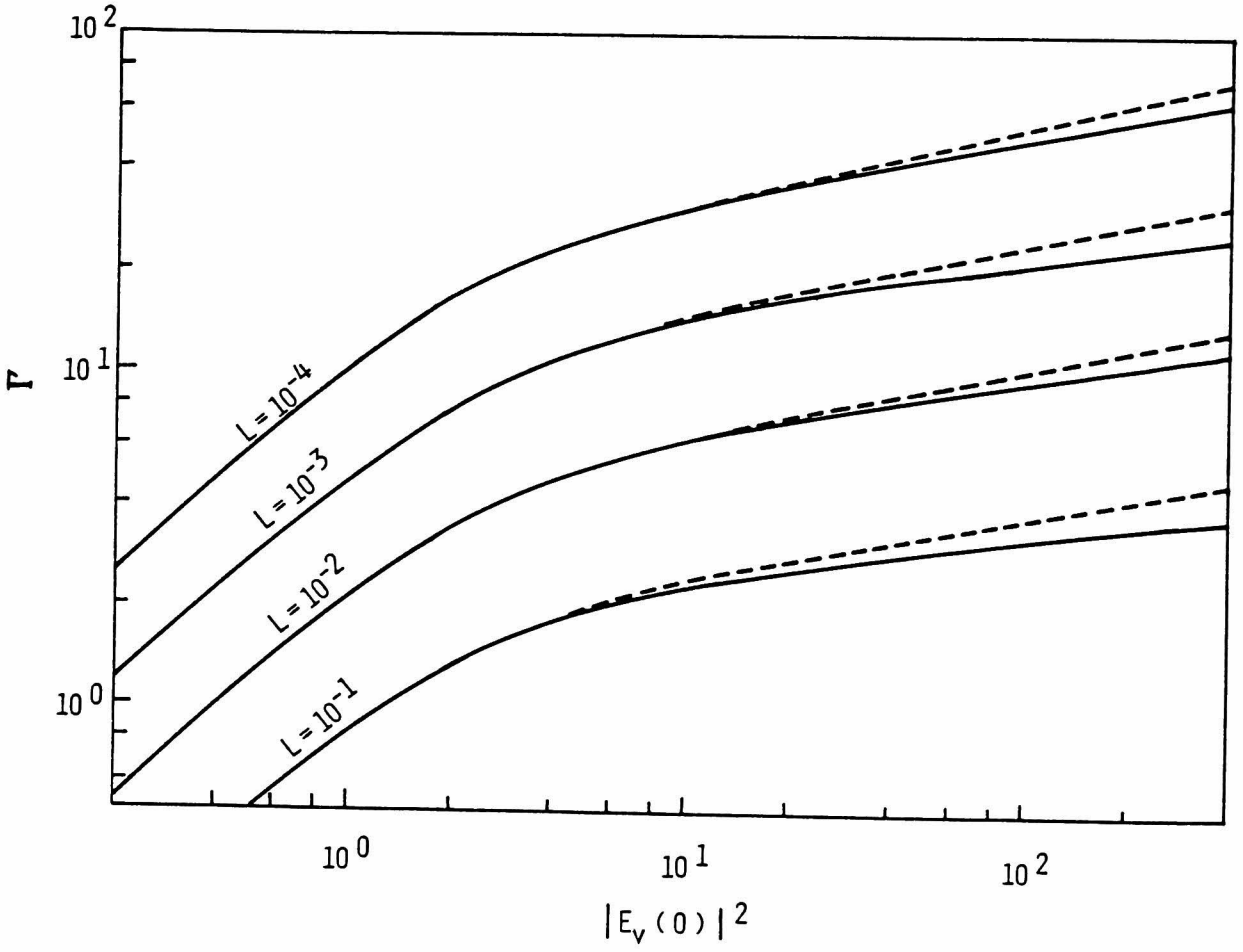

Fig.3.8 Energy flow Γ versus $|E_v(0)|^2$ for numerical results (Solid line) and for analytical results of the approximation model (Broken line).

$\mu_s = 0$. In Fig.3.8, a relationship between the power density Γ and the squared amplitude of the electric field $|E_v(0)|^2$ at the waveguide mouth is plotted for different values of L, the characteristic length of the density gradient. Whenever $|E_v(0)|^2$ is small, Γ increases linearly with it (linear regime) but, as soon as $|E_v(0)|^2 > 1$, Γ tends to saturate, as is shown in Fig.3.9 for $L = 0.01$, due probably to an increase of the width of the cutoff region ($n < n_{co}$). The broken lines in Fig.3.8 denote analytical results of

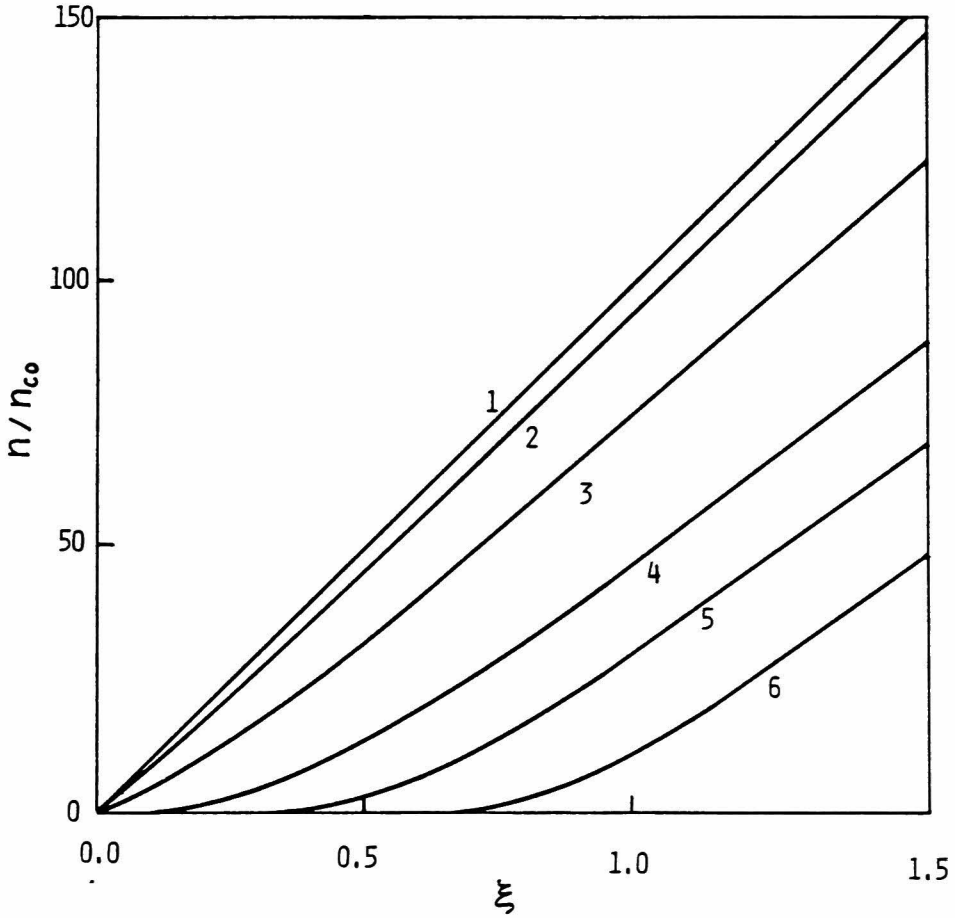

Fig.3.9 Power-density dependence of the density profile with $L = 10^{-2}$ and $\mu_s = 0$: for (1) $\Gamma = 0$, (2) $\Gamma = 0.68$, (3) $\Gamma = 2.56$, (4) $\Gamma = 5.20$, (5) $\Gamma = 6.60$ and (6) $\Gamma = 8.06$.

the approximation model. Although the density profile delicately differs in the analytical and the numerical models, results obtained with the analytical model are accidentally in satisfactory agreement with the numerical results. When $|E_v(0)|^2 >> 1$, a plasma in front of the waveguide mouth is pushed away and thus the electric field decays almost exponentially as in a vacuum up to the shifted cut-off point where the reduced density exceeds the cutoff density. Since the amplitude of the electric field at this point is determined by the cutoff condition and has only a weak dependence on $|E_v(0)|^2$, the power density Γ increases very little with $|E_v(0)|^2$.

In Fig.3.10, the power reflection coefficient R is given as a function of Γ with $N_{//} = 5$ and for different values of L. In a region where Γ is small (linear regime), the steeper the density gradient (i.e. the smaller the values of L), the smaller the reflection coefficient. This implies that the width of the cutoff layer decreases with increasing density gradient. If L is too small, however, a mode conversion may occur abruptly and a matching between the wave source and the plasma bulk can hardly be obtained. With further increasing Γ, the reflection coefficient increases for any value of L. This can be explained as an increase of the width of the cutoff region due to the density concavity in the ξ-direction. In Fig.3.11, we depict the reflection coefficient as a function of $N_{//}$ for different values of $\Gamma' = (N_{//}^2 - 1)^{-1/2}\Gamma$, since Γ' is independent of $N_{//}$. Results suggest that the coupling efficiency becomes optimum with $N_{//} = 2 \sim 3$ for this case (with $k_0 L_n = 10^{-2}$), and consequently the reflection coefficient varies little with increasing Γ.

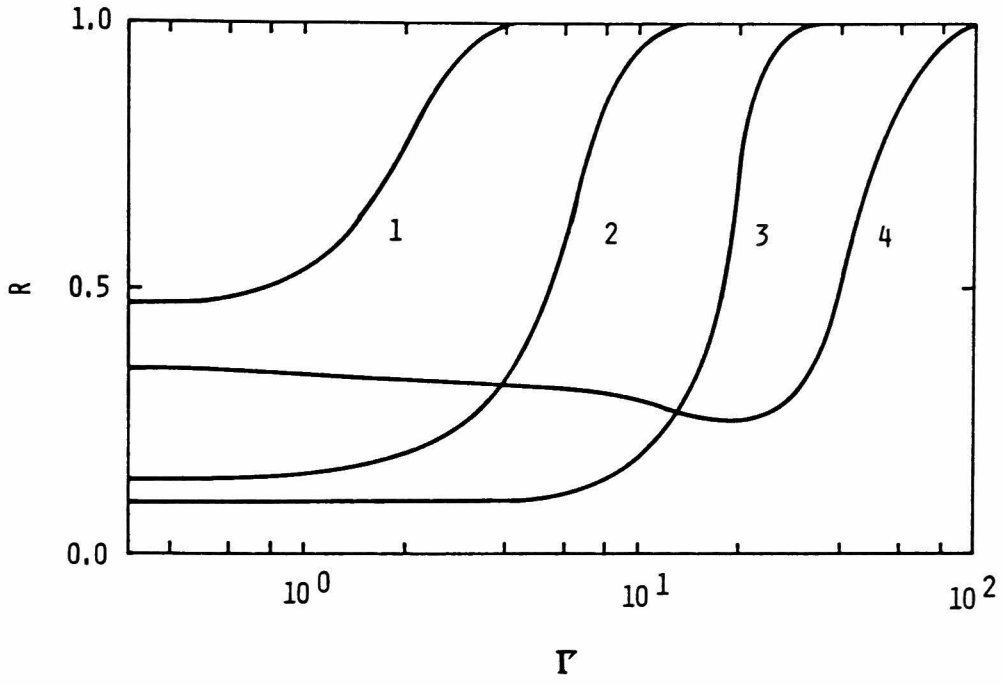

Fig.3.10 Reflection coefficient R versus Γ with $N_{//} = 5$ and $\mu_s = 0$: for (1) $k_0 L_n = 2 \times 10^{-2}$, (2) $k_0 L_n = 2 \times 10^{-3}$ (3) $k_0 L_n = 2 \times 10^{-4}$ and (4) $k_0 L_n = 2 \times 10^{-5}$.

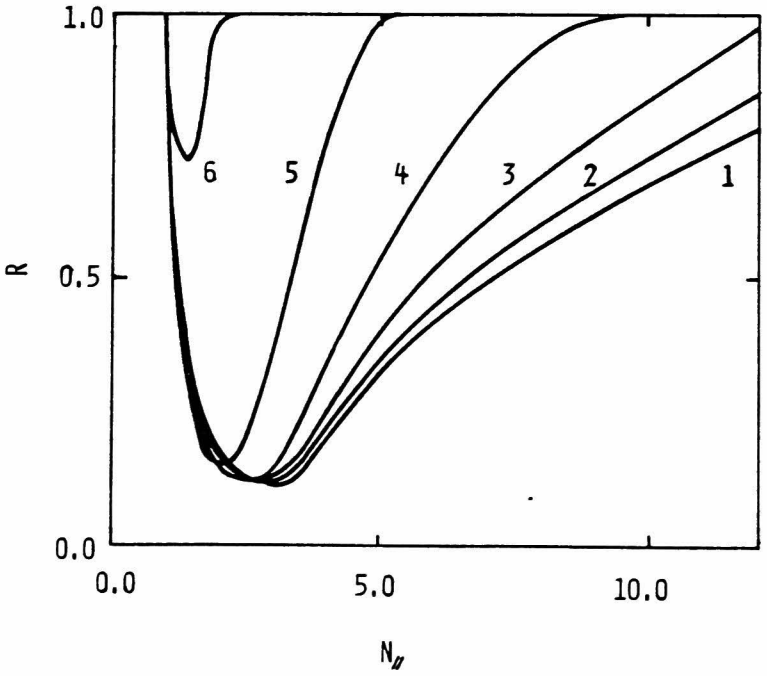

Fig.3.11 Reflection coefficient R versus $N_{//}$ with $k_0 L_n = 10^{-2}$: for

(1) $\Gamma' = (N_{//}^2 - 1)^{-1/2}\Gamma$ $= 0.05$,

(2) $\Gamma' = 0.1$,

(3) $\Gamma' = 0.2$,

(4) $\Gamma' = 0.4$,

(5) $\Gamma' = 1.0$ and

(6) $\Gamma' = 7.0$.

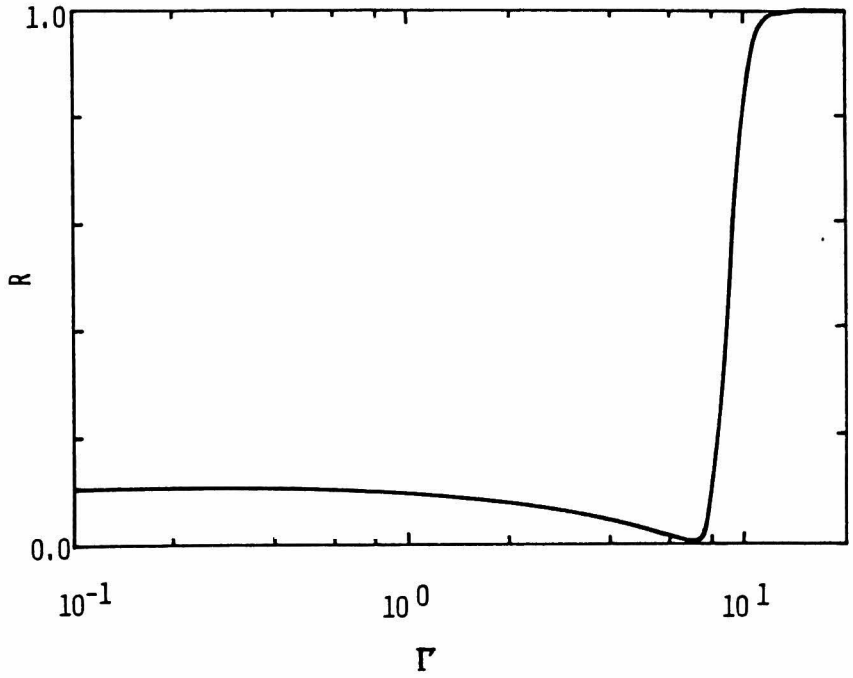

Fig.3.12 Reflection coefficient R versus Γ with $N_{//} = 5$, $k_0 L_n = 3 \times 10^{-3}$ and $\mu_s = 100$.

Several results obtained with $\mu_s = 100$, $x_s = 0$ and $N_{//} = 5$ are shown in Fig.3.12 and 13. The reflection coefficient (see Fig.3.12) decreases until the power density Γ exceeds 7 and then quickly increases up to unity. The modified density profiles depicted in Fig.3.13 indicate that the coupling is optimized when the surface plasma density μ_s is reduced to $20 \sim 30$. This result is consistent with that of the linear analysis given in §§3-1-3, which states, by virtue of eq.(3.17) for the high-density limit, that the normalized surface impedance $\bar{Z}_s$ becomes unity for $\mu_s = N_{//}^2$ and that therefore the reflection coefficient R vanishes. In case where $N_{//} = 5$, an optimum coupling is expected to occur when the surface density decreases to $\mu_s = 25$. For a higher power-density, a cut-off region reappears and then the reflection increases.

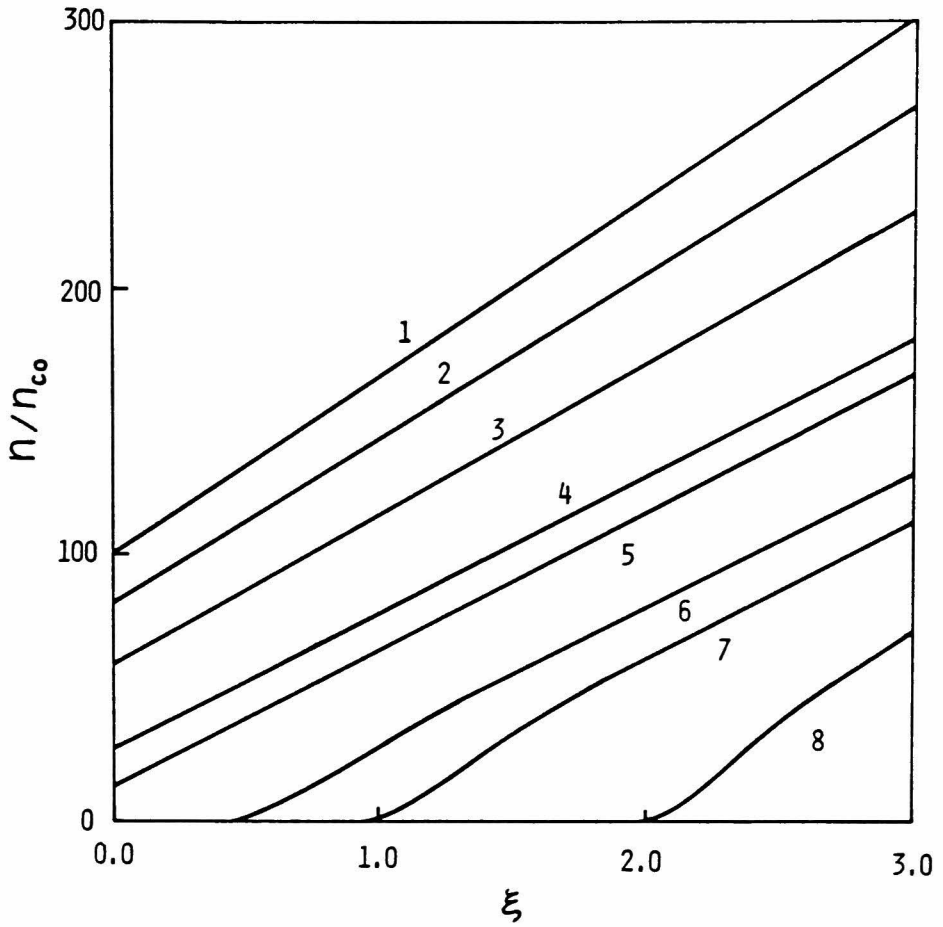

Fig.3.13 Power-density dependence of the density profile with $k_0 L_n = 3 \times 10^{-3}$ and $\mu_s = 100$: for (1) $\Gamma = 0$, (2) $\Gamma = 1.92$, (3) $\Gamma = 4.09$, (4) $\Gamma = 6.72$, (5) $\Gamma = 7.65$, (6) $\Gamma = 9.50$, (7) $\Gamma = 10.4$ and (8) $\Gamma = 12.1$.

The parameters in Figs.3.12 and 13 are chosen to simulate the JFT-2 experiment[10] and the result of the linear analysis in §§3-1-4 For the choice of parameters: $f = 750\text{MHz}$, $\partial n/\partial x = 3.5 \times 10^{19}\text{m}^{-4}$, $T = T_i + T_e = 30\,\text{eV}$ and $N_{//} = 5$ for $\Delta\Phi = \pi/2$, we obtain $n_{co} \sim 7 \times 10^{15}\text{m}^{-3}$, $L_n \sim 2 \times 10^{-4}\text{m}$, $\beta \sim 8.4 \times 10^{-11}\text{m}^2\text{V}^2$ and $\Gamma_x \sim 5 \times 10^{6}\Gamma\ \text{W m}^{-2}$. Therefore, we may conclude that, if the surface density is assumed to be about $7 \times 10^{17}\text{m}^{-3}$, the reflection coefficient decreases until the power

density Γ_x exceeds 3.5 kW/cm^2 and that the maximum transmitted power-density is about 5 kW/cm^2. Since the transmitted power in actual experiments in JFT-2 is less than 2 kW/cm^2, it seems natural that the reflection coefficient tends to decrease with the increasing power density.

§3-4. Discussion

Taking account of a static density depression due to the ponderomotive force, we have derived a nonlinear wave equation which governs the electromagnetic field near a plasma surface. Numerical computations on the one-dimensional model have shown the power-density dependence of the coupling with the LH wave of the phased waveguide array.

When the surface plasma density is lower than the cutoff one, the reflection usually increases with increasing power density, since the cutoff region gets wider under the influence of the ponderomotive force. Since the power-density spectrum described by eq.(3.22) is proportional to $k_{\parallel}^{-4/3}$ for a given fixed amplitude of the electric field which characterizes a magnitude of the density depression, the upper limit of the transmitted power-density tends to decrease for larger values of $k_{\parallel}$ (see Fig.3.11). Therefore the electron heating which requires large values of $k_{\parallel}$ seems to be unfavourable in order to maximize the transmitted power-density.

If the surface plasma density exceeds the optimum value which is $N_{\parallel}^2$ times the cutoff density, the reflection coefficient will be minimized under the action of the ponderomotive force which lowers the surface density to the optimum value. This result may explain the power-density dependence of the reflection coefficient measured in the LH heating experiment on Petula.[9)]

Finally, we shall briefly discuss the effects of the two-dimensional density rippling. Not only an actual waveguide array has a finite width along the static magnetic field, but the

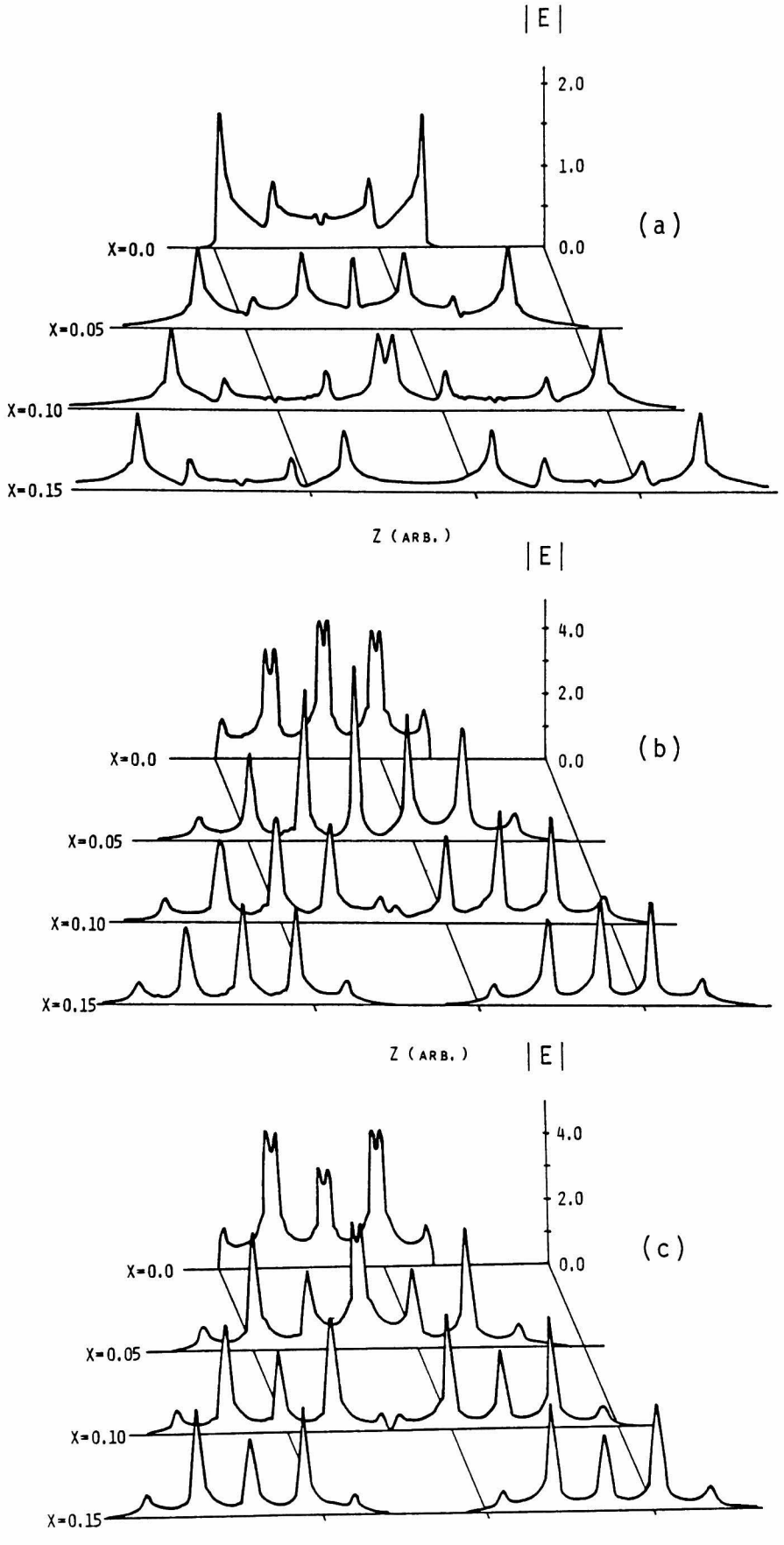

Fig.3.14 Absolute values of the electric field in front of the waveguide array with $L_n = 5 \times 10^{-4}$ m and $\mu_s = 20$: for
(a) $\Delta\Phi = 0°$,
(b) $\Delta\Phi = 90°$ and
(c) $\Delta\Phi = 180°$.

electric field in front of the array has strong peaks around a metal edge of the waveguides. Profiles of the electric field in front of a four-waveguide launcher calculated by linear theory is illustrated in Fig.3.14 for parameters deduced from experimental data on JFT-2.[10] If the density perturbation due to the ponderomotive force has a period $2\pi/k_r$, which is typically a width of the waveguide, the electromagnetic field with parallel wave number $k_{//}$ excites new modes with $k_{//} \pm k_r$, which can propagate beyond the cutoff point even if $k_{//}^2 < k_0^2$. A reduction of the reflection coefficient and/or a modification of the $N_{//}$-spectrum are plausible. The power-density spectrum given by eq.(3.22) suggests, however, that the contribution of large-$N_{//}$ components to the power-density is small because of the factor $k_{//}^{-4/3}$. Also, large-$N_{//}$ components tend to be attenuated in the cutoff region localized around the metal edge. Therefore this problem would require further careful and self-consistent analyses.
In addition to the two-dimensional effects, the wave-particle interaction in this intense localized electric field and parametric phenomena are left open to further studies.

Chapter 4

NONLINEAR PROPAGATION OF LOWER HYBRID WAVES

The problem of the nonlinear propagation of large-amplitude LH waves has received since several years a great deal of attention. In this chapter, we intend to elucidate this problem and especially wish to focus our attention to characteristic behaviour of these LH waves near the linear mode-conversion point.

Before reaching an inner region of a confined plasma, a LH wave has to propagate a long way nearly along the static magnetic field. If a certain nonlinear mechanism could affect the propagation characteristic and/or give rise to a localization of the electric field (filamentation or self-focussing), the linear theory is incapable of predicting the deposition of the wave energy to the medium, since the intense localized electric field can be responsible for a local heating and for a generation of high-energy charged particles. Specifically, if such a filamentation occurs near the plasma surface, not only the absorbed energy is fated to be lost rapidly, but also the unconfined high-energy particles may enhance an impurity influx.

Nonlinear propagation of the LH wave was first treated by Morales and Lee[43] as the problem of the two-dimensional steady-state propagation in a homogeneous plasma. Taking account of the competition between a thermal dispersion and a density depression due to the ponderomotive force, they have shown that the wave field is governed by the complex modified Korteweg-de Vries (CMKdV) equation, which has not yet been solved analytically.[53] In the limit of a rapid phase variation, Newell and Kaup[54] have

reduced the CMKdV equation into the nonlinear Schrödinger (NLS) equation, which is soluble by means of the inverse scattering method[55] and has envelope-soliton solutions. Several authors have tried to extend the theory to an inhomogeneous plasma.[56-58]

Since a group velocity perpendicular to the magnetic field becomes zero at the linear mode-conversion point (see §2-2), it is expected that an electric field has a large amplitude there. Sanuki and Ogino[56] have analysed the case of an inhomogeneous plasma, including the LH resonance point. Their numerical computation suggests that the nonlinear distortion of the wave packet which occurs near the LH resonance point renders the electric field spiky. Their analysis may not, however, describe the linear mode-conversion since a finite-temperature effect is treated only as a perturbation to the wave trajectory derived from the cold-plasma dispersion.

In the first section, we describe a model and derive a basic equation. The nonlinear propagation far from the mode-conversion point is also discussed. In §4-2, linear properties of the wave equation is analysed and the WKB solutions are connected at the conversion point with no recourse to the usual asymptotic solution of the fourth-order differential equation. Incorporating the nonlinear term in the linear equation, it is shown that a nonlinear behaviour of the LH wave packet near the mode-conversion point is governed by the NLS equation involving a linearly increasing potential, which is the same equation as that describing the wave near the plasma cutoff in an inhomogeneous unmagnetized plasma. Numerical results are also presented. The last section is devoted to the discussion of the results.

§4-1. Basic formulation

§§4-1-1. Model and basic equation[59)]

We consider a plasma immersed in a uniform static magnetic field $\vec{B}_0 = B_0\vec{z}$. The unperturbed plasma density n_0 is assumed to increase slowly in the x- direction but the temperature gradient is neglected for the sake of simplicity. So far as a low- β plasma is concerned, the diamagnetic effect due to the density gradient is also neglected. Since the density depression due to the ponderomotive force is a temporally slow process, characterized by a spatial extent of the wave packet along the static magnetic field and the sound velocity, we deal with a steady-state two-dimensional problem.

Three-dimensional effects, which may become important whenever there exist such nonzero-k_y modes as parametrically excited waves, will be referred to in §§ 4-1-2.

As is illustrated in Fig.4.1, an incoming wave packet is assumed to be localized along the z-axis and its k_z-spectrum to be also localized around a certain value $k_{//}$ which is determined by an external wave source. This model simulates an actual heating experiment with a finite-length slow wave structure such as a waveguide array. The parallel wave number $k_{//}$ is assumed to be large enough to well satisfy the accessibility condition (2.12), $N_{//}^2 > N_{//acc}^2$, and thus the electrostatic approximation is applicable (see §2-1). Remark, however, that it is not too large neither to neglect the wave-particle interaction. With these considerations in mind, we start from the two-fluid MHD equations for electrons and ions and

the Poisson equation,

$$\frac{\partial n_\sigma}{\partial t} + \vec{\nabla}\cdot(n_\sigma \vec{v}_\sigma) = 0 \ ,$$

$$\frac{\partial \vec{v}_\sigma}{\partial t} + (\vec{v}_\sigma \cdot \vec{\nabla})\vec{v}_\sigma = \frac{q_\sigma}{m_\sigma}(-\vec{\nabla}\phi - \vec{v}_\sigma \times \vec{B}_0) - \frac{T_\sigma}{n_\sigma m_\sigma}\vec{\nabla} n_\sigma \ , \qquad (4.1)$$

$$-\nabla^2\phi = \frac{1}{\varepsilon_0}\sum_\sigma q_\sigma n_\sigma \ .$$

In these equations, N_σ, $\vec{v}_\sigma$ and T_σ are the density, the fluid velocity and the temperature of the species σ, respectively, and ϕ is the electrostatic potential.

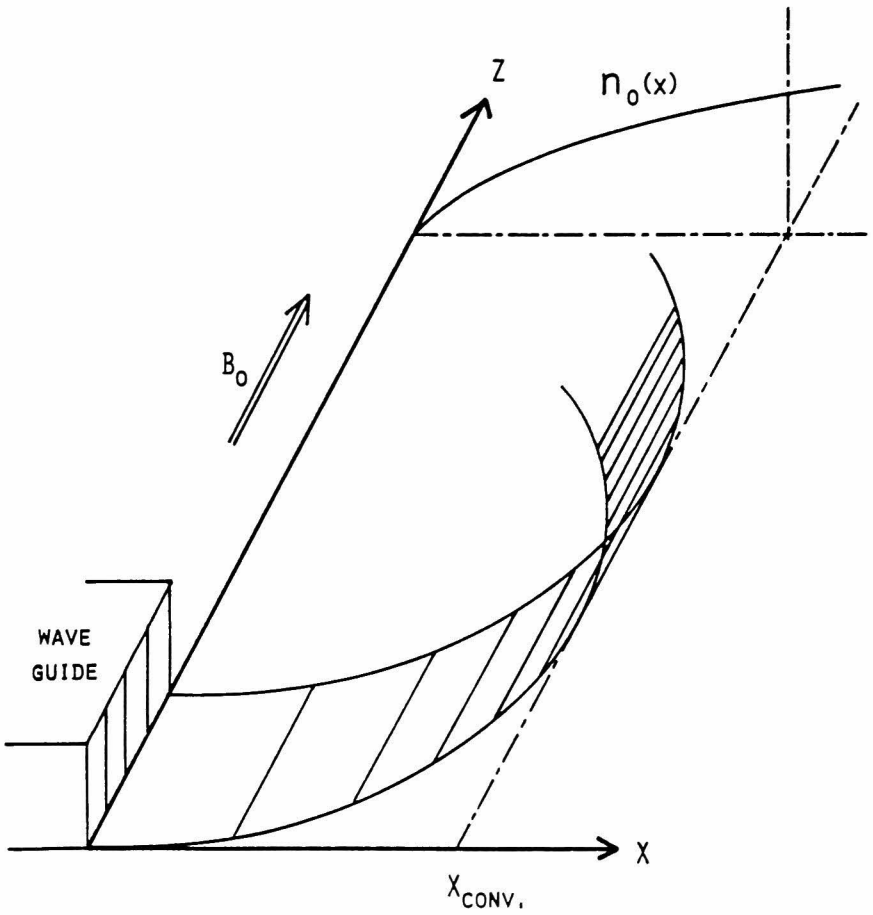

Fig.4.1 Geometry of the model.

In order to obtain a nonlinear equation which accounts for both the thermal dispersion and the density depression, the thermal effect as well as the wave amplitude are assumed to be of the order of ε with ε a small expansion parameter. To be precise, the ratio of an excursion length to the wave length is assumed to be of the order of ε and the quantity $q\phi/T$ is regarded as of the order of unity. In contrast to the ordering in §§3-2-1, this ordering enables us to include the lowest-order thermal dispersion effect. Now we look for a solution of the form

$$X(x,z) = X^{(0)}(x,z) + \sum_{n=1}^{2} \varepsilon^n \sum_{\ell=-2}^{2} X_\ell^{(n)}(x,z) \exp(-i\ell\omega t) \ . \tag{4.2}$$

Substituting eq.(4.2) into eqs.(4.1), we obtain to the second order in ε the electrostatic dispersion relation

$$\begin{aligned} \nabla^2\phi_1^{(1)} - \sum_\sigma \Bigg[\vec{\nabla}\cdot\frac{in^{(0)}q_\sigma}{\varepsilon_0\omega} \overleftrightarrow{\mu}_\sigma\cdot\vec{\nabla}\phi_1^{(1)} + \vec{\nabla}\cdot\frac{in_0^{(1)}q_\sigma}{\varepsilon_0\omega} \overleftrightarrow{\mu}_\sigma\cdot\vec{\nabla}\phi_1^{(1)} \\ + \vec{\nabla}\cdot\frac{in^{(0)}q_\sigma}{\varepsilon_0\omega}\frac{T_\sigma}{q_\sigma} \overleftrightarrow{\mu}_\sigma\cdot\vec{\nabla}\frac{1}{i\omega n^{(0)}} \vec{\nabla}\cdot n^{(0)} \overleftrightarrow{\mu}_\sigma\cdot\vec{\nabla}\phi_1^{(1)} \Bigg] = 0 \end{aligned} \tag{4.3}$$

and the density perturbation

$$n_0^{(1)} = n_{e0}^{(1)} = n_{i0}^{(1)} = -\frac{\varepsilon_0}{T}\sum_\sigma \left(\frac{\omega^2}{\omega^2 - \omega_{c\sigma}^2} \left|\frac{\partial\phi_1^{(1)}}{\partial x}\right|^2 + \left|\frac{\partial\phi_1^{(1)}}{\partial z}\right|^2 \right) , \tag{4.4}$$

where $\overleftrightarrow{\mu}_\sigma$ is the mobility tensor for the cold plasma, defined by

$$\overleftrightarrow{\mu}_\sigma = -\frac{iq_\sigma}{m_\sigma\omega}\begin{pmatrix} \dfrac{\omega^2}{\omega^2-\omega_{c\sigma}^2} & \dfrac{i\omega\omega_{c\sigma}}{\omega^2-\omega_{c\sigma}^2} & 0 \\ \dfrac{-i\omega\omega_{c\sigma}}{\omega^2-\omega_{c\sigma}^2} & \dfrac{\omega^2}{\omega^2-\omega_{c\sigma}^2} & 0 \\ 0 & 0 & 1 \end{pmatrix}$$

and $T = T_e + T_i$. The third term in eq.(4.3) comes from the density depression due to the ponderomotive force and the fourth term from the thermal dispersion through the kinetic pressure. Combining eqs. (4.3) and (4.4), we derive the basic equation accurate up to the order of ε^2, which is equivalent to eq.(9) of Ref.56,

$$\begin{aligned} &\frac{\partial}{\partial x}\left[\varepsilon_\perp\frac{\partial\phi}{\partial x}\right] + \varepsilon_\parallel\frac{\partial^2\phi}{\partial z^2} + \frac{\partial^2}{\partial x^2}\left[\alpha\frac{\partial^2\phi}{\partial x^2}\right] + \frac{\partial}{\partial x}\left[2\beta\frac{\partial^3\phi}{\partial x\partial z^2}\right] + \gamma\frac{\partial^4\phi}{\partial z^4} + \frac{\partial}{\partial x}\left[\alpha g\frac{\partial\phi}{\partial x}\right] \\ &\quad + \frac{\partial}{\partial x}\left\{\frac{\varepsilon_0}{n_0 T}(1-\varepsilon_\perp)\left[(1-\varepsilon_\perp)\left|\frac{\partial\phi}{\partial x}\right|^2 + (1-\varepsilon_\parallel)\left|\frac{\partial\phi}{\partial z}\right|^2\right]\frac{\partial\phi}{\partial x}\right\} \qquad (4.5) \\ &\quad + \frac{\partial}{\partial z}\left\{\frac{\varepsilon_0}{n_0 T}(1-\varepsilon_\parallel)\left[(1-\varepsilon_\perp)\left|\frac{\partial\phi}{\partial x}\right|^2 + (1-\varepsilon_\parallel)\left|\frac{\partial\phi}{\partial z}\right|^2\right]\frac{\partial\phi}{\partial z}\right\} = 0 , \end{aligned}$$

where

$$\varepsilon_\perp = 1 - \sum_\sigma \frac{\omega_{p\sigma}^2}{\omega^2-\omega_{c\sigma}^2} , \quad \varepsilon_\parallel = 1 - \sum_\sigma \frac{\omega_{p\sigma}^2}{\omega^2} , \quad g = \frac{d}{dx}\left[\frac{1}{n_0}\frac{dn_0}{dx}\right] ,$$

$$\alpha = \sum_\sigma \frac{T_\sigma}{m_\sigma\omega^2}\frac{\omega^2\omega_{p\sigma}^2}{(\omega^2-\omega_{c\sigma}^2)^2} , \quad \beta = \sum_\sigma \frac{T_\sigma}{m_\sigma\omega^2}\frac{\omega_{p\sigma}^2}{\omega^2-\omega_{c\sigma}^2} , \quad \gamma = \sum_\sigma \frac{T_\sigma}{m_\sigma\omega^2}\frac{\omega_{p\sigma}^2}{\omega^2} ,$$

with $\omega_{p\sigma}$ and $\omega_{c\sigma}$ denoting the plasma frequency and the cyclotron frequency, respectively.

§§4-1-2. Nonlinear propagation far from the linear mode-conversion point

We wish to derive first the CMKdV equation for the LH wave far from the mode-conversion point, in parallel with Ref.56. To this end, we introduce the stretched coordinates ξ and η defined by

$$\begin{cases} \xi = \delta^{1/2} \left[\int^{x} q(x')\, dx' - z \right] , \\ \eta = \delta^{3/2} z , \end{cases} \tag{4.6}$$

and expand $\phi(\xi,\eta)$ as $\phi = \phi^{(0)} + \delta\phi^{(1)}$. The quantity $q(x)$[†] designates an angle between the group velocity and the static magnetic field in the x - z plane, which will be determined later. Within the WKB approximation, that is, when the inequalities

$$\left|\frac{\partial}{\partial\xi} \ln \phi\right| >> \left|\frac{\partial}{\partial\xi} \ln \varepsilon_{\perp}\right| \quad \text{and} \quad \left|\frac{\partial}{\partial\xi} \ln q\right| \sim O(\delta)$$

hold, we obtain to the lowest order in δ

$$\left[q^2(\xi)\, \varepsilon_{\perp}(\xi) + \varepsilon_{\parallel}(\xi) \right] \frac{\partial^2 \phi^{(0)}}{\partial \xi^2} = 0 . \tag{4.7}$$

Since $\partial^2\phi^{(0)}/\partial\xi^2 \neq 0$, $q(\xi)$ must satisfy the relation

$$q^2(\xi) = - \frac{\varepsilon_{\parallel}(\xi)}{\varepsilon_{\perp}(\xi)} , \tag{4.8}$$

which characterizes the propagation cone for the LH wave in an inhomogeneous plasma. Introducing now a function $\psi(\xi,\eta) = (\partial/\partial\xi)\phi^{(0)}(\xi,\eta)$, the second-order equation with respect to δ takes the form

[†] More precisely, $\arctan[q(x)]$.

$$\frac{\partial \psi}{\partial \eta} + A \frac{\partial}{\partial \xi} (|\psi|^2 \psi) + B \frac{\partial^3 \psi}{\partial \xi^3} + C \psi = 0 \quad , \tag{4.9}$$

where

$$A(\xi) = \frac{\varepsilon_0}{n_0 T} \frac{(q^2+1)^2}{-2\varepsilon_{//}} > 0, \qquad B(\xi) = \frac{\alpha q^4 + 2\beta q^2 + \gamma}{-2\varepsilon_{//}} > 0$$

and

$$C(\xi) = \frac{q^2}{-2\varepsilon_{//}} \frac{\partial \varepsilon_{\perp}}{\partial \xi}$$

In a homogeneous plasma, eq.(4.9) is reduced to the CMKdV equation, since A and B are non-zero constants and C vanishes. Morales and Lee have treated ψ as a real quantity in their pioneering paper[43] and derived the modified KdV equation, which has been shown to have exact N-soliton solutions.[60,61] If ψ is real, however, the solution has been proved to be a stationary wave and thus no energy flow takes place, which is not applicable to the present discussion on the propagation of the externally excited wave. Karney *et al*[53] have studied the properties of the CMKdV equation and, by means of numerical analysis, have found two types of solitary waves, the one with a constant phase and the other with an envelope pulse. These two pulses are not identified, however, as solitons.

The limit of a rapid phase variation of the CMKdV equation has been treated by Newell and Kaup.[54] Introducing new variables, $\zeta = \xi + 3\kappa^2 \eta$, $\tau = 6\kappa\eta/B$ and $\psi(\xi,\eta) = (6/AB)^{1/2} u(\zeta,\tau) \exp[-i(\kappa\xi + \kappa^3\eta/B)]$,

they have obtained

$$i\frac{\partial u}{\partial t} + \frac{1}{2}\frac{\partial^2 u}{\partial \zeta^2} + |u|^2 u + \frac{i}{6\kappa}\frac{\partial^3 u}{\partial \zeta^3} + \frac{i}{\kappa}\frac{\partial}{\partial \zeta}(|u|^2 u) = 0 \ .$$

In the limit $|\partial \ln u/\partial\zeta| << \kappa$, this equation reduces to the NLS equation

$$i\frac{\partial u}{\partial t} + \frac{1}{2}\frac{\partial^2 u}{\partial \zeta^2} + |u|^2 u = 0 \ , \qquad (4.10)$$

which, like the modified KdV equation, is soluble by the inverse scattering method and has envelope solitons.

In an inhomogeneous plasma, an additional term $iCu/6\kappa$ has to be included in eq.(4.10). This case has recently been investigated by Leclert, Karney, Bers and Kaup,[58] who have concluded that the inhomogeneity suppresses the occurrence of solitons for such parameters (power density, plasma density and temperature gradient) of the LH heating as will be envisaged for present and future tokamak plasmas. The original equation (4.9) is, however, valid only far from the mode-conversion point, because the stretching (4.6) is implicitly based on the assumption that

$$[\ \alpha q^4 + 2\beta q^2 + \gamma\ ]\frac{\partial^4 \phi(0)}{\partial \xi^4} << \varepsilon_{\prime\prime}\frac{\partial^2 \phi(0)}{\partial \xi^2} \ ,$$

which is not satisfied near the LH resonance point, where q diverges. The propagation near the LH resonance point or, more precisely, the mode-conversion point will be discussed at length in the next section.

Three dimensional effects on the nonlinear propagation of the LH waves have been studied by several authors.[57,62,63] They have shown that the two-dimensional soliton solution to the NLS equation is linearly unstable for the transverse envelope modulation ($\partial/\partial y \neq 0$), though the e-folding growth distance is estimated to be rather long compared with a plasma size for a reasonable wave-energy density $\varepsilon_0 |E|^2 << n_0 T$. Another three-dimensional effect is relevant to the coupling due to the $\vec{E} \times \vec{B}$ drift motion of electrons. If there exists such a nonzero-k_y mode as a parametrically excited wave, the daughter wave grows through this parametric coupling at the expense of a pump wave. The depletion of the pump wave can be in fact quite large and the self-modulation discussed above can be completely masked, if the daughter wave saturates with an amplitude comparable with that of the pump wave.[63] However, the saturation level of the parametric decay is not yet well known, even in a homogeneous plasma. As for the threshold of parametric phenomena,[18] it is rather high for the LH wave with a finite pump width in an inhomogeneous plasma, compared with the homogeneous case. Therefore the three-dimensional effects will not be considered in the subsequent sections because of its complexity, especially near the linear mode-conversion point where the effect of the inhomogeneity becomes strong.

§4-2. Nonlinear behaviour near the linear mode-conversion point[59)]

§§4-2-1. Linear Analysis

In this subsection, we shall study, by means of the WKB approximation, the linear behaviour of the LH wave near the conversion point, by using the linear version of eq.(4.5), in which the last two nonlinear terms are deleted. The linear local dispersion relation derived from eq.(4.5) is expressed as

$$k_{\perp}^4 - \frac{1}{\alpha}[\,\varepsilon_{\perp} - 2\beta k_{\parallel}^2\,]\,k_{\perp}^2 + \frac{1}{\alpha}[\,-\varepsilon_{\parallel} + \gamma k_{\parallel}^2\,]\,k_{\parallel}^2 = 0 \ , \tag{4.11}$$

which has four real solutions $\pm k_1$ and $\pm k_2$ on the lower-density side of the conversion point (Fig.4.2). When two wave numbers k_1 and k_2 are combined as

$$k_{\pm} = \frac{1}{2}[\,k_2 \pm k_1\,] \quad > 0 \ , \tag{4.12}$$

it is shown that k_- vanishes at the conversion point. Furthermore, calculation of the group velocity shows that the branches $-k_+ + k_-$ and $-k_+ - k_-$ correspond to the incoming LH mode and the outgoing ion plasma mode, respectively. Other two modes are irrelevant to externally excited LH waves.

The phase of the potential ϕ rapidly oscillates near the conversion point because of the condition $k_+ >> k_-$. As for k_z, it is localized around $k_{\parallel}$, as was assumed in §§4-1-1. Therefore we can define a new ordering parameter δ and a slowly varying amplitude ψ as

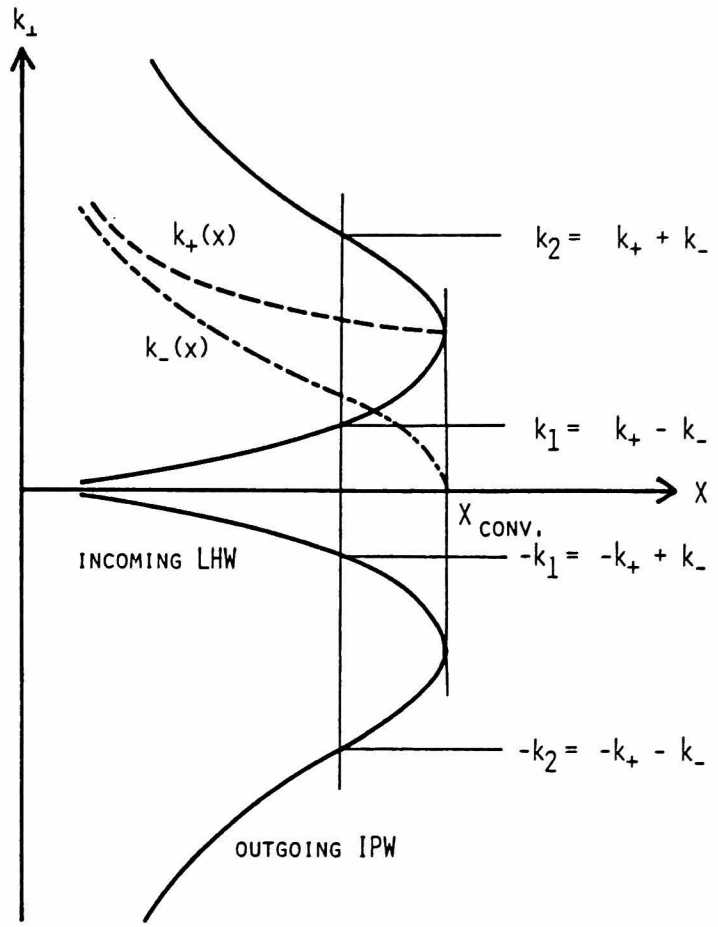

Fig.4.2 Behaviour of local wave numbers perpendicular to the magnetic field as a function of x.

$$\phi(x,z) = \psi(\delta x, \delta^2 z) \exp\left[-i \int^{x} k_{+}(x')\, dx' + i k_{\parallel} z \right] . \qquad (4.13)$$

Since we consider a region near the conversion point where $k_{-} \lesssim \delta k_{+}$ holds, we obtain, upon substituting eq.(4.13) into eq. (4.5), the lowest-order equation in δ as

$$i \frac{k_{\perp}^2}{2k_{\parallel}} \left[1 + \frac{2\beta k_{\parallel}^2}{\alpha k_{+}^2} + \frac{\gamma k_{\parallel}^4}{\alpha k_{+}^4} \right] \frac{\partial \psi}{\partial z} + \frac{\partial^2 \psi}{\partial x^2} + k_{-}^2 \psi = 0 . \qquad (4.14)$$

In this equation and in the sequel, x and z should obviously be interpreted as stretched asymptotic variables as are defined by eq.(4.13). We note that terms proportional to the density gradient are neglected in eq.(4.14) because of the weak inhomogeneity, that is, $(k_{\pm}L_n)^{-1}$ is assumed to be at most of the order of δ^2, where $L_n^{-1} = \mathrm{d}\ \ln n_0/\mathrm{d}x$.

In the remaining part of this subsection, we wish to determine two coefficients which appear in a WKB solution of the linear version of eq.(4.5), which is briefly discussed in Appendix A in the plane-wave limit $\partial\psi/\partial z = 0$. This WKB solution, valid far from the conversion point and generally expressed as a linear combination of two independent WKB solutions representing, respectively, the incoming and the reflected (outgoing) waves, has to be connected with an asymptotic solution of eq.(4.14), valid near the conversion point where $\mathrm{d}k_{-}/\mathrm{d}x$ diverges. The latter can be exactly obtained if we choose the conversion point as the origin of the x-axis and assume the small density gradient,

$$k_{-}^2 \simeq -\frac{x}{4\,\alpha\,L_n} . \tag{4.15}$$

In the plane-wave limit, a solution of eq.(4.14), which satisfies the boundary condition $\psi \to 0$ as $x \to \infty$, can thus be expressed in terms of the Airy function as

$$\psi(x) = C\ \mathrm{Ai}(x / x_L) , \tag{4.16}$$

where $x_L = (4\alpha L_n)^{1/3}$ and the constant C will be determined below by connecting it, in an asymptotic region, with a solution pertinent to the incoming wave. The result is

$$\psi(x) = \left(\frac{\Gamma}{2\varepsilon_0\omega}\right)^{1/2} \left(\frac{1}{4\alpha k_+ k_-}\right)^{1/2} \tag{4.17}$$

$$\times \left[\frac{\exp\left[\, i\int^x k_-(x')\,dx'\right]}{(k_+ - k_-)^{1/2}}\, e^{i\pi/4} + \frac{\exp\left[\, -i\int^x k_-(x')\,dx'\right]}{(k_+ + k_-)^{1/2}}\, e^{-i\pi/4}\right]$$

where Γ denotes the incoming power-density (W/m^2) and $C = [\pi x_L \Gamma/(2\varepsilon_0\omega)]^{1/2} \cdot [(\alpha k_+^2)_{x=0}]^{-1/2}$. This is nothing but the asymptotic solution of the fourth-order differential equation,[23,27,30] which usually needs a lengthy calculation. The simple treatment given above applies also to such other linear mode conversion as between the upper-hybrid mode and the Bernstein mode, where a converted wave is reflected at the conversion point.

§§4-2-2. Model Equation

In order to investigate the nonlinear effect, we substitute eq.(4.13) into the basic equation (4.5). If we assume $q\phi/T$ to be of the order of δ, the lowest-order equation becomes

$$i\frac{k_+^2}{2k_{//}}\, d\, \frac{\partial\psi}{\partial z} + \frac{\partial^2\psi}{\partial x^2} + k_-^2\psi + \frac{\varepsilon_0}{n_0 T}\frac{k_+^2}{4\alpha}\left[\, 1 + k_+^2\alpha d\,\right]^2 |\psi|^2\psi = 0\ , \tag{4.18}$$

where $d = 1 + 2\beta k_{//}^2/\alpha k_+^2 + \gamma k_{//}^4/\alpha k_+^2$. Near the conversion point ($x = 0$) where we may use eq.(4.5) with n_0 evaluated at $x = 0$, eq.(4.18) is simplified and expressed in a normalized form as

$$i\frac{\partial\psi}{\partial z} + \frac{1}{2}\frac{\partial^2\psi}{\partial x^2} - x\psi + |\psi|^2\psi = 0 \ , \tag{4.19}$$

where x, z and ψ are normalized, respectively, by x_n, z_n and ψ_n which are defined by

$$x_n = 2\rho_i\left(rs^2\frac{m_e}{m_i}\frac{L_n}{\rho_i}\right)^{1/3}, \quad z_n = \frac{1}{4s}\frac{m_i}{m_e}\frac{x_n^2}{\rho_i} \quad \text{and} \quad \frac{\varepsilon_0 k_{+n}^2\psi_n^2}{n_0 T} = \frac{x_n}{L_n} \ ,$$

where

$$k_{+n}^2 = \frac{m_i}{m_e}\frac{k_{\prime\prime}}{\rho_i s} \ , \qquad r = \left.\frac{\omega_{pi}^2}{\omega^2}\right|_{x=0} = \left(1 + 2k_{\prime\prime}\rho_i s - \frac{\omega^2}{\omega_{ci}|\omega_{ce}|}\right)^{-1} \ ,$$

$$s^2 = \frac{\omega_{ci}|\omega_{ce}|}{\omega^2} + \frac{T_e}{T_i}\frac{\omega^2}{\omega_{ci}|\omega_{ce}|} \qquad \text{and} \qquad \rho_i^2 = \frac{T_i}{m_i\omega_{ci}^2} \ .$$

In the above, the approximation $d \simeq 1$ is used, which is valid for typical experimental conditions, i.e., whenever $k_{\prime\prime}\rho_i << 1$. The NLS equation with a linearly increasing potential, eq.(4.19), has been extensively studied in connection with resonant absorption of laser light in a non-uniform plasma[64]. By the simple transformation[65]

$$\zeta = x + \frac{1}{2}(z - z_0)^2, \qquad \tau = z - z_0$$

$$\text{and} \quad \psi(x,z) = u(\zeta,\tau)\exp\left\{i\left[x(z - z_0) + \frac{1}{6}(z - z_0)^3\right]\right\} \ , \tag{4.20}$$

eq.(4.19) can be reduced to the usual NLS equation with no potential term, eq.(4.10), the initial-value problem of which is analyticaly soluble by means of the inverse scattering method. It has been

proved[66] that there is no soliton solution if an initial profile satisfies

$$\int_{-\infty}^{\infty} |u(\zeta,0)|\, d\zeta < 0.904 \ . \qquad (4.21)$$

Although this is nothing else than the threshold condition for a filamentation, it will be a difficult task to rewrite it for $\psi(x,z)$ at a certain initial point in the x-direction. Therefore we shall content ourselves to present numerical results in the next sub-section.

§§4-2-3. Numerical analysis

In order to visualize the behaviour of a wave packet near the mode-conversion point, we have numerically solved the model equation (4.19) by using the difference method. In view of realizing an actual experimental set-up, a finite-size wave source with width l is assumed to be located at $x = -8$ and has a particular spatial profile

$$\psi = a \sin[\pi z / l] \qquad \text{for} \qquad 0 < z < l \ . \qquad (4.22)$$

The computation is carried out in the region $-16 < x < 12$ and $z > 0$. To reduce the effect of spurious reflections at both boundaries, an extra damping term is added to eq.(4.19) in the regions $-16 < x < -12$ and $8 < x < 12$. In Figs. 4.3 to 7 the envelopes of the potential are plotted. The actual potential is, of course, given by a carrier $\exp(-ik_+ x + ik_{//} z - i\omega t)$ modulated by ψ.

i) Small-amplitude case ($a = 0.01$)

For a large-size wave source ($l = 6.0$), a standing wave is built up near the conversion point ($x = 0$) and its shape is similar to the Airy function, eq.(4.16), weighted with the spatial profile, eq.(4.22), as is illustrated in Fig.4.3. On the other hand, in Fig.4.4, we can see that the wave packet produced by a small-size wave source ($l = 1.0$) diffuses due to thermal dispersion. Since the k_z-spectrum of the incoming wave has a relatively

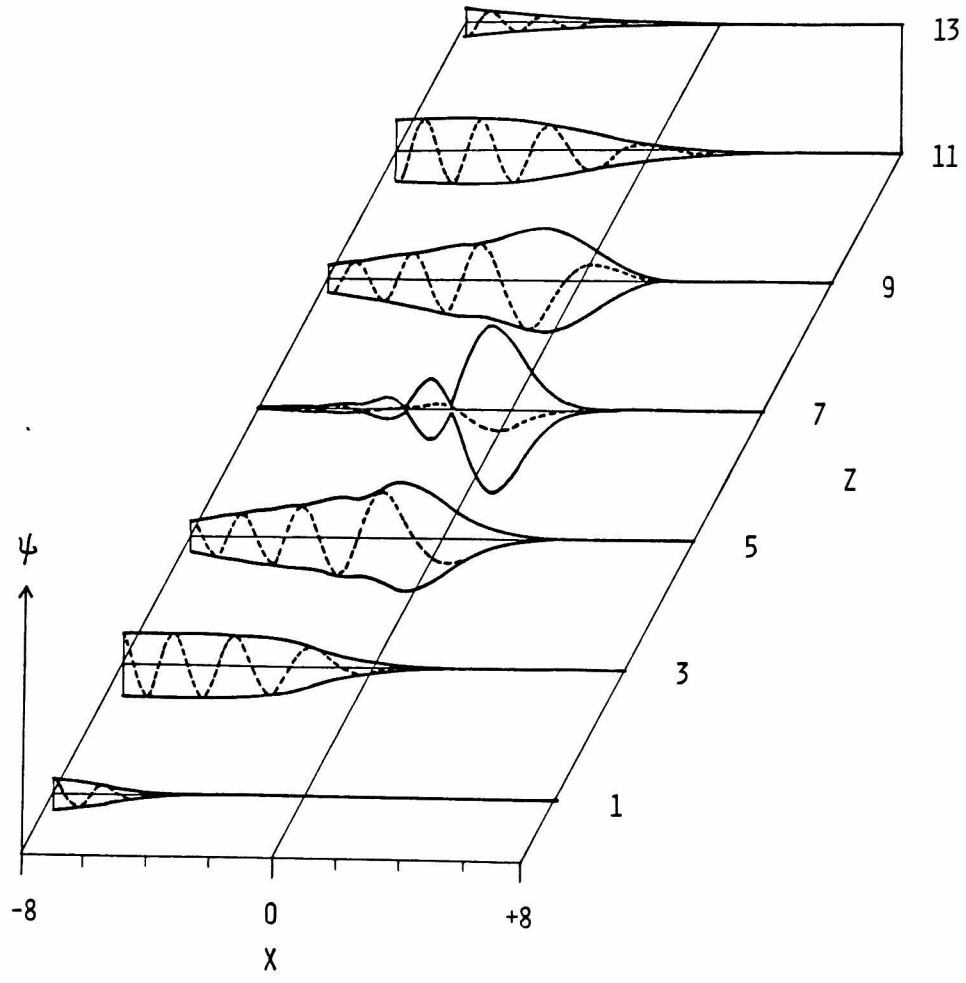

Fig.4.3 Potential profile for a small-amplitude wave with $a = 0.01$, launched by a large-size wave source with $l = 6.0$. The solid line indicates the envelope $|\psi|$ and the broken line the real part of ψ.

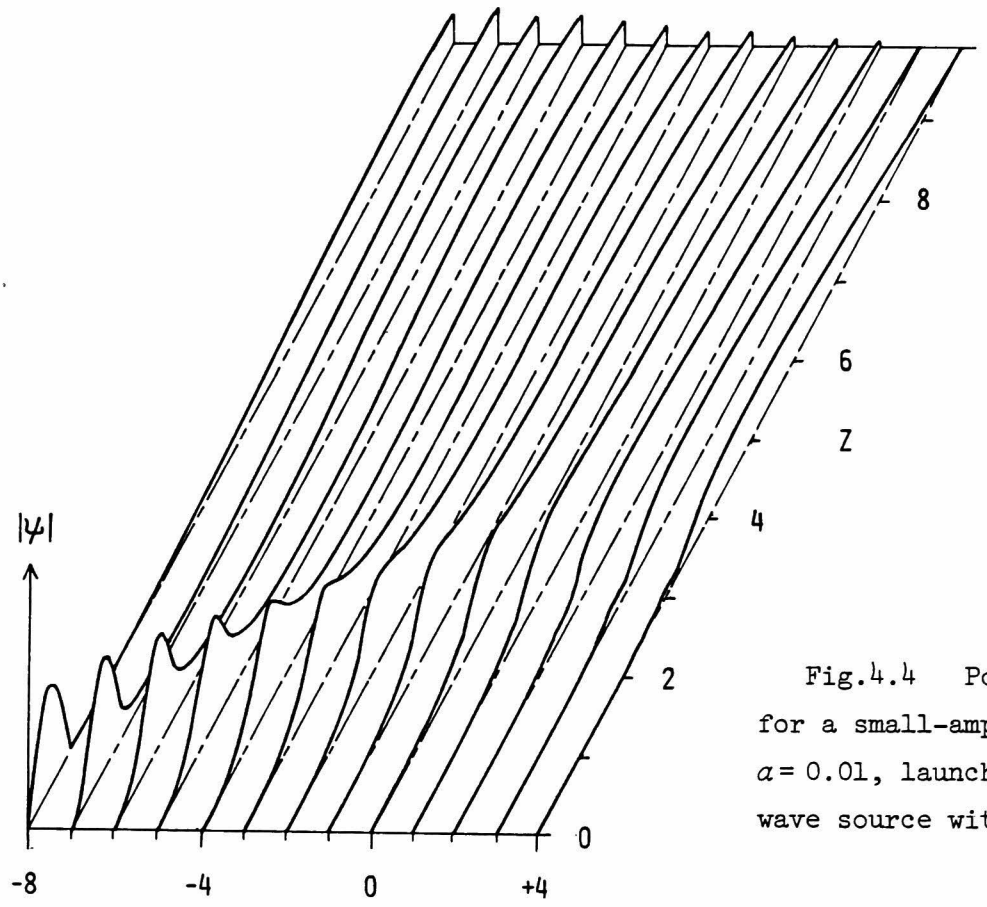

Fig.4.4 Potential profile for a small-amplitude wave with $a = 0.01$, launched by a small-size wave source with $\ell = 1.0$.

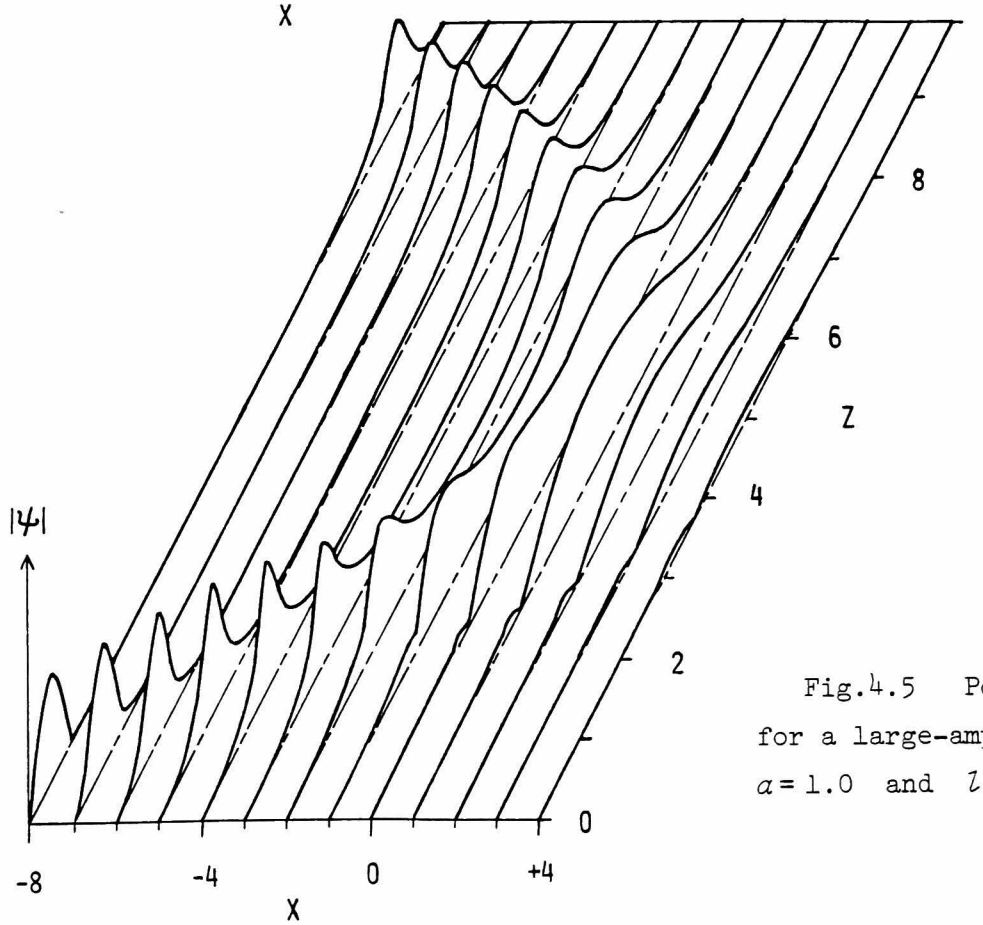

Fig.4.5 Potential profile for a large-amplitude wave with $a = 1.0$ and $\ell = 1.0$.

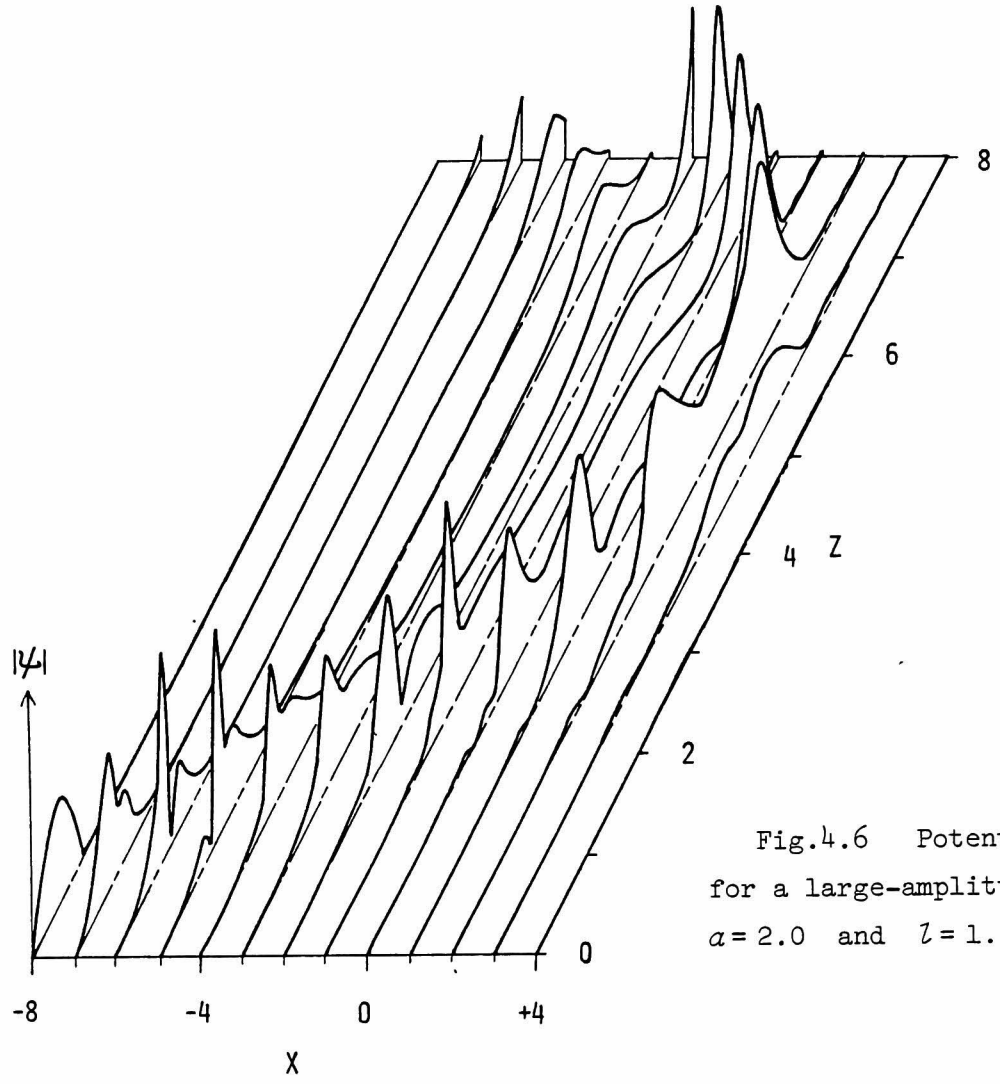

Fig.4.6 Potential profile for a large-amplitude wave with $a = 2.0$ and $l = 1.0$.

broad peak around $k_z = k_{//}$, the mode conversion of the k_z-component with $k_z > k_{//}$ occurs on the lower-density side, while the components with $k_z < k_{//}$ penetrate, beyond the conversion point, deep into the higher-density side. Therefore the wave packet spreads and the maximum amplitude decreases monotonically.

ii) Large-amplitude case $(a \geq 1.0)$

When an amplitude becomes so large that the nonlinear effect (steepening) competes with the dispersion effect (broadening), even the wave emitted by a small-size wave source remains localized

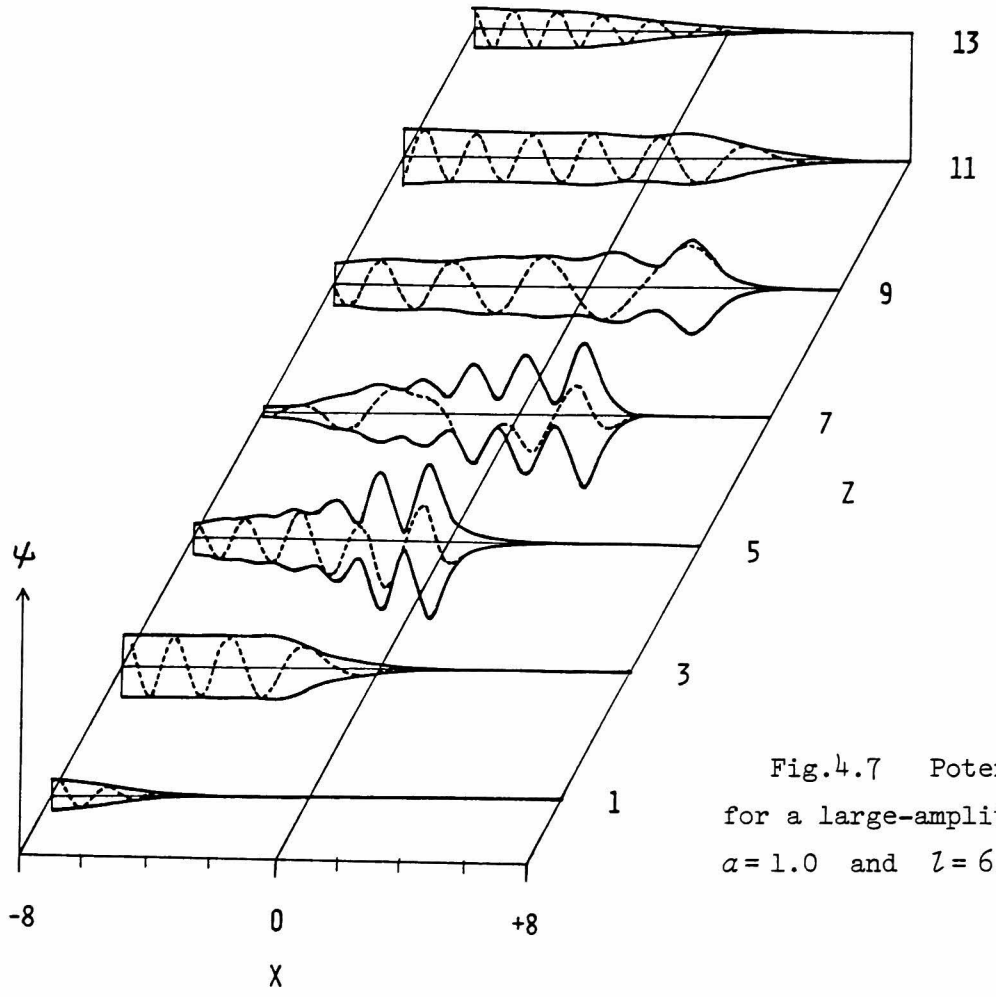

Fig.4.7 Potential profile for a large-amplitude wave with $a = 1.0$ and $\ell = 6.0$.

after the conversion (Fig.4.5). This explains the formation of an envelope soliton, as is suggested by its sech-like profile. When the amplitude is increased further ($a = 2.0$), the wave packet splits into two solitons (Fig.4.6). For a large-size wave source ($\ell = 6.0$), the Airy-function-like peaks are enhanced by the non-linear effect and some of the sharp peaks penetrate beyond the conversion point. However, they spread after the conversion and no soliton is clearly observed within our limited system-size of the computation (Fig.4.7).

§4-3. Discussion

So far, we have derived and solved the model equation describing the weakly nonlinear LH wave propagating near the linear mode-conversion point. Although our treatment is based on the assumption of the rapid phase variation, the model equation accounts well for the linear mode conversion, which was not examined with scrutiny in the past.[56)]

According to our numerical results, a small-amplitude wave packet diffuses due to thermal dispersion, in the case of a small-size wave source. As the amplitude increases, the stable localized wave packet is set up $(a \sim 1)$ and then splits into solitons, namely, the filamentation occurs $(a \gtrsim 2)$. For a large-size wave source, the standing wave, built up near the conversion point, is composed of several peaks on the envelope. These peaks get larger with increasing amplitude. However, it is observed that the formation of solitons requires a longer propagation length, compared with the case of the small-size wave source.

As an example, we may recall the LH heating experiments carried out on the JFT-2. Relevant parameters are[10)] :
$n_0 = 2 \times 10^{19} \mathrm{m}^{-3}$, $B_0 = 1.3$ T, $T = T_e + T_i = 900$ eV, $f = 750$ MHz, $k_{//}c/\omega = 5$, $L_n = 0.25$ m, $L_z = 0.056$ m and $L_y = 0.29$ m, where L_z and L_y are the sizes of the wave-guide array. When we estimate from eq.(4.16) the incident power $P(= \Gamma L_x L_y)$ so that $\psi = 1$, we obtain $P = 40$ kw, which is much lower than the experimentally observed value $P \lesssim 135$ kW. Even with this power, a filamentation is not expected to occur because the small-size of the wave source, $l = L_z/z_n = 0.09$, acts to spread the wave packet due to strong thermal dispersion and reduces

its amplitude rapidly. The tendency for a filamentation to occur more and more difficult with decreasing l has also been confirmed by numerical analysis. It may be observable, however, when a power is increased and/or a waveguide array is lengthened.

Finally, let us remark that it is easy to include in the model the effect of collisional damping which cannot be neglected in a low temperature plasma such as a linear machine. Using the electron collision frequency ν_e, we find that the damping term $i(\nu_e/\omega)(\omega_{pe}^2/\omega_{ce}^2)(L_n/x_n)\psi$ should be added to eq.(4.19). Since the factor L_n/x_n is larger than unity under the usual experimental condition, this enhanced effect of damping as well as the thermal dispersion would obstruct an experimental detection of the converted wave.

Chapter 5

STOCHASTIC HIGH-ENERGY TAIL FORMATION BY A SINGLE WAVE IN A MAGNETIZED PLASMA

The formation of a high-energy tail in a perpendicular velocity distribution of ions has often been observed in LH wave heating experiments.[5-10] Existence of the high-energy tail is now considered to be essential to LH wave heating, because wave energy seems to be absorbed by bulk ions through collisional relaxation of the high-energy tail. Although production of high-energy ions enhances a fusion reaction rate in a well-confined plasma, it has a drawback of also increasing energy loss by yielding poorly-confined or banana particles, especially in present-day experimental devices. Therefore a satisfactory explanation on the mechanism of the tail formation has been called for.

Recently, it has been argued that nonlinear interaction of charged particles with a monochromatic wave can be responsible for their stochastic motion in a uniform magnetic field. In the case of an oblique propagation, Smith and Kaufman[67] have shown the occurrence of a stochastic acceleration along a magnetic field, which is followed by a perpendicular acceleration because of energy conservation in the wave frame. Since a threshold of the wave amplitude is very large when $k_{\parallel} v_{Ti} \ll \omega_{ci}$, however, their results are not applicable to the tail formation by a LH wave. In order to explain the case of a LH wave, we shall consider an electrostatic wave with a frequency lying near a cyclotron harmonic and demonstrate that, if the wave amplitude exceeds a threshold of reasonable magnitude, the motion of ions becomes stochastic even if $k_{\parallel} = 0$

(perpendicular propagation) and that the formation of a high-energy tail may be expected.

In this chapter, a nonlinear motion of charged particles is extensively studied in the presence of both a uniform magnetic field and a monochromatic electrostatic wave for the cases of an oblique and a perpendicular propagation. Appearance of secondary islands in phase space as well as primary ones is discussed. The overlapping of secondary islands taken into account, a wave amplitude required for the onset of a stochasticity is estimated analytically. The results are in good agreement with numerical results. For the case of the perpendicular propagation, it is shown that production of high-energy particles is most efficient if the wave frequency is a multiple of the cyclotron frequency. As the wave amplitude increases, numerical calculations show that a steady velocity distribution is insensitive to the wave frequency.

In the first section, we survey the concept of the intrinsic stochasticity and its application to RF heating. In §5-2, we introduce a Hamiltonian of the test particle and formulate in its most general form the overlapping of secondary islands. The case of the oblique propagation is analysed in §5-3 and the case of the perpendicular propagation in §5-4. The last section is devoted to a discussion of the results obtained.

§5-1. Intrinsic stochasticity in RF heating

In the range of a density and a temperature appropriate for a controlled nuclear fusion, a Coulomb mean free path is extremely long compared with a device size and an anisotropy in the particle velocity distribution is relaxed only slowly through long-range Coulomb collisions. It is then reasonable to ask on what time scale RF energy is absorbed by a plasma, since the argument of quasi-linear theory shows that RF interaction tends to produce local plateaus in a space-averaged velocity distribution. Recently it has been shown[68] in a number of RF heating processes that trapped adiabatic orbits in RF waves (superadiabaticity) can be destroyed by collision-free stochasticity as effectively as by Coulomb collisions. Since this stochasticity originates in nonlinearity of the deterministic equation of motion and relies on neither an external random force nor statistical average, the term "intrinsic stochasticity" has recently come into use. This mechanism is called as universal instability,[69,70] or Arnold diffusion, in the field of dynamical systems. A peculiar feature of this mechanism results in an irregular, or stochastic, motion of the system as if the latter were influenced by a random perturbation even though, in fact, the motion is governed by purely dynamical equations. This stochasticity generally takes place for very special initial conditions (inside the so-called stochastic layers) which are, however, everywhere *dense* in the phase space of the system.

The concept of intrinsic stochasticity has been introduced into Plasma Physics in order to explain a mechanism of destruction of magnetic surfaces by magnetic-field irregularities.[71]

Recently, destroyed magnetic surfaces have been studied by several authors in relation to anomalous electron heat transport in tokamaks.[72,73] Until now, analyses based on intrinsic stochasticity have been worked out in various fields of Plasma Physics: electron cyclotron resonance heating in a mirror field,[74,75] adiabatic invariance of particles' motion in mirror machines,[76] instability saturation in a coupled three-wave system, onset of MHD turbulence and so on.[77]

Intrinsic stochasticity in the wave-particle interaction was first treated by Zaslavskii and Filonenko.[78] They have treated the motion of a charged particle trapped by two electrostatic waves with different phase velocities and discussed the stochasticity of particles with reference to a quasilinear process. Recently, Smith and Kaufman[67] have demonstrated that, in a magnetized plasma, a single electrostatic wave propagating obliquely to a uniform magnetic field can give rise to a stochastic motion of charged particles and can produce a tail in a velocity distribution. Since their analysis is valid only in the order of approximation where primary islands, first appear, the threshold obtained by them gives a rough estimate of the wave amplitude for the onset of the intrinsic stochasticity. A portion in phase space becomes stochastic for amplitudes smaller than the threshold and an other portion remains adiabatic even if the amplitude becomes several times the threshold value. In order to estimate an area of a phase space where the motion becomes stochastic, we shall take account of an overlapping of secondary islands in subsequent sections.

§5-2. Hamiltonian formulation for the motion of a charged particle

§§5-2-1. Hamiltonian of a test particle

We consider the motion of a charged particle, with mass m and charge e, placed in a uniform magnetic field $B_0\vec{z}$ and subject to a monochromatic electrostatic wave $\phi\cos(k_\perp x + k_\parallel z - \omega t)$. In order to analyse systematically the formation and the overlapping of islands, we make use of the Hamiltonian formalism.

The Hamiltonian of a test particle takes the form,

$$H = \frac{1}{2m}[P_x^2 + (P_y - m\omega_c x)^2 + P_z^2] + e\phi\cos(k_\perp x + k_\parallel z - \omega t) , \qquad (5.1)$$

where $\omega_c = qB_0/m$ is the cyclotron frequency. The quantities P_x, P_y and P_z are the canonical momenta such that $P_x = mv_x$, $P_y = mv_y + m\omega_c x$ and $P_z = mv_z$. Since H is independent of y, the momentum P_y is a constant of the motion. Defining the normalized magnetic moment P_ψ and the cyclotron phase ψ by the relations

$$\begin{cases} P_\psi = \dfrac{1}{2m\omega_c}[P_x^2 + (P_y - m\omega_c x)^2] = \dfrac{m v_\perp^2}{2\omega_c} , & (5.2) \\ \\ \psi = \arcsin\left(\dfrac{x - P_y/m\omega_{ci}}{\sqrt{2P_\psi/m\omega_{ci}}}\right) = \arctan\left(-\dfrac{v_y}{v_x}\right) , & (5.3) \end{cases}$$

we can rewrite the Hamiltonian, after the canonical transformation from (x, P_x) to (P_ψ, ψ), as

$$H(\psi, z, P_\psi, P_z, t) = \omega_c P_\psi + \frac{P_z^2}{2m} + e\phi\cos\left(k_\perp\sqrt{\frac{2P_\psi}{m\omega_c}}\sin\psi + k_\parallel z - \omega t\right) \qquad (5.4)$$

$$= \omega_c P_\psi + \frac{P_z^2}{2m} + e\phi \sum_{n=-\infty}^{\infty} J_n(k_\perp \sqrt{\frac{2P_\psi}{m\omega_c}}) \cos(n\psi + k_\parallel z - \omega t) ,$$

where the cosine function is expanded on the basis of the Bessel function J_n.

This equation indicates that, for a small-amplitude wave, a charged particle in a static magnetic field moves as if there exist a number of waves with frequencies $\omega - n\omega_c$. If the motion of a particle is subject to the resonance condition

$$n\omega_c + \frac{k_\parallel P_z}{m} - \omega \simeq 0 \qquad \text{for any integer } n , \quad (5.5)$$

the particle will be trapped in a potential well and thus the trajectories of trapped particles in a phase space form an island enclosed by a separatrix. In the case of obliquely propagating waves, the width of the island increases with the wave amplitude and, when two separatrices of the adjacent islands with harmonic numbers n and $n+1$ approach to each other, the interaction of the two islands results in a formation of secondary islands near the separatrices. This is explained by an interaction between the nonlinear motion of particles in the n-th primary island and the $(n+1)$ - th cyclotron harmonic. Although primary islands never overlap in the case of perpendicularly propagating waves $(k_\parallel = 0)$, the secondary islands are produced near the separatrices of the primary ones. They also grow with the wave amplitude and the higher-order islands are generated whenever the secondary ones come to overlap. In view of analysing this hierarchic structure, a general formulation is presented in the next subsection.

§§5-2-2. General formulation[79)]

In terms of the action-angle variables $(\hat{p},\hat{w})$, the Hamiltonian is assumed to consist of two parts and is given by

$$\hat{H}(\hat{p},\hat{w},t) = \hat{H}_0(\hat{p}) + \varepsilon \sum_{mn} \hat{H}_{mn}(\hat{p}) \exp\left[i\,(n\hat{w} - m\omega t)\right] , \tag{5.6}$$

where $H_0(\hat{p})$ represents the unperturbed part and ε is a small number. The unperturbed motion is simply expressed as

$$\begin{cases} \dfrac{d\hat{p}}{dt} = - \dfrac{\partial \hat{H}_0}{\partial \hat{w}} = 0 , \\ \dfrac{d\hat{w}}{dt} = \dfrac{\partial \hat{H}_0}{\partial \hat{p}} = \Omega_0(\hat{p}) . \end{cases} \tag{5.7}$$

If the unperturbed frequency $\Omega_0(\hat{p})$ is close to a resonance, i.e. $N\Omega_0 - M\omega \simeq O(\varepsilon)$, it is appropriate to make use of a canonical transformation in a rotating frame[80)]

$$\begin{cases} w = N\hat{w} - M\omega t , \\ p = \dfrac{\hat{p}}{N} . \end{cases} \tag{5.8}$$

Since the new coordinate w varies slowly compared with ωt, the transformed Hamiltonian

$$H(p,w,t) = H_0(p) - M\omega p + \varepsilon \sum_{mn} H_{mn}(p) \exp\left\{ i\left[\frac{n}{N} w + \left(\frac{nM}{N} - m \right)\omega t \right] \right\} \tag{5.9}$$

can be averaged over ωt to give

$$\overline{H}(p,w) = H_0(p) - M\omega p + \varepsilon \sum_{\ell} H_{\ell M, \ell N}(p) \exp(i\ell w) \ . \qquad (5.10)$$

When the nonlinear motion describable by $\overline{H}(p,w)$ is periodic, it may be expressed in terms of the new action-angle variables,

$$I = \frac{1}{2\pi} \oint p \, dw \qquad \text{and} \qquad \theta = \frac{\partial}{\partial I} \int^{w} p \, dw \ , \qquad (5.11)$$

and the new Hamiltonian $h_0(I) = \overline{H}$ yields the equation of motion

$$\frac{dI}{dt} = 0 \qquad \text{and} \qquad \frac{d\theta}{dt} = \frac{dh_0(I)}{dI} \equiv \Omega(I) \ . \qquad (5.12)$$

These equations describe a nonlinear oscillation which takes place when only one of the primary resonances comes into play.

Then we go back to the exact Hamiltonian, eq.(5.9), and treat eqs.(5.11) as a canonical transformation from (p,w) to (I,θ). Though p and w are periodic with respect to θ, the quantity $H_{mn}(p)\exp(inw/N)$ is not in general periodic, since nw/N may change by $2\pi n/N$ during a period of θ. The dominant contribution comes, however, from periodic terms when $|n - N| << N$. This is the case of our primary interest. The procedure of retaining the periodic term, $H_{mn}(p(I,\theta)) \exp[inw(I,\theta)/N] \simeq \sum_{s} h_{mns}(I) \exp(is\theta)$, yields

$$H(I,\theta,t) = h_0(I) + \varepsilon \sum_{mns}{}' h_{mns}(I) \exp\left\{ i \left[s\theta + \left(\frac{nM}{N} - m \right) \omega t \right] \right\}, \qquad (5.13)$$

where Σ' indicates that terms with $n = \ell N$ and $m = \ell M$ are deleted for all integers ℓ. It should be noted that eq.(5.13) bears similarity to eq.(5.6), except that perturbations which figure in

the former has components of the lower frequency, ω/N. Repetition of the above procedure will lead to an appearance of a dense frequency spectrum of the perturbation and this in turn affects the renormalized nonlinear oscillation.

If the nonlinear oscillation, derivable from $h_0(I)$, resonates with the perturbation at $I = I_{rs}$, i.e.,

$$s\,\Omega(I_{rs}) + \left(\frac{nM}{N} - m\right)\omega = 0 \,, \tag{5.14}$$

the secondary island is generated on the primary resonant trajectory. Taking account of only the resonant perturbation and expanding both $\Omega(I)$ and $h_{mns}(I)$ in Taylor series around I_{rs}, we can reduce the Hamiltonian (5.13) into the form

$$\begin{aligned} H_r(I,\theta,t) = {} & h_0(I_{rs}) \\ & + \frac{d\Omega(I_{rs})}{dI}\,\frac{(\Delta I)^2}{2} - 2\varepsilon\,|h_{mns}(I_{rs})|\cos(s\,\Delta\theta) \,, \end{aligned} \tag{5.15}$$

where $\Delta I = I - I_{rs}$ and $\Delta\theta = \theta - (nM/N - m)(\omega t/s) + \pi/s + [\arg h_{mns}(I_{rs})]/s$, and the relation $h_{-m,-n,-s} = h^*_{mns}$ has been used. The reduced Hamiltonian enables us to estimate the width of the secondary island as

$$\Delta I_s = \left| 8\varepsilon\, h_{mns}(I_{rs}) / \left[d\Omega(I_{rs})/dI \right] \right|^{1/2} \,. \tag{5.16}$$

In the derivation of eq.(5.15), we have neglected the term $2\varepsilon\,(dh_{mns}/dI)\Delta I\cos(s\Delta\theta)$, compared with $(d\Omega/dI)(\Delta I)^2/2$. Therefore the estimation (5.16) is justified *a posteriori* if the perturbation satisfies the condition

$$2\,\varepsilon\,\frac{(dh_{mns}/dI)^2}{(d\Omega/dI)h_{mns}} \ll 1 \quad , \tag{5.17}$$

which usually holds near the separatrices of primary islands where $d\Omega/dI$ approaches infinity.

When the adjacent secondary island of width ΔI_{s*} is separated by $\delta I_{ss*} = |I_{rs*} - I_{rs}|$ from the trajectory with $I = I_{rs}$, the overlap condition for the secondary islands, known as Chirikov's criterion[69] for the onset of intrinsic stochasticity, is given by

$$K \equiv [(\Delta I_s + \Delta I_{s*})/\delta I_{ss*}]^2 \gtrsim 1 \quad . \tag{5.18}$$

§5-3. Case of oblique propagation

§§5-3-1. Analysis of the primary resonance

When an amplitude of the electrostatic wave is small, we may regard the Hamiltonian (5.4) of a test particle as a sum of an unperturbed Hamiltonian H_0 and a perturbation V, that is,

$$H = H_0 + V \ , \tag{5.19}$$

where

$$H_0 = \frac{P_z^2}{2m} + \omega_c P_\psi \ ,$$

$$V = e\phi \sum_{n=-\infty}^{\infty} J_n(k_\perp \sqrt{2P_\psi/m\omega_c}) \cos(k_\parallel z + n\psi - \omega t) \ ,$$

The canonical equations of H_0 immediately give the unperturbed motion,

$$z = \frac{P_{z0}}{m} t + z_0 \ , \qquad \psi = \omega_c t + \psi_0 \ ,$$

$$P_z = P_{z0} \qquad \text{and} \qquad P_\psi = P_{\psi 0} \ , \tag{5.20}$$

where the suffix 0 designates the initial value. Inserting eqs. (5.20) into the perturbation V, we obtain the first-order approximation

$$V \simeq e\phi \sum_{n=-\infty}^{\infty} J_n(k_\perp \sqrt{2P_\psi/m\omega_c}) \cos\left[(k_z P_z/m + n\omega_c - \omega)t + k_\parallel z_0 + n\psi_0\right] . \tag{5.21}$$

This expression indicates that a resonant term, satisfying the resonance condition (5.5), is responsible for the motion of a particle, since the contribution of non-resonant terms vanishes by taking the time-average over an time interval longer than the cyclotron period.

We now transform to the new variables $(\xi, \zeta, P_\xi, P_\zeta)$, using the generating function

$$S(z, \psi, P_\xi, P_\zeta, t) = \left(P_\xi - \frac{Nm\omega_c}{k_\parallel^2} + \frac{m\omega}{k_\parallel^2}\right)\left(k_\parallel z + N\psi - \omega t + \pi\right) + \psi P_\zeta . \tag{5.22}$$

In terms of the old variables, the new ones turn out to be

$$\begin{aligned} \xi &= k_\parallel z + N\psi - \omega t + \pi , \\ \zeta &= \psi , \\ P_\xi &= \frac{P_z}{k_\parallel} + \frac{Nm\omega_c}{k_\parallel^2} - \frac{m\omega}{k_\parallel^2} , \\ P_\zeta &= P_\psi - \frac{NP_z}{k_\parallel} , \end{aligned} \tag{5.23}$$

with an integer N satisfying the condition $N \sim (\omega - k_\parallel P_z/m)/\omega_c$. This canonical transformation serves as passing simultaneously to the wave frame moving along the magnetic field with the phase velocity $\omega/k_\parallel$ and to the rotating frame discussed in §§5-2-2. The new Hamiltonian now reads

$$H(\xi,\zeta,P_\xi,P_\zeta) = \frac{k_{//}^2}{2m}P_\xi^2 + \omega_c P_\zeta - e\phi \sum_n J_n(k_\perp\rho)\cos[\xi + (n-N)\zeta] \ , \tag{5.24}$$

which is independent of time. The Larmor radius ρ which satisfies the relation

$$\rho^2 = \frac{2P_\psi}{m\omega_c} = \frac{2}{m\omega_c}\left[P_\zeta + NP_\xi - \frac{m\omega_c N^2}{k_{//}^2} \right] \tag{5.25}$$

is not taken to change considerably from the initial value ρ_0. Then we divide the Hamiltonian into two parts: the one independent of the rapidly varying phase ζ and the other dependent both on ζ and on ρ i.e.,

$$H_0 = \frac{k_{//}^2}{2m}P_\xi^2 + \omega_c P_\zeta - e\phi J_N(k_\perp\rho_0)\cos\xi \ , \tag{5.26}$$

$$H_1 = -e\phi \sum_{n\neq N} J_n(k_\perp\rho)\cos[\xi + (n-N)\zeta]$$

$$-e\phi[J_N(k_\perp\rho) - J_N(k_\perp\rho_0)]\cos\xi \ . \tag{5.27}$$

We first consider in detail the averaged Hamiltonian H_0. There are two constants of the motion; the time-independent Hamiltonian H_0 itself and the canonical momentum P_ζ conjugate to the cyclic coordinate ζ. Since $H_0 - \omega_c P_\zeta$ is a constant, it is obvious that eq.(5.26) is equivalent to the Hamiltonian of a simple pendulum. When $H_0 - \omega_c P_\zeta$ becomes smaller than $|e\phi J_N(k_\perp\rho_0)|$, the particle is trapped in a potential well with the half-width in v_z as

$$\Delta v_z^{(N)} = \frac{k_{\parallel}}{m} \Delta P_{\xi} = 2\left|\frac{e\phi}{m} J_N(k_{\perp}\rho_0)\right|^{1/2} \tag{5.28}$$

around the resonance velocity,

$$v_z^{(N)} = \frac{\omega - N\omega_c}{k_{\parallel}} . \tag{5.29}$$

as is illustrated in Fig.5.1. As the width of this primary island in a phase plane (ξ, P_{ξ}) is proportional to $\phi^{1/2}$, the adjacent

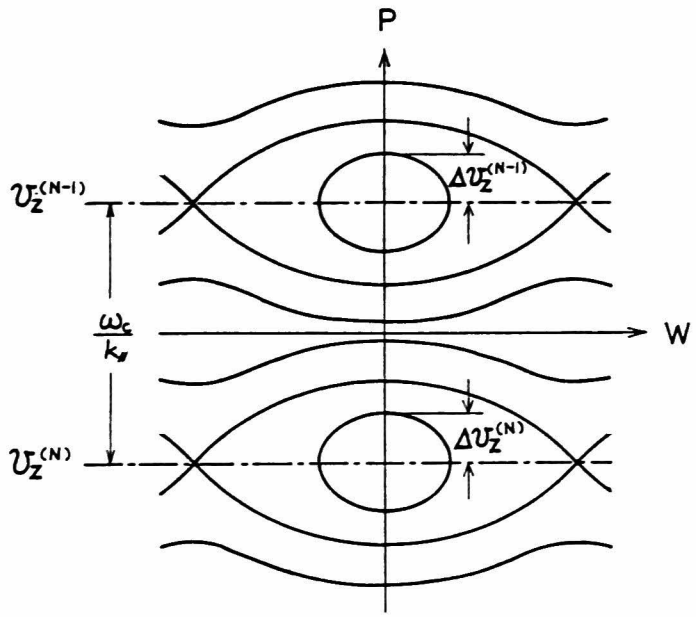

Fig.5.1 A sketch of primary resonances on the phase plane (P, W).

islands with N and $N-1$ may overlap above a critical amplitude. Smith and Kaufman[67] have argued that Chirikov's criterion which allows to predict a disappearance of the constant of motion is given by the overlapping condition

$$\Delta v_z^{(N)} + \Delta v_z^{(N-1)} > v_z^{(N-1)} - v_z^{(N)} = \frac{\omega_c}{k_{\parallel}}$$

or, equivalently,

$$16 \left| \frac{k_{\parallel}^2 e\phi \, J_N(k_{\perp}\rho_0)}{m\,\omega_c^2} \right| > 1 \quad , \tag{5.30}$$

if two Bessel functions J_N and J_{N-1} have comparable amplitudes. This simple formula gives a rough estimate of the threshold for the onset of a stochastic motion. As will be shown later in the light of numerical computations, however, the motion becomes stochastic in only a portion of phase space if the above criterion is fulfilled. In the following subsections, we shall develop an analysis which accounts for an appearance of the secondary islands, in order to predict an area of phase space indicating nonadiabatic motions.

§§5-3-2. Analysis of the secondary resonance

The averaged Hamiltonian (5.26) may be simplified, by the use of the normalized bounce frequency ω_b, to give

$$h_0(P,W) = \frac{k_{\parallel}^2}{m\omega_c^2}(H_0 - \omega_c P_\zeta) = \frac{P^2}{2} - \omega_b^2 \cos W , \tag{5.31}$$

where

$$P = \frac{k_{\parallel}^2 P_\xi}{m\omega_c} = \frac{1}{\omega_c}(k_{\parallel} v_z + N\omega_c - \omega) , \qquad W = \xi \quad \text{and}$$

$$\omega_b = \left| \frac{k_{\parallel}^2 e\phi}{m\omega_c^2} J_N(k_\perp \rho_0) \right|^{1/2} .$$

In order to analyse the nonlinear oscillation, it is convenient to introduce the action-angle variables,

$$\begin{cases} I = \dfrac{1}{2\pi}\oint P\, dW = \dfrac{1}{2\pi}\oint 2\omega_b q\left[1 - \dfrac{1}{q^2}\sin^2\dfrac{W}{2}\right]^{1/2} dW , \\ \\ \theta(W,h_0) = \dfrac{\partial}{\partial I}\displaystyle\int^W P\, dW , \end{cases} \tag{5.32}$$

where the quantity q, defined by

$$q^2 = \frac{1}{2}\left(1 + \frac{h_0}{\omega_b^2} \right) ,$$

vanishes at the center of the island and becomes unity on the separatrices and will be used as the parameter of the elliptic functions. The action I is proportional to an area of phase space

enclosed by the trajectory and the angle θ corresponds to a phase on the trajectory (see Fig.5.2). The equation of motion for I and θ is simply expressed by eq.(5.12). Note also that the quantity $\Omega(I)$, corresponding to a bounce frequency which depends on I, approaches zero near the separatrix where a period of the oscillation goes to infinity.

We now summarize a solution to the equation of motion, without giving computational details. Several useful formulae of the Jacobian elliptic functions, sn, cn and dn, are found in Appendix B. For a trapped particle with $0 < q < 1$, we obtain

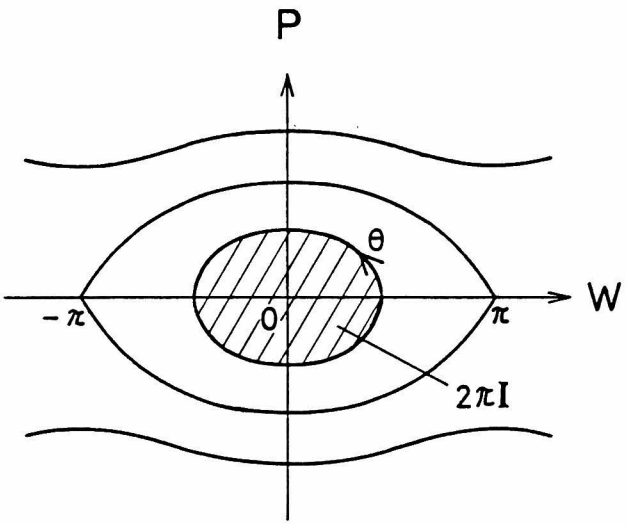

Fig.5.2 Illustration of the relationshop between the action-angle variables (I, θ) and the original ones (P, W).

$$P = 2\omega_b q\, \mathrm{cn}(\omega_b\theta/\Omega) \ ,$$

$$\sin W = 2\,\mathrm{sn}(\omega_b\theta/\Omega)\,\mathrm{dn}(\omega_b\theta/\Omega), \quad \cos W = 1 - 2q^2\,\mathrm{sn}^2(\omega_b\theta/\Omega),$$

$$I = \frac{8}{\pi}[\,E - (1-q^2)\,F\,]\,\omega_b \quad \text{and} \quad \Omega(I) = \frac{dh_0(I)}{dI} = \frac{\pi}{2F}\,\omega_b \ , \qquad (5.33)$$

where $F(q)$ and $E(q)$ denote the complete elliptic integral of the first kind and of the second kind, respectively. For an untrapped particle with $q > 1$ and $P > 0$, we find

$$P = 2\omega_b q\, \tilde{\mathrm{dn}}(q\omega_b\theta/\Omega) \ ,$$

$$\sin W = 2\,\tilde{\mathrm{sn}}(q\omega_b\theta/\Omega)\tilde{\mathrm{cn}}(q\omega_b\theta/\Omega), \quad \cos W = 1 - 2\,\tilde{\mathrm{sn}}^2(q\omega_b\theta/\Omega),$$

$$I = \frac{4q}{\pi}\,\tilde{F}\,\omega_b \qquad \text{and} \qquad \Omega(I) = \frac{\pi q}{\tilde{F}}\,\omega_b \ , \qquad (5.34)$$

where, tildes on the elliptic functions and the elliptic integrals indicate that the parameter q in the corresponding functions should be replaced by q^{-1}.

Since the perturbed Hamiltonian H_1 retains a number of terms periodic in ζ which varies approximately as $\omega_c t$, the nonlinear periodic motion due to H_0 may resonate with the perturbation and thus may give rise to secondary islands on the resonant trajectory. The total Hamiltonian in the normalized form becomes

$$H(W,\zeta,P,\overline{P}_\zeta) = \frac{P^2}{2} - \omega_b^2 \cos W + \overline{P}_\zeta - \sum_{n\neq N} \gamma_n \omega_b^2 \cos [W + (n-N)\zeta]$$

$$- \sum_n \omega_b^2 \frac{J_n(k_\perp \rho) - J_n(k_\perp \rho_0)}{J_N(k_\perp \rho_0)} \cos [W + (n-N)\zeta] \quad , \quad (5.35)$$

where

$$P_\zeta = \frac{k_\parallel^2 P_\zeta}{m\omega_c} \qquad \text{and} \qquad \gamma_n = \frac{J_n(k_\perp \rho_0)}{J_N(k_\perp \rho_0)}$$

Assuming the variation of $k_\perp \rho$ to be small, i.e.,

$$|J_n(k_\perp \rho) - J_n(k_\perp \rho_0)| \ll |J_n(k_\perp \rho_0)| \qquad (5.36)$$

which serves to neglect the last term in eq.(5.35), we may express the Hamiltonian as

$$H(W,\zeta,P,\overline{P}_\zeta) = \frac{P^2}{2} - \omega_b^2 \cos W + \overline{P}_\zeta$$

$$- \sum_{n\neq N} \gamma_n \omega_b^2 [\cos W \cos (n-N)\zeta - \sin W \sin (n-N)\zeta] . \qquad (5.37)$$

Taking account of the differential identities of the Jacobian elliptic functions and their Fourier expansions, recalled in Appendix B, we may rewrite eq.(5.37), in terms of the action-angle variables I and θ, as

$$H(I,\theta,\zeta,\bar{P}_\zeta) = h_0(I) + \bar{P}_\zeta - \sum_{n\neq N} \gamma_n \omega_b^2 \left\{ \left[1 - \frac{2(F-E)}{F}\right] \cos(n-N)\zeta \right.$$

$$+ \frac{\pi^2}{F^2} \sum_{\substack{s=-\infty \\ s\neq 0}}^{\infty} \frac{2s\, a^s}{1-a^{2s}} \cos[2s\theta + (n-N)\zeta] \qquad (5.38)$$

$$\left. + \frac{\pi^2}{F^2} \sum_{s=-\infty}^{\infty} \frac{(2s+1)a^{s+1/2}}{1+a^{2s+1}} \cos[(2s+1)\theta + (n-N)\zeta] \right\}$$

for a trapped particle and

$$H(I,\theta,\zeta,\bar{P}_\zeta) = h_0(I) + \bar{P}_\zeta - \sum_{n\neq N} \gamma_n \omega_b^2 \left\{ \left[1 - \frac{2(\tilde{F}-\tilde{E})q^2}{\tilde{F}}\right] \cos(n-N)\zeta \right.$$

$$+ \frac{2q^2\pi^2}{\tilde{F}^2} \sum_{s=1}^{\infty} \frac{2s\, \tilde{a}^s}{1-\tilde{a}^{2s}} \{ \cos[s\theta + (n-N)\zeta] \qquad (5.39)$$

$$\left. + \tilde{a}^{2s} \cos[s\theta - (n-N)\zeta] \} \right\}$$

for an untrapped particle, where

$$a = \exp\left(-\frac{\pi F(\sqrt{1-q^2})}{F(q)}\right) \quad \text{and} \quad \tilde{a} = \exp\left(-\frac{\pi F(\sqrt{1-1/q^2})}{F(1/q)}\right).$$

It is obvious from eqs.(5.38) and (5.39) that the secondary resonance occurs on the trajectory $I = I_{rs}$ if the relation

$$s\Omega(I_{rs}) + (n-N) = 0 \qquad \text{for} \qquad n \neq N\,, \qquad (5.40)$$

is satisfied for certain integers s . In order to estimate a width of the secondary island, we may single out only one resonant term, approximate ζ by $\omega_c t$ and reduce the Hamiltonian to the simpler form,

$$H(I,\theta,\tau) = h_0(I) - h_{ns}(I)\cos[\, s\theta + (n - N)\tau\,] \,, \tag{5.41}$$

with $\tau = \omega_c t$. Following the similar procedure discussed in §§5-2-2, the half-width of the secondary island is estimated to be

$$\Delta I_s = \left| \frac{4\, h_{ns}(I_{rs})}{d\Omega(I_{rs})/dI} \right|^{1/2} \tag{5.42}$$

in the action variable or

$$\Delta\Omega_s = \left| 4 \frac{d\Omega(I_{rs})}{dI}\, h_{ns}(I_{rs}) \right|^{1/2} \tag{5.43}$$

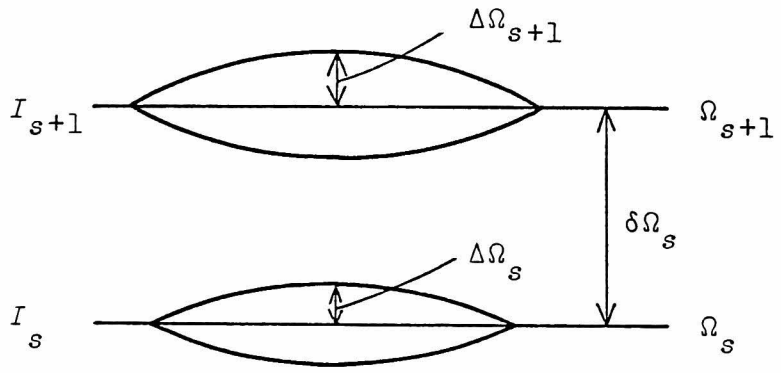

Fig.5.3 A sketch of the half-width $\Delta\Omega$ of the secondary island and the frequency spacing $\delta\Omega$ between adjacent secondary resonances.

in the normalized bounce frequency, where $d\Omega(I_{rs})/dI$ stands for $d\Omega/dI|_{I=I_{rs}}$. On the other hand, the frequency spacing $\delta\Omega$ between adjacent secondary resonances becomes

$$\delta\Omega_s = \begin{cases} \Omega_{2s} - \Omega_{2s+1} \sim \dfrac{n-N}{4s^2} = \dfrac{\pi^2}{4F^2}\dfrac{\omega_b^2}{n-N} & \text{(trapped)}, \\ \Omega_s - \Omega_{s+1} \sim \dfrac{n-N}{s^2} = \dfrac{\pi^2 q^2}{\tilde{F}^2}\dfrac{\omega_b^2}{n-N} & \text{(untrapped)}, \end{cases} \tag{5.44}$$

if the condition $s \gg 1$ is fulfilled (see Fig.5.3). Finally, we introduce a quantity K which gives an indication to an overlapping of the secondary islands and express Chirikov's criterion for the onset of a stochastic motion as

$$K = \left| \frac{2\,\Delta\Omega_s}{\delta\Omega_s} \right|^2 > 1 , \tag{5.45}$$

The stochastic parameter K for a trapped particle ($0 < q < 1$) is defined by

$$K = \frac{8}{\pi}\frac{1}{A_{\prime\prime}^3}\frac{E-(1-q^2)F}{q^2(1-q^2)}(\gamma_n + \gamma_{2N-n})\left(\sqrt{\frac{b}{1-b^2}} + \sqrt{\frac{b}{1+b^2}}\right)^2 \tag{5.46}$$

and for an untrapped particle ($q > 1$),

$$K = \begin{cases} \dfrac{4}{\pi}\dfrac{1}{A_{\prime\prime}^3}\dfrac{\tilde{E}}{q(q^2-1)}\gamma_n\dfrac{\tilde{b}}{1-\tilde{b}^4} & \text{for} \quad n < N , \\ \dfrac{4}{\Pi}\dfrac{1}{A_{\prime\prime}^3}\dfrac{\tilde{E}}{q(q^2-1)}\gamma_n\dfrac{\tilde{b}^3}{1-\tilde{b}^4} & \text{for} \quad n > N , \end{cases} \tag{5.47}$$

where

$$A_{\prime\prime} = \frac{\omega_b}{|n - N|}, \qquad b = \exp\left\{ - \frac{F(\sqrt{1 - q^2})}{A_{\prime\prime}} \right\}$$

and $$\tilde{b} = \exp\left\{ - \frac{F(\sqrt{1 - 1/q^2})}{A_{\prime\prime}} \right\} .$$

We have so far classified the motion of untrapped particles in two groups, according as whether $n < N$ or $n > N$, because a perturbation ($n < N$) propagating with a phase velocity $(\omega - n\omega_c)/k_{\prime\prime}$, greater than the phase velocity $(\omega - N\omega_c)/k_{\prime\prime}$ at the primary resonance, may affect the motion of the untrapped particles ($P > 0$) more strongly than that with a slower phase velocity ($n > N$).

§§5-3-3. Results of numerical analysis

Numerical calculations, based on the exact Hamiltonian (5.1), has been carried out with the purpose of confirming analytical results given in length in the previous subsections. In order to visualize the numerical result, we have made use of the surface-of-section method. Since a phase point moves with time on a three-dimensional energy surface which is contained in the four-dimensional phase space, a trajectory has to be well plotted in a two-dimensional phase plane so that we can easily understand whether a motion is adiabatic or not. To this end, we plot in a $\xi - P_\xi$ plane the intersection of a trajectory with a phase surface defined by the cyclotron phase $\zeta = \pi$. If there exists another constant of the motion in addition to energy, the trajectory lies on a

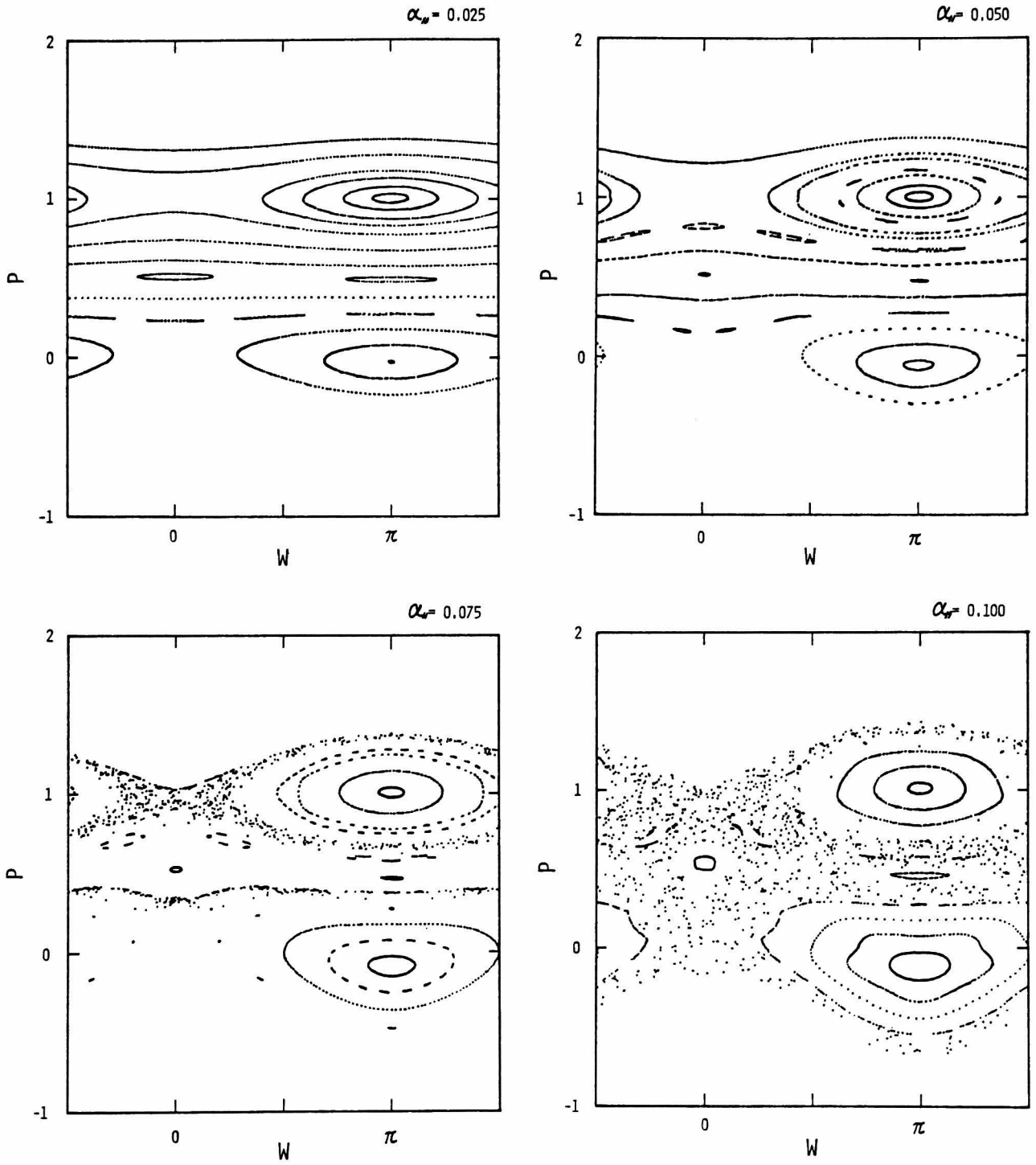

Fig.5.4 Numerically calculated trajectories for $k_{\perp}\rho_E = 1.48$ are plotted by the use of the surface-of-section method at $\psi = \pi$. 15 particles with different initial conditions are tracked until $\tau = 300$.

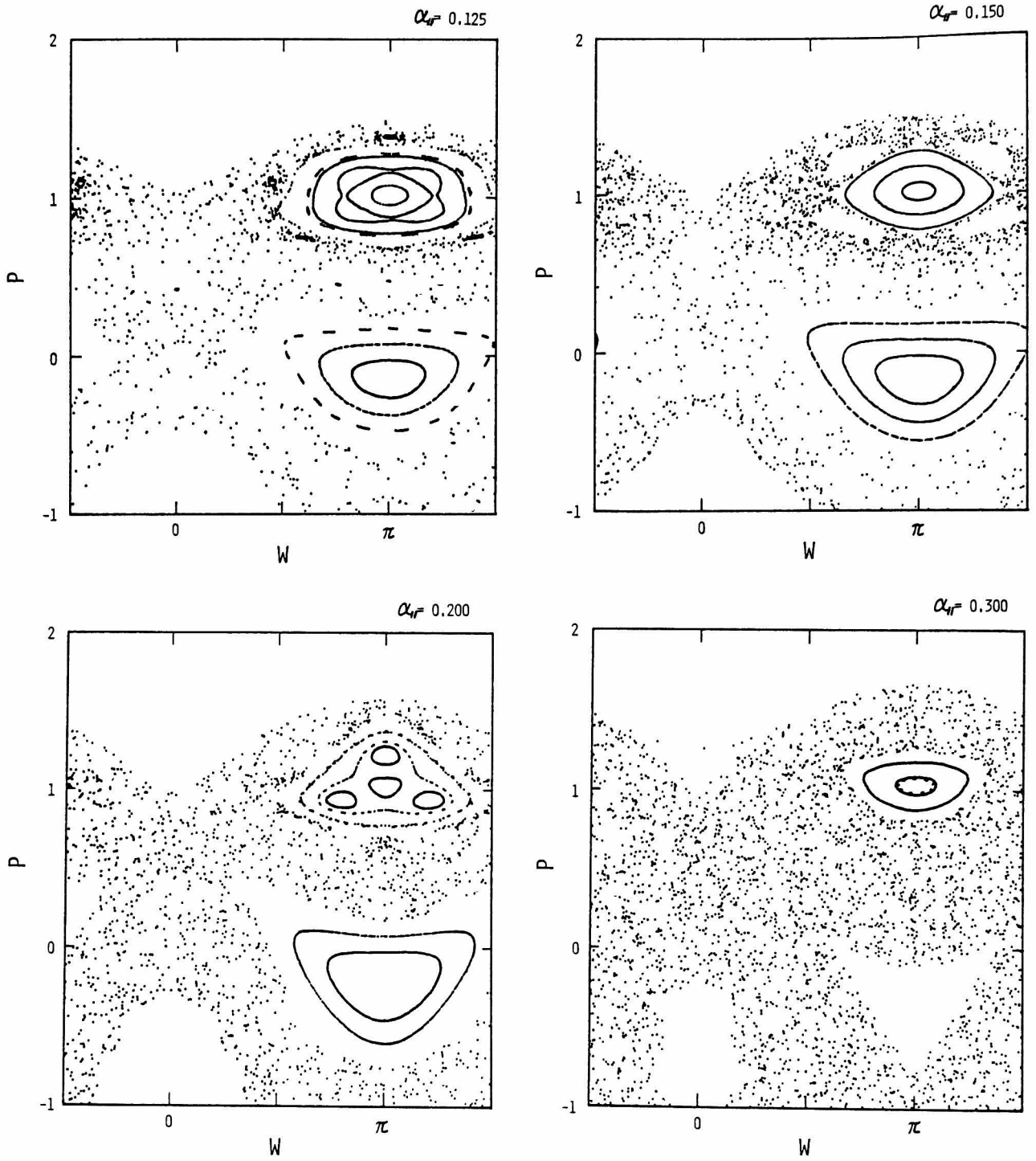
α_{II}= 0.125
α_{II}= 0.150
α_{II}= 0.200
α_{II}= 0.300
P
W
2
1
0
-1
0
π

Fig.5.4 (conti.)

two-dimensional phase surface and its intersection with the surface of section $\zeta = \pi$ is a curve in (ξ, P_ξ, P_ζ) space. A set of plotted points falls on a curve in the $\xi - P_\xi$ plane, while the points fill an area if no other constant of the motion exists.

Fig.5.4 shows the surface of section for various values of $\alpha_{\prime\prime}$ which is related to the wave amplitude as

$$\alpha_{\prime\prime} = k_{\prime\prime}^2 e\phi / m\omega_c^2 \quad . \tag{5.48}$$

The propagation angle of the wave with respect to the static magnetic field is $\pi/4$, i.e. $k_{\prime\prime} = k_\perp$, and the energy is given by $k_\perp \rho_E = k_\perp (2H_0/m)^{1/2}/\omega_c = 1.48$ for any initial condition. The motion of a particle is followed in the wave frame moving with the phase velocity. With $\alpha_{\prime\prime} = 0.025$, we can see that a constant of the motion indeed exists and two primary islands with $N = 0$ and -1 are formed. As the amplitude increases, secondary islands appear in the primary island ($\alpha_{\prime\prime} = 0.05$) and the motion of several particles near the separatrix becomes nonadiabatic ($\alpha_{\prime\prime} = 0.075$). Further increase of the wave amplitude causes a chaotic motion of the phase points over almost all the phase plane accessible for the constant energy $k_\perp \rho_E = 1.48$, except near the center of primary islands.

In order to compare numerical results with the analytical one, we have estimated an area of the primary island filled up with the phase points. The areas normalized by the total area of the primary island are indicated by crosses in Fig.5.5. The solid lines show the normalized area S_K for various values of $\gamma = \gamma_n + \gamma_{2N-n}$, where Chirikov's criterion (5.45) holds.

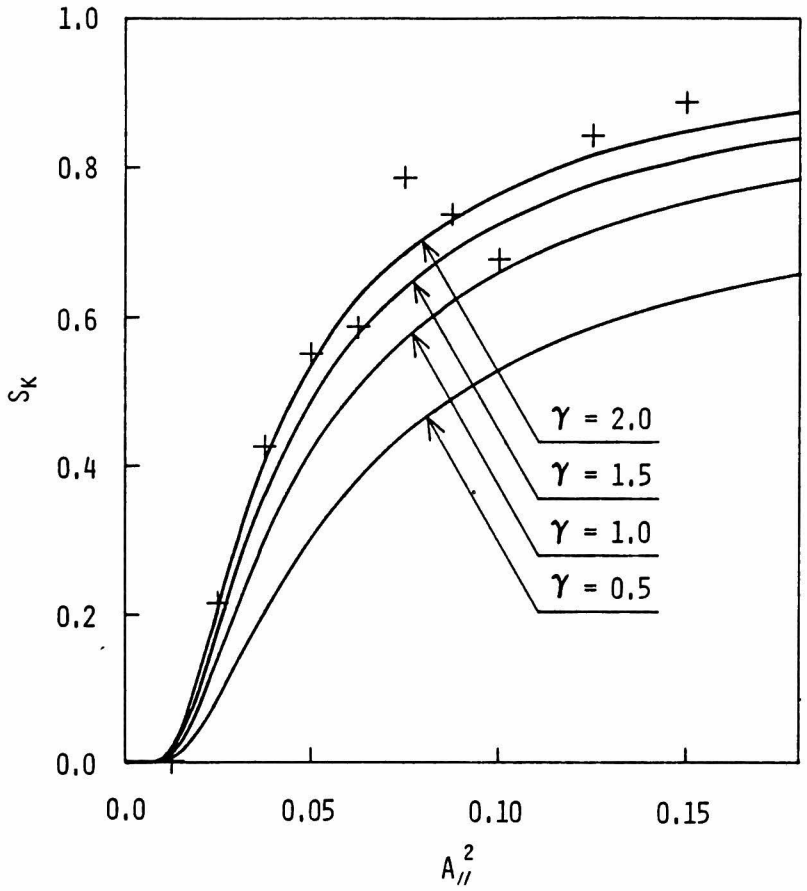

Fig.5.5 The normalized area S_K satisfying Chirikov's criterion vs. the normalized wave amplitude $A_{//}^2 (\propto \phi)$. Crosses indicate the result obtained from numerical computations. At the center of the island $(P=1)$ which we have observed, the coefficient γ takes a value of 1.84.

As soon as $A_{//}^2$ $[= \alpha_{//} J_1(k_\perp \rho)]$ exceeds the threshold value, 0.02, a stochastic layer suddenly appears at the vicinity of the separatrix and grows rapidly with $A_{//}^2$. In the small-$A_{//}$ limit, the area of the stochastic layer is approximated by

$$S_K \sim \frac{12}{A_{\prime\prime}^4} \gamma \exp\left[- \pi / 2 A_{\prime\prime} \right] , \qquad (5.49)$$

which is non-analytic at the vicinity of $A_{\prime\prime} = 0$. Compared with the rough estimate of the threshold derived from the overlapping of the primary islands, $A_{\prime\prime}^2 = 1/16 = 0.0625$, it is obvious that the above analysis which takes into account the secondary islands gives a more accurate description of an onset of the stochastic motion.

§5-4. Case of perpendicular propagation

§§5-4-1. Analytical treatment[79,81,82]

Since the LH wave has a small parallel wave number, results of the previous section for the obliquely propagating wave anticipate an extremely high threshold of the wave amplitude for the onset of stochastic motions. In this section, we wish to show that another mechanism, which a monochromatic wave with $k_{\parallel} \simeq 0$ may be responsible for, can bring about a stochastic motion of high-energy particles with $v_{\perp} > \omega/k_{\perp}$.

To simplify the analysis, we assume a wave propagating perpendicularly to the static magnetic field. The effect of a finite $k_{\parallel}$ will be discussed in §5-5. Since P_z is also a constant of the motion in case where $k_{\parallel} = 0$, the Hamiltonian (5.4) may be reduced to

$$H(\psi, P_\psi, t) = \omega_c P_\psi + e\phi \sum_n J_n(k_\perp \sqrt{2P_\psi/m\omega_c}) \cos(n\psi - \omega t) \ . \qquad (5.50)$$

By the use of a canonical transformation similar to eq.(5.8),

$$w = N\psi - \omega t \qquad \text{and} \qquad p = \frac{k_\perp^2 P_\psi}{Nm\omega_c} \qquad (5.51)$$

with an integer N nearest to ω/ω_c, the Hamiltonian (5.50) is expressed as the sum of the time-independent part $H_0(p,w)$ and the time-dependent one $H_1(p,w,\tau)$;

$$H_0(p,w) = \delta p + \alpha_\perp J_N(r) \cos w \ , \tag{5.52}$$

$$H_1(p,w,\tau) = \alpha_\perp \sum_{n\neq N} J_n(r) \cos[\frac{n}{N} w + \frac{n-N}{N} \nu\tau] \ , \tag{5.53}$$

with $\tau = \omega_c t$, $\nu = \omega/\omega_c$, $\delta = N - \nu$, $r = \sqrt{2Np} = k_\perp v_\perp/\omega_c$ and $\alpha_\perp = k_\perp^2 e\phi/m\omega_c^2$.

Let us first consider a motion derived from the averaged Hamiltonian $H_0(p,w)$.[83,84] The equations of motion obtained from eq.(5.52) read

$$\begin{cases} \dfrac{dr}{d\tau} = -\alpha_\perp \dfrac{N}{r} J_N(r) \sin w \ , \\ \dfrac{dw}{d\tau} = \delta + \alpha_\perp \dfrac{N}{r} J_N'(r) \cos w \ . \end{cases} \tag{5.54}$$

Qualitative phase trajectories ($H_0 = \text{const}$) are illustrated in Fig.5.6. We see that several particles are trapped whenever $r \gtrsim N$, if the frequency mismatch δ is smaller than $\alpha_\perp \max[NJ_N'(r)/r]$. with δ approaching zero, untrapped regions diminish and, finally, all ions are trapped in rectangular cells, which are enclosed by separatrices represented by $w = \pm\pi/2$ and $r = r^*$, where $J_N(r^*) = 0$. In contrast to the case of the oblique propagation, however, rectangular cells or primary islands never overlap, because an equi-H_0 surface in phase space is one-dimensional. Since no stochasticity appears in this order of approximation, we are led to pursue an analysis of the secondary island which is essential in the case of the perpendicular propagation. In order to obtain an analytic expression for the motion due to H_0, we shall consider

the case of high-energy particles with $v_\perp >> \omega/k_\perp$ and waves with a frequency lying near a cyclotron harmonic. The former condition, $r >> N$, enables us to use the asymptotic expansion of J_N :

$$J_N \sim \sigma \left(2/\pi r_0 \right)^{1/2} \cos \tilde{r} ,$$

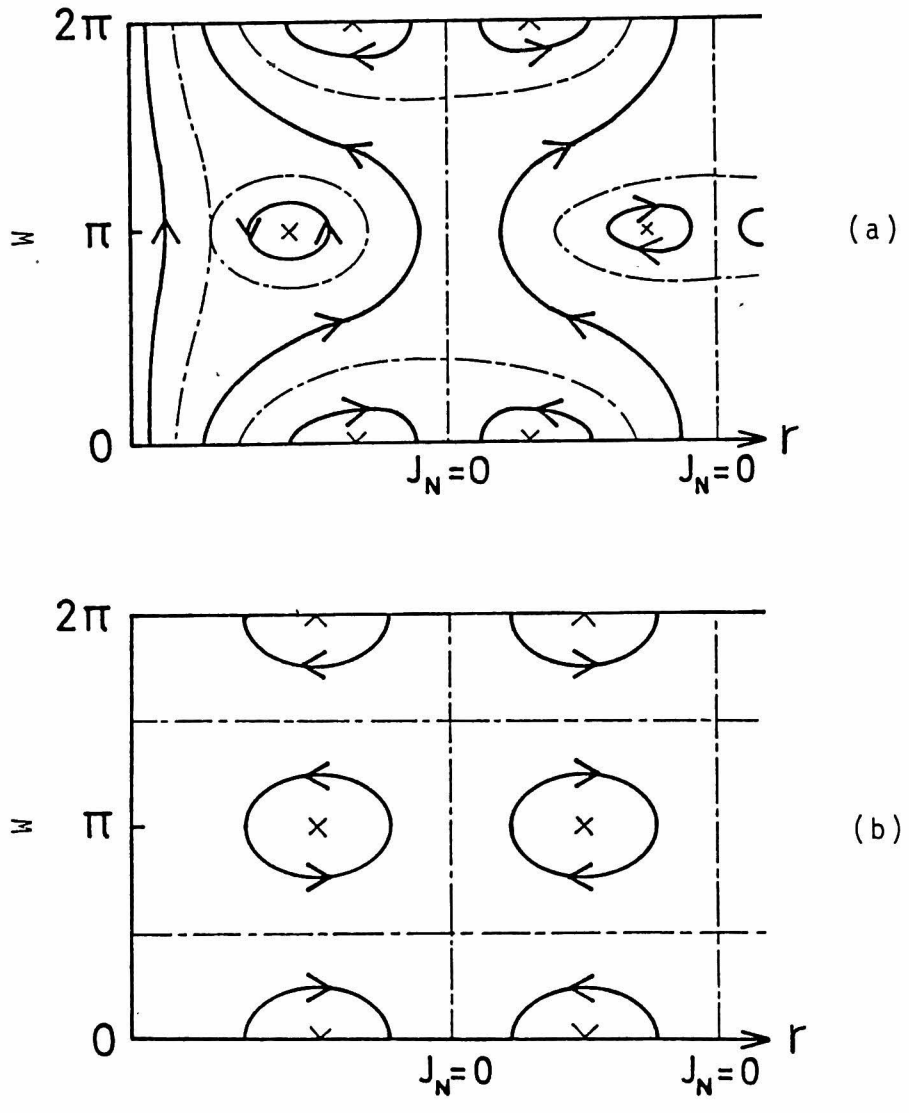

Fig.5.6 Qualitative phase trajectories derived from the time-independent part $H_0(p,w)$ for (a) $\delta \neq 0$ and (b) $\delta = 0$.

where r_0 satisfies $J_N'(r_0) = 0$ and $\tilde{r} = r - r_0 << r_0$. The quantity σ takes the value ± 1 depending on a value of r_0. Making use of the bounce frequency ω_t evaluated at the center of the trapping region,

$$\omega_t = \alpha_1 \frac{N}{r_0} |J_N(r_0)| \sim \alpha_1 \frac{2^{1/2}}{\pi^{1/2}} \frac{N}{r_0^{3/2}} , \tag{5.55}$$

we may express the latter condition as $\delta << \omega_t$. Under these conditions, the equation of motion of particles in the cell may be simplified to give

$$\frac{d\tilde{r}}{d\tau} = \omega_t \left[q^2 - \sin^2 \tilde{r} \right]^{1/2} , \tag{5.56}$$

the solution of which is given, in terms of the Jacobian elliptic functions, as

$$\begin{aligned} \sin \tilde{r} &= q \, \mathrm{sn}(\omega_t \tau) , & \cos \tilde{r} &= \mathrm{dn}(\omega_t \tau) , \\ \sin w &= q \frac{\mathrm{cn}(\omega_t \tau)}{\mathrm{dn}(\omega_t \tau)} , & \cos w &= \frac{\sqrt{1 - q^2}}{\mathrm{dn}(\omega_t \tau)} . \end{aligned} \tag{5.57}$$

The parameter q defined by

$$q^2 = 1 - \left(\frac{H_0}{\alpha_1 |J_N(r_0)|} \right)^2$$

vanishes at the center of the cell and becomes unity on the separatrix. It has been suppressed in the expressions for both the Jacobian elliptic functions and the elliptic integrals which will be introduced below.

Taking account of the periodicity of the elliptic functions, we can express the motion derived from H_0 in terms of the action-angle variables (I,θ) :

$$\frac{dI}{d\tau} = 0 \qquad \text{and} \qquad \frac{d\theta}{d\tau} = \Omega(I) = \frac{\pi}{2\,F(q)}\,\omega_t \ . \tag{5.58}$$

The relationship between the old and the new variables is given by the equations

$$\begin{cases} I(H_0) = \dfrac{1}{2\pi}\oint p\ dw = \dfrac{2}{\pi}\dfrac{r_0}{N}\displaystyle\int_0^q \frac{q}{(1-q^2)^{1/2}}\,F(q)\ dq\ , \\[2ex] \theta(w,H_0) = \dfrac{\partial}{\partial I}\displaystyle\int^w p\ dw = \dfrac{\pi}{2}\,\frac{F[\arcsin(q^{-1}\sin w\,),q]}{F(q)}\ , \end{cases} \tag{5.59}$$

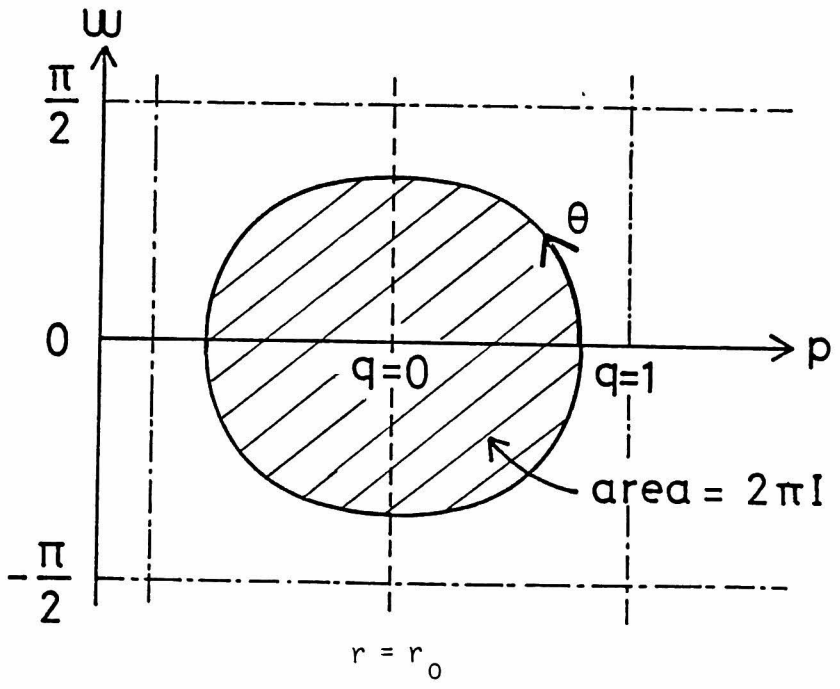

Fig.5.7 Illustration of the relationship between the action-angle variables (I,θ) and the original ones (p,w).

where the complete and the incomplete elliptic integrals of the first kind are denoted by $F(q) = F(\pi/2, q)$ and $F(\xi, q)$, respectively. It is readily seen from Fig.5.7 that a phase space area enclosed by a trajectory is equal to the action $2\pi I$ and an angle θ signifies a phase on the trajectory, $I =$ constant.

Since, in addition to the periodicity already involved in r and w, the time-dependent part H_1 has the period $(N - n)\nu/N$, a force derived from H_1 can resonate with particles in periodic motion which is determined by eqs.(5.58) and can form secondary islands on a resonant trajectory. When we use the asymptotic expansion of J_n, H_1 is approximated by

$$H_1 = 2\omega_t \frac{r_0}{N} \sum_{m=1}^{\infty} \left\{ \cos\tilde{r} \cos w \cos\frac{m\pi}{2} \cos m\frac{w + \nu\tau}{N} - \sin\tilde{r} \sin w \sin\frac{m\pi}{2} \sin m\frac{w + \nu\tau}{N} \right\} . \tag{5.60}$$

In the case of our present interest, $N >> 1$, the temporal variation of $\nu/N \sim O(\omega_t/N)$ may be neglected. Then the transformation of variables to (I, θ) gives the total Hamiltonian of the form

$$H(I, \theta, \tau) = H_0(I) + \sum_{m=-\infty}^{\infty} \sum_{s=-\infty}^{\infty} H_{ms}(I) \exp i[2(2s+1)\theta - (2m+1)\nu\tau/N] , \tag{5.61}$$

where

$$H_{ms}(I) = \omega_t \frac{r_0}{N} (-1)^m \frac{2\pi}{F(q)} \frac{a^{2s+1}}{1 - a^{2(2s+1)}}$$

and $\alpha = \exp[-\pi F(\sqrt{1-q^2})/F(q)]$. Also we have used the Fourier expansion of the Jacobian elliptic functions (Appendix B). The resonance condition for the secondary resonance is then given by

$$2(2s+1)\,\Omega(I_{rs}) = (2m+1)\omega / N\omega_c \sim 2m+1 \tag{5.62}$$

and therefore the frequency spacing of adjacent resonances can be approximated, for a integer $s >> 1$, as

$$\delta\Omega = \Omega(I_{r,s-1}) - \Omega(I_{rs}) \sim \frac{\pi^2}{F^2(q)} \frac{\omega_t^2}{2m+1} . \tag{5.63}$$

Following the discussion of §§5-2-2, we may estimate the width of secondary islands as

$$\Delta\Omega = 2 \left| 2 \frac{d\Omega(I_{rs})}{dI} H_{ms}(I_{rs}) \right|^{1/2} . \tag{5.64}$$

Finally, we obtain the stochastic parameter

$$K = \left(\frac{2\,\Delta\Omega}{\delta\Omega}\right)^2 = \frac{16}{\pi} \frac{1}{A_I^2} \frac{E - (1-q^2)F}{(1-q^2)^{1/2} q^2} \frac{b}{1-b^2} , \tag{5.65}$$

where $A_I = \omega_t / |2m+1|$, $b = \exp[-F(\sqrt{1-q^2})/A_I]$ and E denotes the complete elliptic integral of the second kind. If the condition $K > 1$ is fulfilled, secondary islands overlap and phase points are expected to move chaotically.

§§5-4-2. Results of numerical computations[79)]

The exact Hamiltonian (5.1) has been solved numerically for the case of the perpendicular propagation, $k_{\parallel} = 0$. Since there exists no adequate wave frame, we have worked out in the laboratory frame. Before illustrating exact numerical results by means of the surface-of-section method, it would be instructive to show in Fig.5.8 an averaged motion derived from H_0 for $\delta = 0$ and $\delta \neq 0$, in view of visualizing an existence of the primary islands which never overlap.

In Fig.5.9, numerically calculated phase points for $\delta = 0$

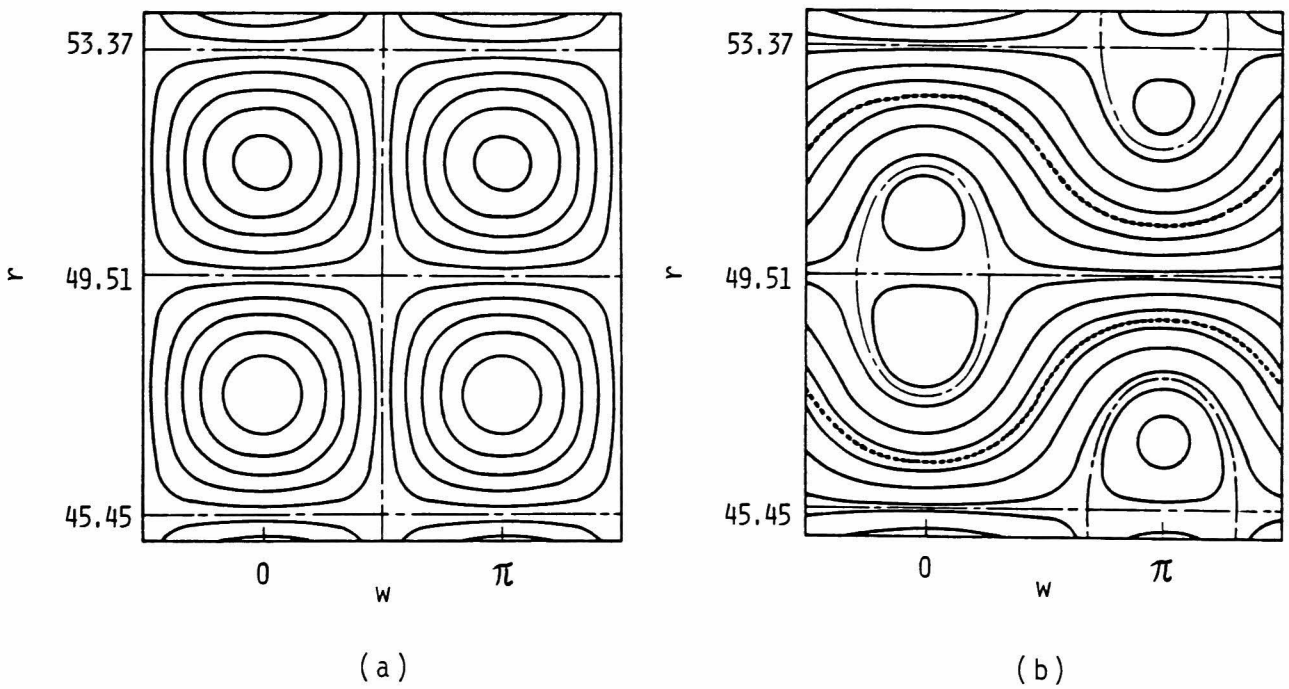

Fig.5.8 Examples of the trajectories derived from H_0 with a) $\nu = 30.00$, b) $\nu = 30.23$ and $\alpha_{\perp} = 6$. The broken line denotes the separatrix and the dotted line the $d\Omega / dI = 0$ trajectory.

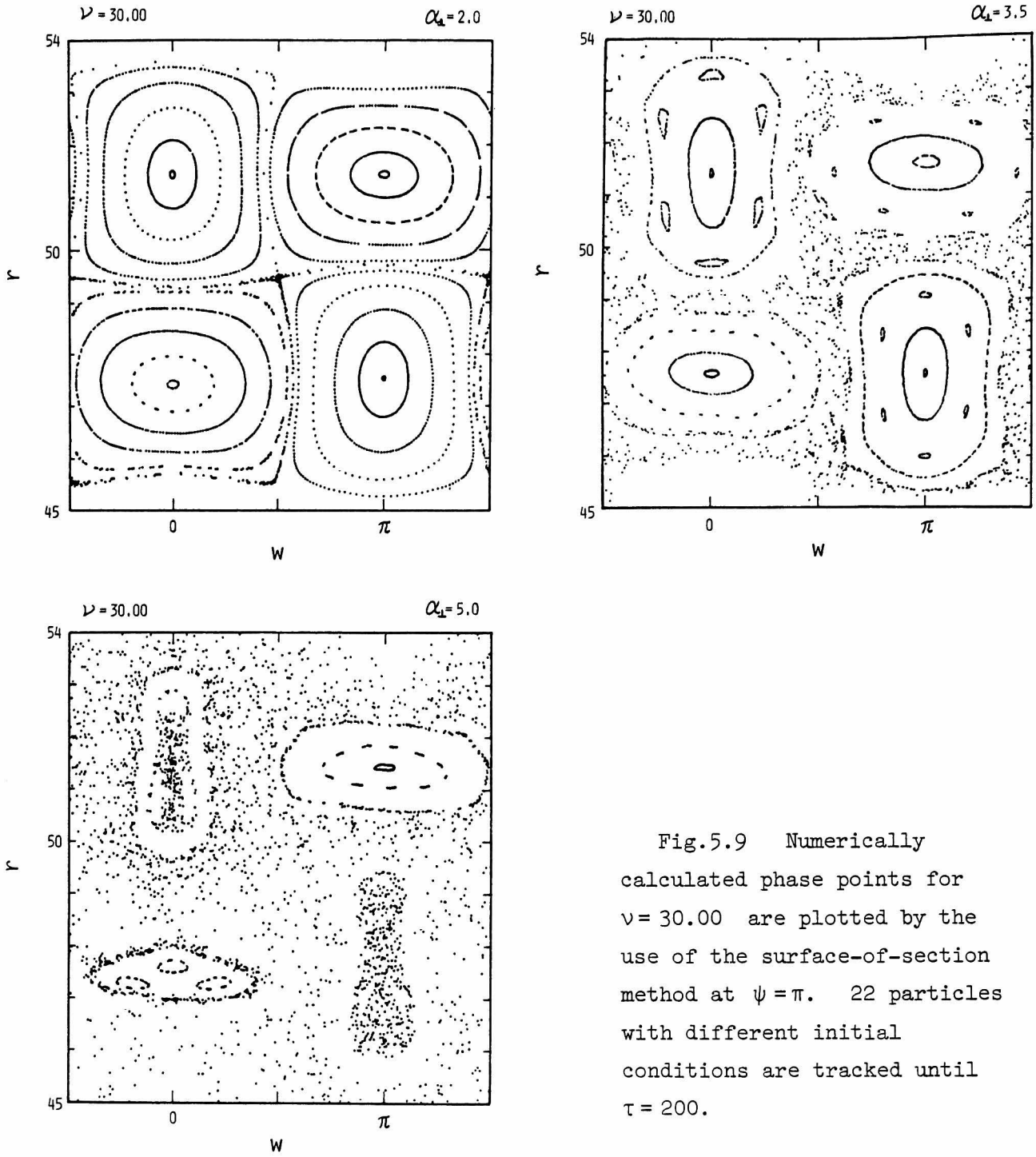

Fig.5.9 Numerically calculated phase points for $\nu = 30.00$ are plotted by the use of the surface-of-section method at $\psi = \pi$. 22 particles with different initial conditions are tracked until $\tau = 200$.

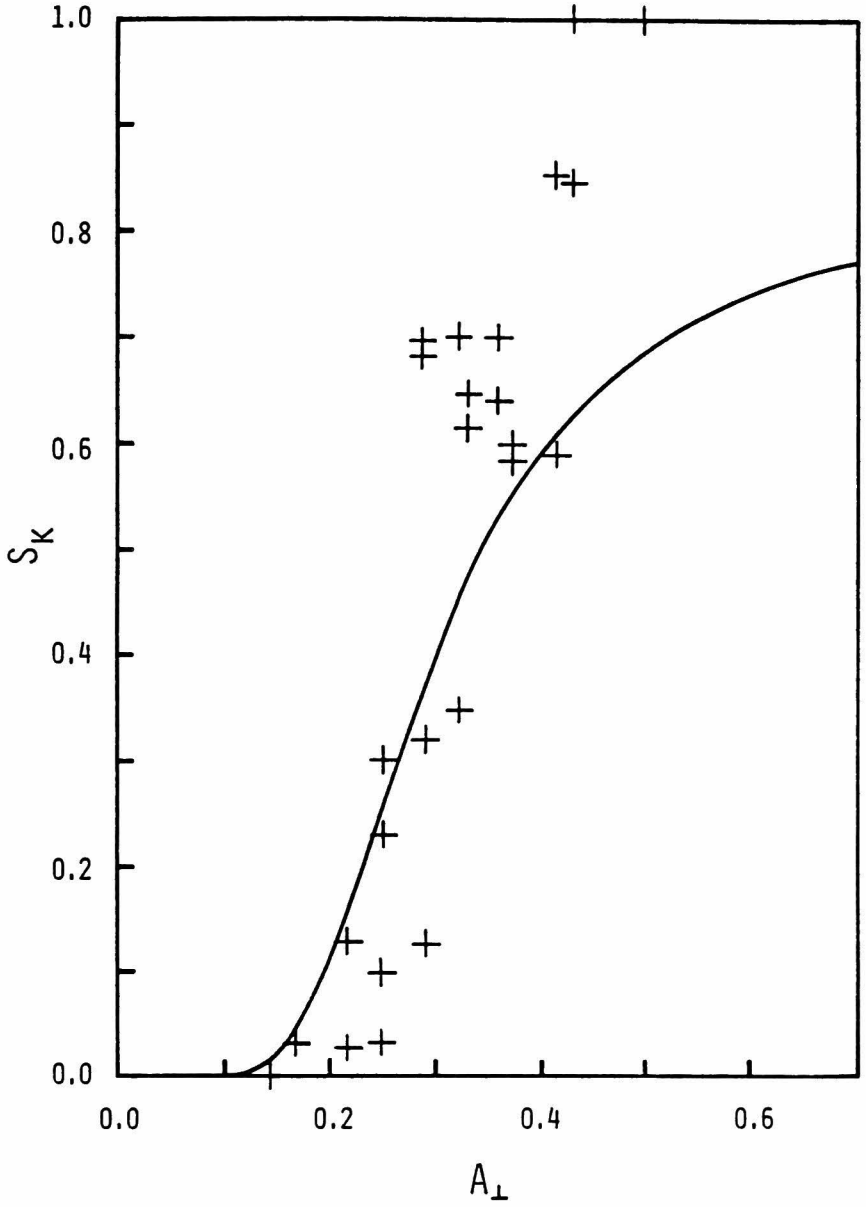

Fig.5.10 The normalized area S_K satisfying Chirikov's condition vs. the normalized amplitude $A_\perp (\propto \phi)$. Crosses indicate the value observed in numerical computations. (We have estimated $A_\perp$ for the dominant perturbation $m = 0$ and -1.)

are plotted as the intersection of the trajectory with a surface of section $\psi = \pi$. When the wave amplitude is small, most of particles move adiabatically in the primary islands. As the amplitude increases, secondary islands overlap near the separatrix and the motion becomes stochastic. Finally particles begin to wonder from one primary island to another. The normalized area S_k introduced in §§5-3-3 is indicated in Fig.5.10. Numerical results are also shown. If $A_1 << 1$, the ratio S_k is approximated by a function non-analytic at the vicinity of $A_1 = 0$ which reads

$$S_K \sim (32 / \pi^2 A_1^3) \exp(-\pi / 2 A_1) . \qquad (5.66)$$

It suggests that, for a small value of A_1, S_k is nonzero but extremely small. In Fig.5.10 we can observe abrupt increase of S_k, as soon as A_1 exceeds 0.15, which agrees well with the numerical results.

On the other hand, when the frequency mismatch is not negligible, i.e., $\delta \sim A_1$, a situation changes considerably. A momentum r of particles in nonlinear periodic motion described by $H_0(I)$ is limited between zeros of Bessel function J_N and secondary islands appear on the trajectory where particles in periodic motion resonates with the perturbation. But they never overlap on the trajectory where $\Omega(I)$ takes an extremum, $d\Omega(I)/dI = 0$ (see Fig.5.8 (b)), since the secondary islands with the same mode number s lie regularly on both sides of this trajectory. The topological development of the secondary islands in this region is illustrated in Fig.5.11, for a perturbation symmetric with respect to this trajectory. Here Δ denotes the frequency mismatch from the

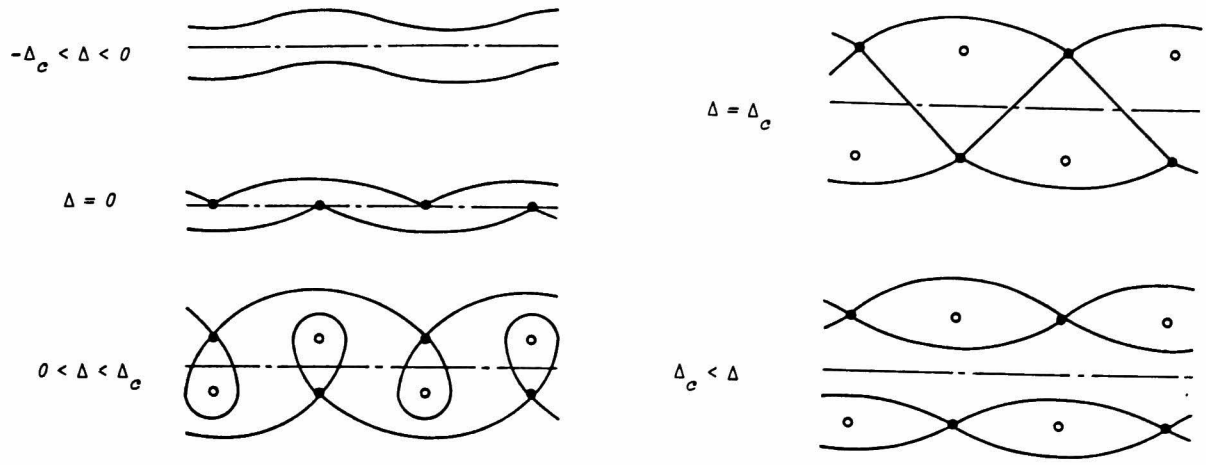

Fig.5.11 Topological development of the secondary islands near the $d\Omega/dI = 0$ trajectory for the symmetric perturbation.

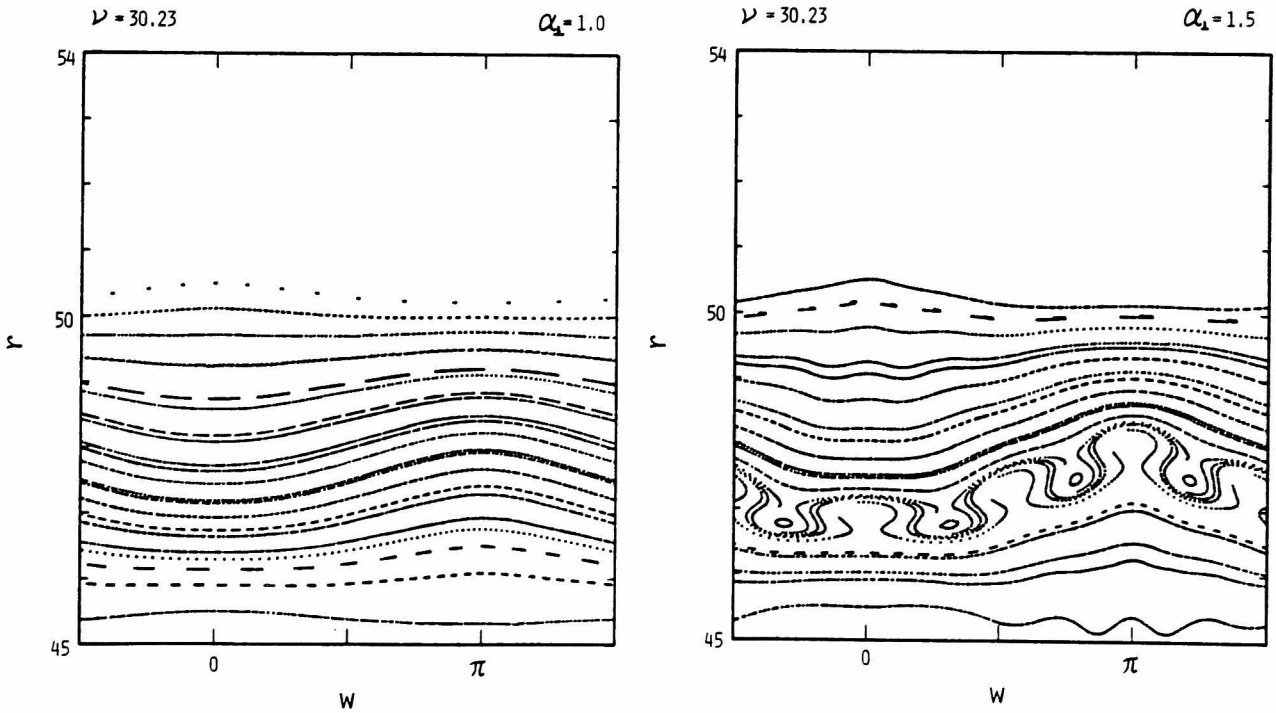

Fig.5.12 Numerically calculated phase points for $\nu = 30.23$.

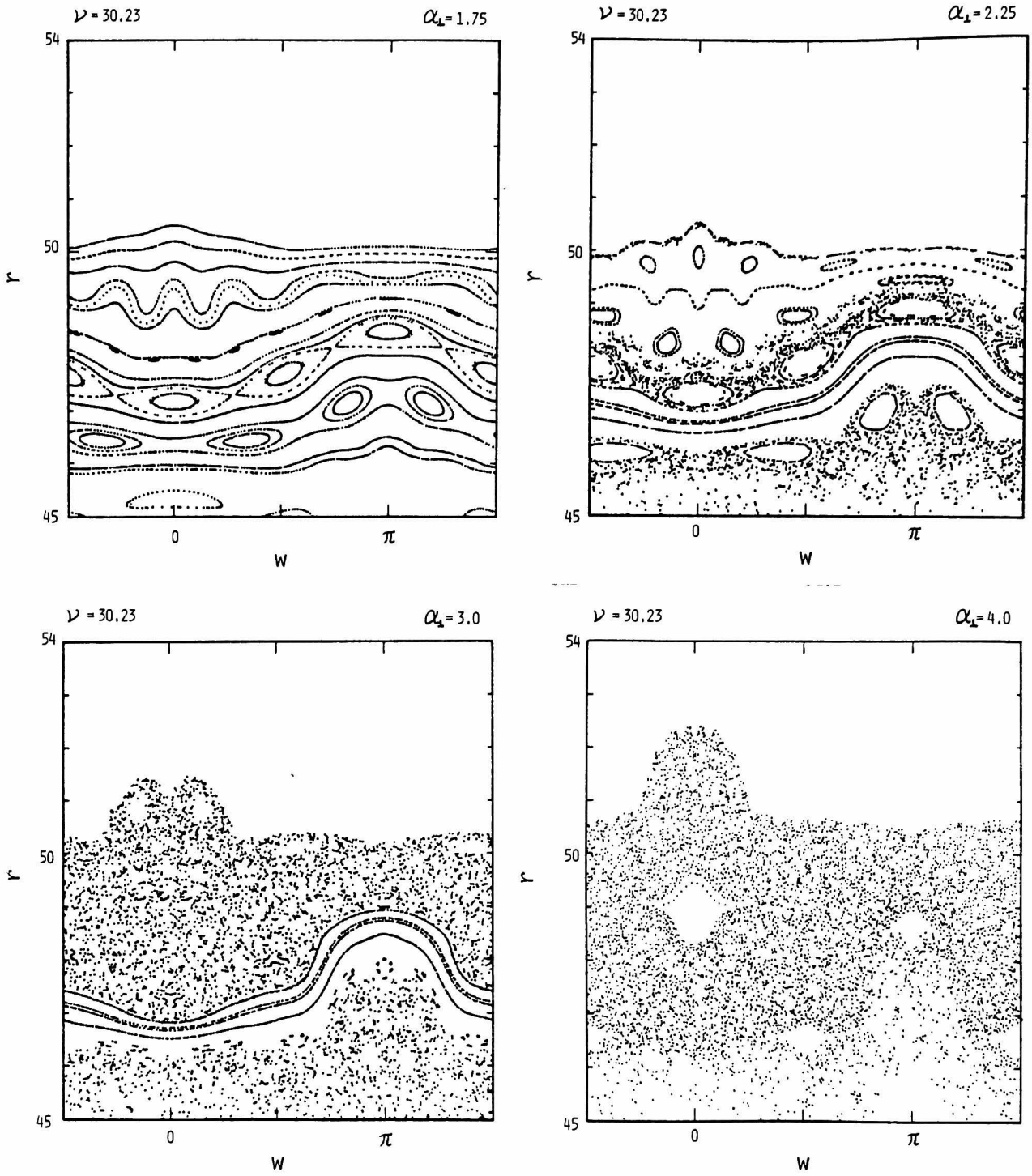

Fig.5.12 (conti.)

secondary resonance $s\Omega_{max} - (nM/N-m)\omega$ (see §5-2-2) and Δ_c is proportional to the perturbation amplitude. In order to obtain a condition that this layer be stochastic, it is necessary to take account of the higher-order resonance. It should be noted, however, that the same analytical difficulty due to the presence of $d\Omega(I)/dI = 0$ trajectory survives in higher-order approximations except the case $\Delta = \Delta_c$, in which two chains of islands contact to each other. Fig.5.12 shows the numerical result : When $\alpha_I = 1.5$, secondary islands $(s = 4)$ begins to grow at the $d\Omega(I)/dI = 0$ trajectory and its shape is similar to the case $0 < \Delta < \Delta_c$, as is seen in Fig.5.11. As the amplitude increases, $s = 4$ islands are separated and eventually overlap with $s = 5$ islands. However, the $d\Omega(I)/dI = 0$ trajectory is adiabatic and particles cannot go across the stopping band until $\alpha_I = 4.0$. For $\alpha_I = 4.0$, the stopping band $(r \sim 47)$ is cleared but another one $(r \sim 51)$ prevents particles from obtaining higher energy.

Including the case of cyclotron off-resonance, Karney and Bers[85] has examined the stochastic threshold numerically and obtained the condition for the onset of stochastic motions in a fraction of phase space of order unity, $A_I > 0.25$, which is independent of δ. However, the above discussion suggests that the stochastic threshold which determines a maximum energy a particle would gain, depends on δ to some extent, since there exists no layer which hardly becomes stochastic if $\delta << A_I$.

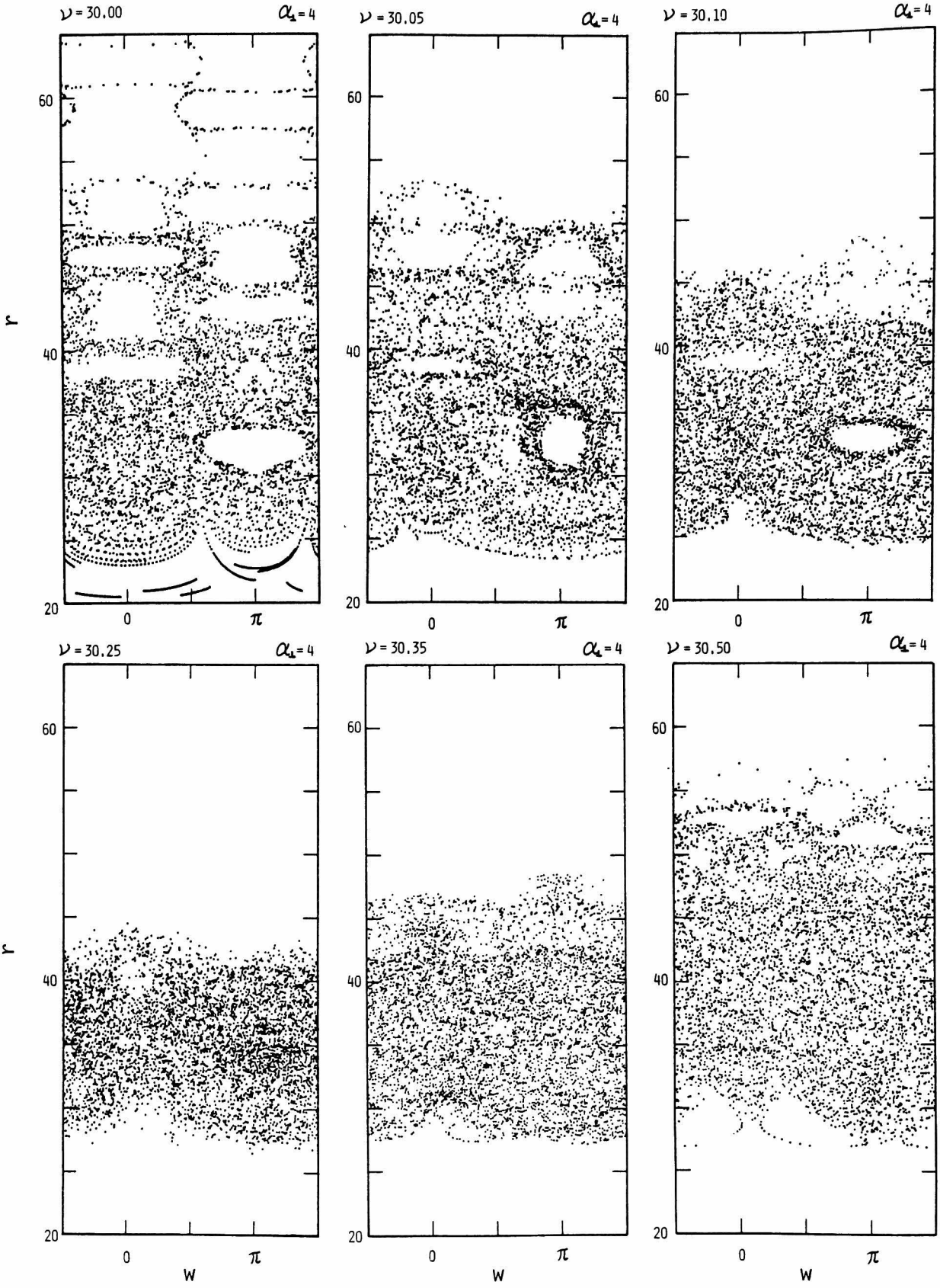

Fig.5.13 Distribution of 100 particles from $\tau = 300$ to 350 for a relatively small amplitude $\alpha_1 = 4$.

We have carried out numerical calculations on the particle distribtuion for various frequencies. Initially 100 particles are distributed randomly between $r = 33.5$ and $33.5 + 2\pi$. Figure 5.13 shows the distributions during the time interval from $\tau = 300$ to 350 for a relatively small amplitude $\alpha_1 = 4$. For a cyclotron resonance $\nu = 30.00$, a fraction of particles, acclerated, enter into a higher-energy region $r = 64$ $(\omega_t \sim 0.19)$ along the narrow stochastic layer near the separatrix. On the other hand, a stopping

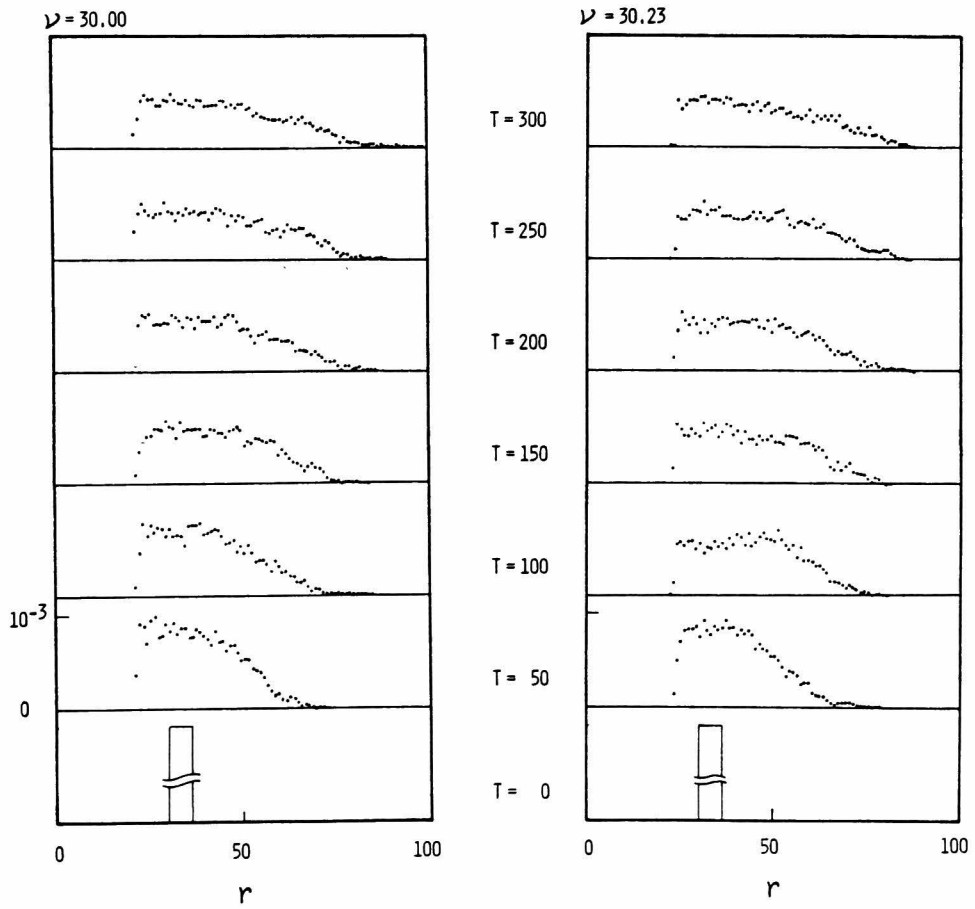

Fig.5.14 Time dependence of the distribution function, normalized by $\int f \cdot r\, dr = 1$ in the case of a large amplitude $\alpha_1 = 12$.

band near $r = 44$ ($\omega_t \sim 0.33$) hinders particles from being further accelerated for an off-resonant case $\nu = 30.25$. That rather higher-energy particles are produced in the case $\nu = 30.50$ is expected to be attributed to a half-integer cyclotron resonance which is of the order of ϕ^2. Another important feature to be mentioned is an attainable lowest energy which determines a number of stochastic particles in a Maxwellian plasma, because of the abundance of particles with low energy. Also in this respect, a wave with frequency close to cyclotron harmonics picks up the lowest-energy particles in spite of the slowness of the motion.

When the wave amplitude is sufficiently large, we find that the δ-dependence of the maximum energy becomes less important. It is partly because the particle number in such a high-energy regime is small and partly because it takes a long time for particles to obtain high energy. Note also that a velocity distribution of stochastic particles becomes almost independent of δ and that the time dependence of the distribution indicated in Fig.5.14 is insensitive to the wave frequency.

§5-5. Discussion

We have investigated the problem of the intrinsic stochasticity of charged particles subject to a uniform magnetic field and an electrostatic wave and have confirmed that results obtained from analytical study on the overlapping of secondary islands are in good agreement with the numerical results. In this section, we shall discuss the stochastic tail formation in LH wave heating.

Since the LH wave in a central part of the plasma column has a very small but finite $k_{\parallel}$ compared with $k_{\perp}$, we have studied this finite-$k_{\parallel}$ effect in Refs. 86 and 87. The result shows that, if we define $\delta = N - \nu + k_{\parallel} v_z/\omega_c$ and the condition

$$\frac{k_{\parallel}^2}{k_{\perp}^2} \ll \frac{k_{\perp}^2 e\phi}{m\omega_c^2} \left(\left[1 - \frac{N^2}{r^2} \right] - \frac{r J_N'^2}{J_N} \right) \frac{N^2}{r^2} J_N \cos\xi - \delta \frac{N J_N'}{J_N} \tag{5.67}$$

is satisfied, the analysis of §5-4 is not altered. Since $(k_{\parallel}/k_{\perp})^2$ is of the order of m_e/m_i, the condition (5.67) may be satisfied in most of phase space where $v_{\perp} \gtrsim \omega/k_{\perp}$, except at the vicinity of the separatrices of primary islands. Another effect of finite $k_{\parallel}$ is a frequency mismatch which increases with increasing perpendicular kinetic energy. The energy conservation in the wave frame leads to the relation,

$$\Delta\delta = \Delta\left(\frac{k_{\parallel} v_z}{\omega_c} \right) \sim \frac{k_{\parallel}^2}{k_{\perp}^2} \frac{\omega_c}{\omega} \frac{1}{2} \Delta\left(\frac{k_{\perp}^2 v_{\perp}^2}{\omega_c^2} \right), \tag{5.68}$$

valid for $\Delta\delta << \omega/\omega_c$. Since the factor $(k_{\parallel}^2/k_{\perp}^2)(\omega_c/\omega)$ is of the order of $(m_e/m_i)^{3/2}$ for the LH wave, however, increase of the perpendicular energy may be very large, before the frequency

mismatch becomes serious.

In the case of the perpendicular propagation, it has been shown in §5-4 that the condition for the appearance of a stochastic layer is given by $\omega_t \gtrsim 0.15$. This condition may be interpreted as a condition which determines an upper bound of the high-energy tail,

$$\frac{\omega}{\omega_c} < \frac{k_\perp v_\perp}{\omega_c} < 3\left(\frac{\omega}{\omega_c}\frac{k_\perp^2 e\phi}{m\omega_c^2}\right)^{2/3}. \tag{5.69}$$

The lower bound is given by the condition that the Bessel function J_N have a considerable magnitude. Although we have assumed that $\delta \ll \omega_t$ in §5-4-1, numerical calculations have shown that, if $\omega_t > 0.33$, particles are accerelated independently of δ. Recently, Abe et al[87] have numerically analysed the tail formation of ions which initially have a Maxwell velocity distribution. They have carefully discussed the effect of finite $k_\parallel$ and the dependences of an acceleration mechanism on both δ and ω/ω_c.

In the LH wave heating experiment on JFT-2, a high-energy tail of the ion perpendicular-energy distrubtuion has been observed at above 2 KeV. This lower-bound energy corresponds to a wave number $k_\perp \sim 8 \times 10^3\ \mathrm{m}^{-1}$ for a wave frequency 750 MHz. If we try to estimate a minimum wave amplitude for the onset of the tail formation by eq.(5.69), we obtain a potential ϕ as small as 3 V. This low threshold is due to the relatively large wave number and a weak magnetic field ($B_0 = 1.3\,\mathrm{T}$). For the wave amplitude $\phi = 30$ V, the maximum attainable energy is calculated to be about 30 KeV. If a power density is roughly estimated as $\Gamma \sim v_{Ti}\varepsilon_0|E_\perp|^2$, we obtain $\Gamma \sim 12.5\ \mathrm{W/cm}^2$ for $\phi = 30$ V. The total power 250 kW, considered to be transmitting through a surface of a torus with $r = 5$ cm

and $R = 90$ cm, is not far from 125 kw observed in actual experiments, if we take account of a nonuniformity of the wave on the torus surface.

In order to calculate a tail temperature and an absorbed power, we have to include in the analysis the effect of a collisional relaxation on the high-energy tail. This problem has recently been attacked by Karney,[88] who approximated the stochastic process by a simple Fokker-Planckequation. Although we have treated only a plane wave, sharply localized electric fields have also been proved to produce a high-energy tail.[89] Extension of our results to an inhomogeneous case is left open for further studies.

Chapter 6

SUMMARY AND CONCLUSIONS

In Chapter 3, we have investigated the coupling of a waveguide array with electromagnetic fields in a low-density low-temperature surface plasma. The linear coupling analysis has shown that the reflection coefficient, seen from a wave source, depends on both the relative phase difference $\Delta\Phi$ and the density gradient in front of the waveguide. When a density at the plasma surface well exceeds the cutoff density, the coupling becomes insensitive to the density gradient for large $\Delta\Phi$. Taking account self-consistently of the static density depression due to the ponderomotive force, we have derived a nonlinear wave equation which governs the propagation of LH waves in a surface plasma. The power-density dependence of the reflection coefficient has been obtained by solving numerically the nonlinear wave equation which has been reduced to a one-dimensional form by retaining only the fundamental mode of the waveguide array. Results reveal the existence of an upper limit of the transmitted power-density, typically of several kW/cm^2, which may be attributed to an enlargement of the cutoff region. Since there exists an optimal surface density imposed by a parallel refractive index $N_{\parallel}$, the reflection coefficient decreases with increasing power-density, whenever the unperturbed surface density exceeds the optimal value. As soon as the power density passes by an optimum corresponding to the optimum value for the surface density, however, the reflection coefficient rapidly increases and approaches unity.

In view of realizing an efficient high-power LH heating,

results of our analysis will serve as an indispensable guide for the design of an optimized waveguide array which launches LH waves with a desirable $N_{\parallel}$-spectrum at as high as possible power-densities.

In Chapter 4, we have analysed the nonlinear propagation of LH waves in a high-density plasma core. First, we have derived the nonlinear equation which well describes the competition between thermal dispersion and density depression due to the ponderomotive force. In a homogeneous plasma, the equation can be reduced to the complex modified Korteweg-de Vries equation, and, in particular, in the limit of a rapid phase variation, to the nonlinear Schrödinger equation. In an inhomogeneous plasma, it has been shown that, near the linear mode-conversion point, a wave packet is governed by the nonlinear Schrödinger equation with a linearly increasing potential. Numerical solutions suggest that, when the wave amplitude is small, a wave packet with a small width in the direction of the magnetic field easily spreads out near the mode-conversion point and its amplitude decreases immediately. On the other hand, a large-amplitude wave packet forms a soliton which preserves its shape even after the mode-conversion. Further increase of the wave amplitude causes a filamentation.

Proper estimate of the parameters taken from actual experimental data on JFT-2 has indicated that, even with sufficiently large power-density, a limited spatial extent of the waveguide array parallel to the magnetic field acts to spread the wave packet before it reaches the mode-conversion point and thus prevents it from forming filaments. Since a longer density scale-length may lead to a further spreading due to thermal dispersion, the

filamentation near the mode-conversion point is not expected to be observable in large-scale fusion devices, unless the extent of the waveguide array be chosen long enough along the magnetic field.

In Chapter 5, the formation of a high-energy tail on a velocity distribution, due to a monochromatic wave propagating through a magnetized plasma, has been extensively analysed, with emphasis laid on a threshold for the onset of stochastic motions. According to the Hamiltonian formulation for the motion of a charged particle, we have treated the cases of both oblique and perpendicular propagations. The onset of an intrinsic stochasticity has been estimated with the aid of Chirikov's criterion which dictates an overlapping condition for the secondary islands in phase space. The analytical prediction of an area of phase space, where the motion of particles becomes non-adiabatic, is in good agreement with results of numerical computations based on the exact Hamiltonian.

Since the parallel wave number $k_{\parallel}$ of the LH wave is very small compared with the perpendicular wave number $k_{\perp}$ in the central part of a plasma column, analysis of the perpendicular propagation can be applied to the LH wave. A threshold for the amplitude of an electric field which is responsible for the onset of an intrinsic stochasticity is therefore proportional to $k_{\perp}^{-1}$. As the threshold decreases near the linear mode-conversion point where $k_{\perp}$ increases considerably, the LH wave after the mode conversion may readily produce high-energy ions at the vicinity of the resonance points of the ion cyclotron harmonics. Since the wave energy is converted mainly into the perpendicular kinetic energy of ions, we may expect the formation of a high-energy tail in the

perpendicular velocity distribution, as is often observed in actual experiments. It should be noted, however, that the intrinsic stachasticity is not a sole mechanism which is responsible for the tail formation.

So far, we have investigated several important nonlinear effects in the problem of LH wave heating. From the engineering point of view, we believe that our results allow us to explore an efficient method for the high-power heating of a magnetically confined plasma by means of the LH wave. This does not mean that all essential problems have been thoroughly understood. We have to be aware of the actual states of art that a number of difficult nonlinear problems are still left open to a future study.

ACKNOWLEDGEMENTS

It is a great pleasure to acknowledge Professor Ryohei Itatani for his continuous guidance and stimulating discussions from the beginning of my research on plasma physics at Department of Electronics, Faculty of Engineering, Kyoto University.

I wish to express my most sincere thanks to Professor Hiromu Momota who has initiated me to the theoretical study of plasma heating by RF waves and, with constant encouragement and enlightening discussions, has helped me to finish this thesis.

I wish to thank Professor Yoichiro Furutani for his critical discussions since my appointment to Department of Electronics, School of Engineering, Okayama University. His efforts for the careful reading of the manuscript should also be acknowledged.

Thanks are due to many plasma physicists. Among them, I should like especially to thank Dr. T. Takizuka of Japan Atomic Energy Research Institute at Tokai, Dr. H. Abe of Department of Electronics, Faculty of Engineering, Kyoto University, Dr. M. Okamoto, Dr. H. Sanuki and Dr. Y. Tomita of Institute of Plasma Physics, Nagoya University, who have helped my scientific evolution with their fruitful and pleasant discussions and criticisms.

Numerical calculations have been carried out at Okayama University Computer Center, Data Processing Center of Kyoto University and Computer Center of Institute of Plasma Physics, Nagoya University.

Appendix A. WKB solution to the linearized version of eq.(4.5)

In the plane-wave limit $(\partial\psi/\partial z = 0)$, we shall consider the linearized version of eq.(4.5). Denoting by L_n the scale length of the density gradient and assuming the small quantity $1/(k_+ L_n)$ to be of the order of δ^4, we obtain an equation correct up to the order of δ^4,

$$
\begin{aligned}
&[k_-^2 - \frac{k_-^4}{4k_+^2}]\psi + i\frac{k_-^2}{k_+}\frac{\partial\psi}{\partial x} + [1 - \frac{k_-^2}{2k_+^2}]\frac{\partial^2\psi}{\partial x^2} + \frac{i}{k_+}\frac{\partial^3\psi}{\partial x^3} - \frac{1}{4k_+^2}\frac{\partial^4\psi}{\partial x^4} \\
&+ i\frac{k_-^2}{2k_+}[\frac{k_+'}{k_+} + \frac{2k_-'}{k_-} + \frac{\alpha'}{\alpha}]\psi + \{2\frac{k_+'}{k_+} - \frac{k_-^2}{k_+^2}\frac{k_-'}{k_-} + [1 - \frac{k_-^2}{2k_+^2}]\frac{\alpha'}{\alpha}\}\frac{\partial\psi}{\partial x} \\
&+ i\frac{3}{2k_+}[\frac{k_+'}{k_+} + \frac{\alpha'}{\alpha}]\frac{\partial^2\psi}{\partial x^2} - \frac{1}{2k_+^2}\frac{\alpha'}{\alpha}\frac{\partial^3\psi}{\partial x^3} = 0 \ ,
\end{aligned}
\tag{A.1}
$$

where the dash stands for the derivative with respect to x. Now, setting

$$
\psi(x) = f(x)\exp[\ \pm\int^x k_-(x')\,dx'\ ]
$$

and using the WKB approximation with the subsidiary ordering $\partial\ln f/\partial x \sim O(1/L_n)$, we obtain

$$
\frac{1}{f}\frac{df}{dx} = -\frac{k_+'}{2k_+} - \frac{k_-'}{2k_-} - \frac{1}{2}\frac{k_+' \mp k_-'}{k_+ \mp k_-} - \frac{1}{2}\frac{\alpha'}{\alpha} \ . \tag{A.2}
$$

Accordingly, the WKB solution to eq.(A.1) is given by

$$
\psi = A\frac{\exp[-i\int^x k_-(x')dx']}{[\alpha k_+ k_-(k_+ + k_-)]^{1/2}} + B\frac{\exp[\ i\int^x k_-(x')dx']}{[\alpha k_+ k_-(k_+ - k_-)]^{1/2}} \ . \tag{A.3}
$$

Appendix B. Formulae of the Jacobian elliptic functions[90)]

1. Relations between the functions

$$\mathrm{cn}^2 u = 1 - \mathrm{sn}^2 u$$

$$\mathrm{dn}^2 u = 1 - q^2 \mathrm{sn}^2 u$$

2. Differential identities

Function	Derivative
$\mathrm{sn}\, u$	$\mathrm{cn}\, u \;\; \mathrm{dn}\, u$
$\mathrm{cn}\, u$	$-\mathrm{sn}\, u \;\; \mathrm{dn}\, u$
$\mathrm{dn}\, u$	$-q^2 \mathrm{sn}\, u \;\; \mathrm{cn}\, u$

3. Series expansions in terms of the nome: $a \equiv \exp[-\pi F(\sqrt{1-q^2})/F(q)]$

$$\mathrm{sn}\, u = \frac{2\pi}{qF} \sum_{s=0}^{\infty} \frac{a^{s+1/2}}{1 - a^{2s+1}} \sin[(2s+1)\, \frac{\pi u}{2F}]$$

$$\mathrm{cn}\, u = \frac{2\pi}{qF} \sum_{s=0}^{\infty} \frac{a^{s+1/2}}{1 + a^{2s+1}} \cos[(2s+1)\, \frac{\pi u}{2F}]$$

$$\mathrm{dn}\, u = \frac{\pi}{2F} + \frac{2\pi}{F} \sum_{s=1}^{\infty} \frac{a^{s}}{1 + a^{2s}} \cos[\, 2s\, \frac{\pi u}{2F}]$$

$$\mathrm{sn}^2 u = \frac{F - E}{q^2 F} - \frac{2\pi^2}{q^2 F^2} \sum_{s=1}^{\infty} \frac{s\, a^{s}}{1 - a^{2s}} \cos[\, 2s\, \frac{\pi u}{2F}]$$

The last formula can be derived by combining eqs. (17.2.10), (17.4.28) and (17.4.38) in Ref. 90.

REFERENCES

1) H. Eubank *et al* : Phys. Rev. Lett. 43 (1979) 270.

2) V.M.Glagolev *et al* : in *Plasma Physics and Controlled Nuclear Fusion Research (Proc. 4th Int. Conf., Wisconsin, 1971)* IAEA-CN-28/L-6.

3) B.V. Galaktionov *et al* : Sov. Phys.-Tech. Phys. 15 (1971) 1809.

4) V.V. Alikaev *et al* : Sov. Phys.-Tech. Phys. 20 (1975) 327.

5) S. Bernabei, C. Daügnney, W. Hooke, R. Motley, T. Nagashima, M. Porkolab and S. Suckewar : in *Plasma Heating in Toroidal Devices (Proc. 3rd Symp. Varenna-Como, Italy, 1976)*, Editrice Compositori, Bologna, 68.

6) M. Porkolab, S. Bernabei, W.M. Hooke, R.W. Motley and T. Nagashima : Phys. Rev. Lett. 38 (1977) 230.

7) H.D. Pacher *et al* : in *Plasma Physics and Controlled Nuclear Fusion Research (Proc. 7th. Int. Conf., Innsbruck, 1978)* 1 97.

8) P. Briand *et al* : in *Plasma Physics and Controlled Nuclear Fusion Research (Proc. 7th. Int. Conf., Innsbruck, 1978)* 1 65.

9) PETULA Group : in *Controlled Fusion and Plasma Physics (Proc. 9th European Conf., Oxford, 1979)* 1 21.

10) T. Fujii *et al* : in *Plasma Physics and Controlled Nuclear Fusion Research (Proc. 7th. Int. Conf., Innsbruck, 1978)* 1 85.

11) T. Imai *et al* : Phys. Rev. Lett. 43 (1979) 586.

12) T. Imai *et al* : Bull. Phys. Soc. Japan (1980) March, 29a-Z-9.

13) V.E. Golant *et al* : in *Plasma Physics and Controlled Nuclear Fusion Research (Proc. 7th. Int. Conf., Innsbruck, 1978)* 1 113.

14) R.L. Freeman *et al* : in *Plasma Physics and Controlled Nuclear Fusion Research (Proc. 7th. Int. Conf., Innsbruck, 1978)* 1 157.

15) J.J. Schuss *et al* : Phys. Rev. Lett. 43 (1979) 274.

16) J. Fujita *et al* : in *Controlled Fusion and Plasma Physics (Proc. 9th. European Conf., Oxford, 1979)* 1 13.

17) M. Porkolab : Phys. Fluids 17 (1974) 1432.

18) M. Porkolab : Phys. Fluids 20 (1977) 2058.

19) R.L. Berger, Liu Chen, P.K. Kaw and F.W. Perkins : Phys. Fluids 20 (1977) 1864.

20) V.K. Tripathi, C.S. Liu and C. Grebogi : Phys. Fluids 22 (1979) 301.

21) T.H. Stix : Phys. Rev. Lett. 15 (1965) 878.

22) V.E. Golant : Sov. Phys.-Tech. Phys. 16 (1972) 1980.

23) H. Momota, A. Fukuyama, M. Azumi, M. Okamoto and T. Takizuka : *Report of Japan Atomic Energy Research Institute*, JAERI-M 6964 (1977).

24) S. Ichimaru : *Basic Principles of Plasma Physics* (Benjamin, 1973).

25) M. Brambilla : Plasma Phys. 18 (1976) 669.

26) A.D. Piliya and V.I. Fedorov : Sov. Phys.-JETP 30 (1970) 653.

27) T.W. Tang : Phys. Fluids 13 (1970) 121.

28) B.N. Moore and M.E. Oakes : Phys. Fluids 15 (1972) 144.

29) P.M. Bellan and M. Porkolab : Phys. Fluids 17 (1974) 1592.

30) M. Okamoto, M. Azumi, T. Takizuka and A. Fukuyama : J. Phys. Soc. Japan 46 (1979) 1333.

31) S.S. Pesic : Plasma Phys. 15 (1973) 193.

32) M.D. Simonutti : Phys. Fluids 18 (1975) 1524.

33) K. Ohkubo, K. Ohasa and K. Matsuura : J. Phys. Soc. Japan, 43 (1977) 642.

34) E. Ott, J.M. Wersinger and P.T. Bonoli : Phys. Fluids 22 (1979) 192.

35) M. Porkolab : private communication.

36) P. Lallia : in *RF Plasma Heating (Proc. 2nd Top. Conf., Lubbok, 1974)*, paper C3.

37) M. Brambilla : Nucl. Fusion 16 (1976) 47.

38) M. Brambilla : Nucl. Fusion 19 (1979) 1343.

39) V. Krapchev and A. Bers : Nucl. Fusion 18 (1978) 519.

40) Yu.F. Baranov and O.N. Shcherbinin : Fiz. Plazmy 3 (1977) 246 [Sov. J. Plasma Phys. 3 (1977) 136].

41) M. Fichet and I. Fidone : Plasma Phys. 21 (1979) 901.

42) S. Bernabei, M.A. Heald, W.M. Hooke, R.W. Motley. F.J. Paolini, M. Brambilla and W.D. Getty : Nucl. Fusion 17 (1977) 929.

43) G.J. Morales and Y.C. Lee : Phys. Rev. Lett. 35 (1975) 930.

44) G.J. Morales : Phys. Fluids 20 (1977) 1164.

45) V.S. Chan and S.C. Chiu : Phys. Fluids 22 (1979) 1724.

46) A. Bers : in *RF Plasma Heating (Proc. 3rd Top. Conf., Pasadena, 1978)* A1-1.

47) T. Imai, T. Nagashima and M. Azumi : *Report of Japan Atomic Energy Research Institute*, JAERI-M 6902 (1977).

48) M. Abramowitz and I.A. Stegun : *Handbook of Mathematical Functions*, Dover Publ. (1970) 10.4.

49) Y. Gomay, N. Fujisawa, M. Maeno, N. Suzuki, K. Uehara, T. Yamamoto and S. Konoshima : Nucl. Fusion 18 (1978) 849.

50) A. Fukuyama, T. Morishita and Y. Furutani : Plasma Phys. 22 (1980) in press.

51) A.N. Kaufman, J.R. Cary and N.R. Pereira : Phys. Fluids 22 (1979) 790.

52) V. Krapchev and A. Bers : in *RF Plasma Heating (Proc. 3rd Top. Conf., Pasadena, 1978)* G5-1.

53) C.F.F. Karney, A. Sen and F.Y.F. Chu : Phys. Fluids 22 (1979) 940.

54) A.C. Newell and D.J. Kaup : Bull.Am.Phys. Soc. 21 (1976) 1095.

55) A.C. Scott, F.Y.F. Chu and D.E. McLaughlin : Proc. IEEE 61 (1973) 1443.

56) H. Sanuki and T. Ogino : Phys. Fluids 20 (1977) 1510.

57) H.Y. Yu, P.K. Shukla and K.H. Spatschek : J.Plasma Phys. 20 (1978) 189.

58) G.P. Leclert, C.F.F. Karney, A. Bers and D.J. Kaup : Phys. Fluids 22 (1979) 1545.

59) A. Fukuyama, K. Hirai and Y. Furutani : J. Phys. Soc. Japan 48 (1980) 601.

60) R. Hirota : J. Phys. Soc. Japan 33 (1972) 1456.

61) M.J. Ablowitz, D.J. Kaup, A.C. Newell and H. Segur : Phys. Rev. Lett. 31 (1973) 125.

62) A. Sen, C.F.F. Karney, G.J. Johnston and A. Bers : Nucl. Fusion 18 (1978) 171.

63) P.K. Kaw, C.Z. Cheng and L. Chen : *Report of Princeton Plasma Physics Laboratory*, PPPL-1305 (1976).

64) G.J. Morales and Y.C. Lee : Phys. Fluids 20 (1977) 1135.

65) H.H. Chen and C.S. Liu : Phys. Fluids 21 (1978) 377.

66) M.J. Ablowitz, D.J. Kaup, A.C. Newell and H. Segur : Study App. Math. 53 (1974) 249.

67) G.R. Smith and A.N. Kaufman : Phys. Rev. Lett. 34 (1975) 1613; G.R. Smith and A.N. Kaufman : Phys. Fluids 21 (1978) 2230.

68) T.H. Stix : *Report of Princeton Plasma Physics Laboratory,* PPPL-1539 (1979).

69) G.M. Zaslavskii and B.V. Chirikov : Sov. Phys.-Usp. 14 (1972) 549.

70) B.V. Chirikov : Phys. Rep. 52 (1979) 263.

71) M.N. Rosenbluth, R.Z. Sagdeev, J.B. Taylor and G.M. Zaslavskii : : Nucl. Fusion 6 (1966) 297; N.N. Filonenko, R.Z. Sagdeev and G.M. Zaslavskii : Nucl. Fusion 7 (1967) 253.

72) J.D. Callen : Phys. Rev. Lett. 39 (1977) 1540.

73) A.B. Rechester and M.N. Rosenbluth : Phys. Rev. Lett. 40 (1978) 38.

74) M.N. Rosenbluth : Phys. Rev. Lett. 29 (1972) 408.

75) F. Jaeger, A.J. Lichtenberg and M.A. Lieberman : Plasma Phys. 14 (1972) 1073; M.A. Lieberman and A.J. Lichtenberg : Plasma Phys. 15 (1973) 125.

76) B.V. Chirikov : Sov. J. Plasma Phys. 4 (1978) 289.

77) for example, see *Intrinsic Stochasticity in Plasmas (Proc. Int. Workshop, Cargese, 1979)* ed. by G. Laval and D. Gresillon, (Editions de Physique, Orsay, 1979) .

78) G.M. Zaslavskii and N.N. Filonenko : Sov. Phys.-JETP 27 (1968) 851.

79) A. Fukuyama : in *Intrinsic Stochasticity in Plasmas (Proc. Int. Workshop, Cargese, 1979)* 207.

80) E.F. Jaeger and A.J. Lichtenberg : Ann. Phys. (N.Y.) 71 (1972) 319.

81) A. Fukuyama, H. Momota and R. Itatani : in *Plasma Heating of Toroidal Devices (Proc. 3rd Int. Symp., Varenna, 1976)* 63.

82) A. Fukuyama, H. Momota, R. Itatani and T. Takizuka : Phys. Rev. Lett. 38 (1977) 701.

83) R.E. Aamodt and S.E. Bodner : Phys. Fluids 12 (1969) 1471.

84) A.V. Timofeev : Nucl. Fusion 14 (1974) 165.

85) C.F.F. Karney and A. Bers : Phys. Rev. Lett. 39 (1977) 550; C.F.F. Karney : Phys. Fluids 21 (1978) 1584.

86) H. Momota, A. Fukuyama and T. Takizuka : in *Theory of Magnetically Confined Plasmas (Proc. Int. School, Varenna, 1977)* 365.

87) H. Abe, H. Momota, R. Itatani and A. Fukuyama : submitted to Phys. Fluids.

88) C.F.F. Karney : Phys. Fluids 22 (1979) 2188.

89) G.J. Morales and Y.C. Lee : Phys. Rev. Lett 33 (1974) 1534.

90) M. Abramowitz and I.A. Stegun : *Handbook of Mathematical Functions*, Dover Publ. (1970) Chaps. 16 and 17.